Nanoparticle Mediated Diagnosis and Combination Therapy of Bacterial Infections

by

İrem Koç

A Dissertation Submitted to the
Graduate School of Sciences and Engineering
in Partial Fulfillment of the Requirements for
the Degree of

Master of Science

in

Materials Science and Engineering

KOÇ ÜNİVERSİTESİ

January 26, 2023

Nanoparticle Mediated Diagnosis and Combination Therapy of Bacterial Infections

Koç University

Graduate School of Sciences and Engineering

This is to certify that I have examined this copy of a master's thesis by

İrem Koç

and have found that it is complete and satisfactory in all respects,
and that any and all revisions required by the final
examining committee have been made.

Committee Members:

_____

Prof. Dr. Havva Yağcı Acar (Advisor)

_____

Prof. Dr. Füsun Can

_____

Prof. Dr. Duygu Avcı Semiz

Date: _____

güneşe gömülenlere...

ABSTRACT

Nanoparticle Mediated Diagnosis and Combination Therapy of Bacterial Infections

İrem Koç

Master of Science in Materials Science and Engineering

January 26, 2023

Treatment of bacterial infections has become one of the challenges over the decades. Adhesion on different surfaces of bacteria and biofilm formation have led to the bacteria species to obtain increased survival rates with high morbidity especially in hospital-related infections. Insufficient treatments result in recurrence of the infection or even death of the patient. Current antibiotic drugs are not capable of eradicating the complex biofilm structure due to the acquired resistance mechanisms of bacteria. Therefore studies have been conducted for alternative therapies against multi-drug resistance bacteria and their biofilm-related infections.

Photodynamic therapy (PDT) is noninvasive, localized, and promising alternative method. There have been extensive studies of PDT for the treatment of cancer and bacterial infections. PDT is composed of a photosensitizer (PS), molecular oxygen, and the appropriate light source. PS is excited from ground state to the triplet state by the light source to produce reactive oxygen species (ROS) with the interaction of molecular oxygen in the environment. Following ROS production, cellular components are exposed to produced ROS and consequently cell death. PDT can be utilized alone or in combination with chemotherapy or photothermal therapy (PTT) for the treatment of bacterial infections.

Photothermal therapy is another alternative, wherein the PS converts light-to-heat and induce local temperature increase, resulting in cell death. It is again controlled, highly-localized, and noninvasive method which has been combined with different therapeutics such as PDT, chemotherapy, immunotherapy or radiotherapy for infectious diseases. Some nanoparticles act as photothermal agents, namely as photothermal nanotherapeutics (PTN).

Superparamagnetic iron oxide nanoparticles (SPIONs), mostly known as Magnetic Resonance Imaging (MRI) agents, have been also recognized as PTT agents

recently. They are the most studied nanoparticles in nanotherapeutics because of the FDA-approval and high biocompability. SPIONs may also be used as nano-carriers by tailoring surface coating with targeting agents or ligands for the targeted delivery of drugs, genes, and DNA/RNA.

Silver sulfide quantum dots (Ag_2S-QDs) are semiconductor nanocrystals with broad absorption in UV-visible region and NIR-emission. Their luminescent properties are superior to commercial fluorescent dyes in particular with properties such as resistance to the photobleaching, higher quantum yield, and stability. They have also been recognized as PTT agents and extensively studied for the treatment of cancer. QDs are another class of nano-carriers which can be used for the targeted delivery of therapeutics with bioimaging properties.

5-Aminolevulinic acid (ALA) is an FDA-approved PS with strong fluorescence in visible region for diagnosis and fast accumulation in the tumor and infectious tissue. ALA, itself is not an active PS molecule but it is internalized and converted into active protoporphyrin IX (PpIX) molecule in cells. ALA is also an endogeneous molecule in heme biosynthetic pathway of cells. However, high solubility and rapid clearance from tissues reduces effect of PDT. Additionally, higher amounts of PpIX accumulation is needed for successful PDT applications.

In this thesis, antibiotic free treatment of bacterial infections via combination of PTT and PDT is proposed. The combination is expected to bring about a synergestic effect at lower doses of PS and mild hyperthermia. In case of the biofilms, permeabilization of the biofilm via mild PTT is expected to take place and enhance the treatment efficiency. For this purpose, ALA loaded SPIONs were produced. Planktonic cells and biofilms of gram-positive (*Staphylococcus epidermidis*) and gram-negative (*Pseudomonas aeruginosa*) bacteria were treated with ALA loaded SPIONs and subjected to dual laser irradiation (640 + 808 nm). ALA-PDT takes place at 640 nm irradiation. SPION-PTT is usually achieved at 808 nm, but here it was determined that light-to-heat conversion efficiency of SPION at 640 nm is also 89.73%. Combination therapy resulted in a higher growth inhibition rate with complete eradication of planktonic cells of P.aeruginosa. Significant growth inhibition rates were achieved for biofilms of *S.epidermidis* and *P.aeruginosa* (10-log and 13-log, respectively).

Fluorescence images supported the enhanced delivery of ALA into P.aeruginosa biofilms. It is important to emphasize that SPIONs are the only FDA-approved nanoparticles, and they show low cytotoxicities. Therefore, they can be good can-

didates for the treatment of multi-drug resistant bacteria infections in vivo and in clinical studies by utilizing combination therapy of aPDT and aPTT.

An alternative composition for combination therapy wherein a single wavelength irradiation would be sufficient is also proposed in this thesis: ALA loaded Ag2S-QDs coupled with 640 nm irradiation. PTT potential of QDs at 640 nm laser irradiation was investigated and reported as 65.7%. These QDs were mostly effective against gram-positive bacteria. Significant growth inhibition rates were observed as 8-and 6-log for P.aeruginosa planktonic cells and biofilms, respectively. Confocal microscopy images showed strong NIR emission highlighting the imaging potential of the QDs. It is also shown that these QDs do not have any cytotoxicity against healthy cell line, Vero. Thus, ALA loaded NAC coated Ag_2S-QDs are promising candidates for in vivo and clinical phototherapies against gram-positive bacteria related infections with the advantage of imaging in the NIR region.

ÖZETÇE

Yüksek Lisans Tez Başlığı
İrem Koç
Malzeme Bilimi ve Mühendisliği, Yüksek Lisans
26 Ocak 2023

Bakteriyel enfeksiyonların tedavisi, on yıllardır karşılaşılan zorluklardan biri haline geldi. Bakterilerin farklı yüzeylere yapışması ve biyofilm oluşturması, bakteri türlerinin özellikle hastane kaynaklı enfeksiyonlarda yüksek morbidite ile artan canlılık oranları elde etmesine yol açmıştır. Yetersiz tedaviler, enfeksiyonun tekrarlamasına ve hatta hastanın ölümüne neden olmaktadır. Mevcut antibiyotik ilaçlar, bakterilerin kazanılmış direnç mekanizmaları nedeniyle karmaşık biyofilm yapısını ortadan kaldıramamaktadır. Bu nedenle çoklu ilaca dirençli bakterilere ve bunların biyofilm ile ilişkili enfeksiyonlarına karşı alternatif tedaviler için çalışmalar yapılmaktadır.

Fotodinamik terapi (FDT), invaziv olmayan ve lokalize bir alternatif yöntemdir. Kanser ve bakteriyel enfeksiyonların tedavisi için birçok kapsamlı FDT çalışmaları yapılmıştır. FDT, bir foto-hassaslaştırıcı (PS), moleküler oksijen ve uygun ışık kaynağından oluşur. PS molekülü, kararlı (taban) durumdan kararsız (üçlü) duruma uyarılır ve ortamdaki moleküler oksijenin ile etkileşime girerek reaktif oksijen türevleri (ROT) üretir. ROT üretimini takiben, hücresel bileşenler üretilen ROT'a ve sonuç olarak hücre ölümüne maruz kalır.

FDT, bakteriyel enfeksiyonların tedavisi için tek başına veya kemoterapi veya fototermal terapi (FTT) ile kombinasyon halinde kullanılabilir. Fototermal terapi, PS'nin ışığı ısıya dönüştürdüğü ve hücre ölümüyle sonuçlanan lokal sıcaklık artışına neden olduğu başka bir alternatiftir. Yine bulaşıcı hastalıklar için PDT, kemoterapi, immünoterapi veya radyoterapi gibi farklı terapötiklerle kombine edilmiş, kontrollü, yüksek lokalize ve invaziv olmayan bir yöntemdir. Bazı nanopartiküller, fototermal ajanlar, yani fototermal nanoterapötikler (PTN) olarak işlev görür.

Çoğunlukla Manyetik Rezonans Görüntüleme (MRI) ajanları olarak bilinen superparamanyetik demir oksit nanoparçacıkları (SPION'lar), son zamanlarda PTT ajanları olarak da tanınmaktadır. FDA onayı ve yüksek biyouyumluluk nedeniyle

nanoterapötiklerde en çok çalışılan nanoparçacıklardır. SPION'lar ayrıca, ilaçların, genlerin ve DNA/RNA'nın hedeflenen iletimi için hedefleme ajanları veya ligandlarla yüzey kaplamasını uyarlayarak nano-taşıyıcılar olarak da kullanılabilir.

Gümüş sülfid kuantum noktaları (Ag_2S-QD'ler), UV-görünür bölgede geniş absorpsiyon ve NIR emisyonu olan yarı iletken nanokristallerdir. Bunların ışıldama özellikleri, özellikle ışıkla ağartmaya karşı direnç, daha yüksek kuantum verimi ve kararlılık gibi özelliklerle ticari floresan boyalardan üstündür. Ayrıca PTT ajanları olarak kabul edilmişler ve kanser tedavisi için kapsamlı bir şekilde çalışılmışlardır. QD'ler, biyogörüntüleme özelliklerine sahip terapötiklerin hedeflenen iletimi için kullanılabilen başka bir nano-taşıyıcı sınıfıdır.

5-Aminolevulinik asit (ALA), tümör ve enfeksiyonlu dokuda tanı ve hızlı birikim için görünür bölgede güçlü flüoresans içeren FDA onaylı bir PS'dir. ALA'nın kendisi aktif bir PS molekülü değildir ancak hücrelere alınarak aktif protoporfirin IX (PpIX) molekülüne dönüştürülür. ALA ayrıca hücrelerin heme biyosentetik yolunda endojen bir moleküldür. Bununla birlikte, yüksek çözünürlük ve dokulardan hızlı temizlenme, PDT'nin etkisini azaltır. Ek olarak, başarılı PDT uygulamaları için daha yüksek miktarlarda PpIX birikimi gereklidir.

Bu tezde, PTT ve PDT kombinasyonu yoluyla bakteriyel enfeksiyonların antibiyotiksiz tedavisi önerilmiştir. Kombinasyonun, daha düşük PS dozlarında ve hafif hipertermide sinerjistik bir etki yaratması beklenmektedir. Biyofilmler söz konusu olduğunda, biyofilmin hafif PTT yoluyla geçirgenleşmesinin gerçekleşmesi ve tedavi etkinliğini artırması beklenir. Bu amaçla ALA yüklü SPION'lar üretilmiştir. planktonik gram-pozitif (*Staphylococcus epidermidis*) ve gram-negatif (*Pseudomonas aeruginosa*) bakterilerin hücreleri ve biyofilmleri, ALA yüklü SPION'larla muamele edildi ve ikili lazer ışınlamasına (640 + 808 nm) tabi tutuldu. ALA-PDT, 640 nm ışınlamada gerçekleşir. SPION-PTT genellikle 808 nm'de elde edilir, ancak burada SPION'un 640 nm'de ışıktan ısıya dönüşüm veriminin de %89.73 olduğu belirlendi. Kombinasyon tedavisi, P.aeruginosa'nın planktonik hücrelerinin tamamen ortadan kaldırılmasıyla daha yüksek bir büyüme inhibisyonu oranıyla sonuçlandı. *S.epidermidis* ve *P.aeruginosa*'nın (sırasıyla 10-log ve 13-log) biyofilmleri için önemli büyüme inhibisyon oranları elde edildi.

Floresan görüntüleri, ALA'nın *P.aeruginosa* biyofilmlerine gelişmiş dağıtımını destekledi. SPION'ların FDA onaylı tek nanopartiküller olduğunu ve düşük sitotoksisite gösterdiklerini vurgulamak önemlidir. Bu nedenle, aPDT ve aPTT'nin kombinasyon tedavisinden yararlanarak çoklu ilaca dirençli bakteri enfeksiyonlarının in

vivo ve klinik çalışmalarda tedavisi için iyi adaylar olabilirler.

Bu tezde, tek bir dalga boyunda ışınlamanın yeterli olacağı kombinasyon terapisi için alternatif bir bileşim de önerilmiştir: 640 nm ışınlama ile birleştirilmiş ALA yüklü Ag_2S-QD'ler. 640 nm lazer ışınlamasında QD'lerin PTT potansiyeli araştırıldı ve %65.7 olarak bildirildi. Bu QD'ler çoğunlukla gram-pozitif bakterilere karşı etkiliydi. P.aeruginosa planktonik hücreleri ve biyofilmleri için sırasıyla 8- ve 6- log olarak önemli büyüme inhibisyon oranları gözlendi. Konfokal mikroskopi görüntüleri, QD'lerin görüntüleme potansiyelini vurgulayan güçlü NIR emisyonu gösterdi. Ayrıca bu QD'lerin sağlıklı hücre dizisi Vero'ya karşı herhangi bir sitotoksisiteye sahip olmadığı gösterilmiştir. Bu nedenle, ALA yüklü NAC kaplı Ag_2S-QD'ler, NIR bölgesinde görüntüleme avantajı ile gram-pozitif bakterilerle ilişkili enfeksiyonlara karşı in vivo ve klinik fototerapiler için umut verici adaylardır.

ACKNOWLEDGMENTS

I would like to deeply thank my advisor Prof. Funda Acar Yağcı for her marvellous teaching in chemistry and guidance. I appreciate the chance to work in her laboratory. I was lucky enough to learn academic field from her perspective.

I would like to thank Prof. Füsun Can for believing in me and allowing me in her laboratory to carry out my bacteria experiments. I also thank her being one of the committee members of my thesis. I would not be able to complete all this work without her support. I will always remember the day I have realized we have so much in common.

I would like to thank Prof. Duygu Avcı Semiz for being one of the committee members of my thesis and giving her time for me.

I especially thank Dr. Sarp Kaya for believing in me and accepting me in his laboratory in the first place. I appreciate his support throughout our time together as student and advisor. I would not achieve any of these experiences without his acceptance. I will always remember his kindness.

I sincerely thank Dr. Uğur Ünal for his kindness and his understanding. I have always felt his support and I appreciate it.

I would like to thank Prof. Alphan Sennaroğlu for allowing me in his laboratory for detailed analysis of my work.

My appreciation goes to all of the members in Koç University Surface Science and Technology Center (KUYTAM) who helped me for the characterizations in my work.

I would like to thank my sincere postdocs Kübra Onbaşlı and Nazlı Ataç for their endless help and scientific discussions. I would not achieve any of these data without them.

I deeply thank my dear friend Eda Çelikbaş. She has not only been a spectacular

colleague but also a very close friend. I will always appreciate her support and her patient for teaching me many things that I would not have known without her. I enjoyed sharing our desks together. I enjoyed staying long hours in laboratory with you. I enjoyed going to gym with you, gym freak.

My appreciation also goes to all my current and former lab-mates for their support and contributions within these years.

I also would like to thank many people that I have met in my last semester for contributing the change in me. All of you will always be remembered.

I would like to acknowledge the financial support from the Scientific and Technological Research Council of Turkey (TUBITAK, project number: 118S547 and 220S035).

Finally, I would like to thank my family for their support and understanding. I especially thank my mother for her endless belief for me since I was a child. I would not achieve any of my academic degrees without her labor.

TABLE OF CONTENTS

List of Tables **xv**

List of Figures **xvi**

Abbreviations **xxi**

Chapter 1: Introduction **1**

1.1 Photodynamic Therapy (PDT) 1

1.1.1 ALA-mediated PDT 3

1.2 Photothermal Therapy (PTT) 4

1.3 Superparamagnetic Iron Oxide Nanoparticles in PDT and PTT . . . 7

1.4 Quantum Dots in PDT and PTT 9

Chapter 2: Enhanced antimicrobial PDT of 5-ALA in combination with antimicrobial PTT using SPIONs **13**

2.1 Abstract 13

2.2 Introduction 13

2.3 Materials and Methods 16

2.3.1 Synthesis of Poly(acrylic Acid) Coated SPIONs 16

2.3.2 ALA Loading on SPIONs 17

2.3.3 Characterization 17

2.3.4 Laser Irradiation of Aqueous Solutions 17

2.3.5 Cell Culture 18

2.3.6 Dark Toxicity 18

2.3.7 Antimicrobial activity and antibiofilm assays 18

2.3.8 Laser Treatment of Bacteria 19

2.3.9 PpIX Detection . . . 19
2.3.10 Uptake of Nanoparticles . . . 20
2.3.11 Statistical Analysis . . . 20
2.4 Results . . . 20
2.4.1 Synthesis and Characterization of Nanoparticles . . . 20
2.4.2 Temperature Increase in Aqueous Solutions with 640 nm Irradiation . . . 22
2.4.3 Antibacterial Activity . . . 23
2.4.4 Antibiofilm Bacterial Activity . . . 26
2.4.5 In vitro Uptake of Nanoparticles . . . 28
2.4.6 PpIX Detection . . . 28
2.4.7 Photothermal Screening During Laser Treatment . . . 29
2.5 Discussion . . . 30
2.6 Conclusions . . . 34

Chapter 3: NAC-Ag2S Quantum Dots For NIR-Image Guided Combination Therapy of Antimicrobial PDT and PTT 36

3.1 Abstract . . . 36
3.2 Introduction . . . 36
3.3 Materials and Methods . . . 39
3.3.1 Synthesis of NAC-Ag2S QDs . . . 39
3.3.2 Electrostatic Loading of ALA on NAC-Ag2S QDs . . . 40
3.3.3 Characterization . . . 40
3.3.4 Laser irradiation of QD solutions . . . 41
3.3.5 Cytotoxicity assay . . . 41
3.3.6 Antimicrobial activity and antibiofilm assays . . . 41
3.3.7 Cell uptake of QDs . . . 42
3.3.8 Measurement of PpIX formation . . . 43
3.3.9 Determination of reactive oxygen species (ROS generation) . . . 43
3.4 Results . . . 44

3.4.1 Synthesis and Characterization of NAC-QDs 44
3.4.2 Measurement of photothermal potential 45
3.4.3 Antibacterial activity 45
3.4.4 Antibiofilm bacterial activity 47
3.4.5 Cell uptake of QDs 48
3.4.6 Measurement of PpIX formation 49
3.4.7 ROS generation 50
3.5 Discussion 51
3.6 Conclusions 56

Chapter 4: Conclusions **58**

Bibliography **60**

LIST OF TABLES

2.1 Dynamic Light Scattering (DLS) Results of Nanoparticles. 21

LIST OF FIGURES

1.1 The Mechanism of PDT. 2

1.2 Heme Biosynthetic Pathway. 3

1.3 Chemical Structures of ALA and PpIX 4

1.4 Different thermal treatments as classified by the corresponding operating temperature. 5

1.5 The spectral extensions of the medical window: First and Second Biological Windows 6

1.6 Size Dependent Fluorescence Properties of QDs. 10

2.1 UV absorbance and TGA analysis of nanoparticles. 21

2.2 ITC Result. 22

2.3 Time dependent change in the temperature of PAA@SPION solutions at different Fe concentrations irradiated at 200 mW. Excitation wavelength = 640 nm 22

2.4 After laser on (20 min)/off (20 min) cycles (600 ug/mL, 200 mW). Excitation wavelength = 640 nm. 23

2.5 Effect of free ALA, only SPIONs, and ALA-SPIONs on the growth inhibition of planktonic cells of *S.epidermidis* were measured both with and without laser irradiation. Control: No substances were applied to planktonic cells. 640 nm, 808 nm, and dual laser irradiation at 300 mW, 1000 mW, and 300 mW 1000 mW for 10 minutes, respectively, were used in all laser experiments. 24

2.6 Effect of free ALA, only SPIONs, and ALA-SPIONs on the growth inhibition of planktonic cells of *P.aeruginosa* were measured both with and without laser irradiation. Control: No substances were applied to planktonic cells. 640 nm, 808 nm, and dual laser irradiation at 300 mW, 1000 mW, and 300 mW 1000 mW for 10 minutes, respectively, were used in all laser experiments. 25

2.7 Effect of free ALA, only SPIONs, and ALA-SPIONs on the growth inhibition of *S.epidermidis* biofilms were measured both with and without laser irradiation. Control: No substances were applied to planktonic cells. 640 nm, 808 nm, and dual laser irradiation at 300 mW, 1000 mW, and 300 mW 1000 mW for 10 minutes, respectively, were used in all laser experiments. 26

2.8 Effect of free ALA, only SPIONs, and ALA-SPIONs on the growth inhibition of *P.aeruginosa* biofilms were measured both with and without laser irradiation. Control: No substances were applied to planktonic cells. 640 nm, 808 nm, and dual laser irradiation at 300 mW, 1000 mW, and 300 mW 1000 mW for 10 minutes, respectively, were used in all laser experiments. 27

2.9 Intracellular quantification of SPIONs and ALA-SPIONs in *P.aeruginosa* and *S.epidermidis* biofilms. 28

2.10 Intracellular formation of PpIX through administration of free ALA and ALA-PAA@SPION after overnight incubation. (PpIX: exc: 405 nm and em: 635 nm) *P.aeruginosa* planktonic cells. 29

2.11 Intracellular formation of PpIX through administration of free ALA and ALA-SPIONs after overnight incubation. (PpIX: exc: 405 nm and em: 635 nm) S.aeruginosa planktonic cells. 30

2.12 Fluorescence microscopy images of P. aeruginosa biofilm at 20X magnification. Blue: Bacteria stained with DAPI, Red: PPIX Fluorescence. LEICA Live Cell Microscope, DAPI Filter Ex:365, Em:465, Alexa 610 Filter Ex:590, Em:630. 31

3.1 a) Absorbance calibrated photoluminescence, b) Absorbance and c) TGA spectra of QDs. 44

3.2 Time dependent change in the temperature of QD solutions at different Ag concentrations irradiated at 200 mW. (Ex = 640 nm). The data are expressed as mean ± S.D. (n = 3) 45

3.3 Effect of ALA, QDs, and ALA-QDs on the growth inhibition of planktonic cells of *S. epidermidis* was measured both with and without laser irradiation. Control: No substances were applied to planktonic cells. Each laser experiment was conducted under 640 nm laser irradiation for 10 minutes. The data are presented as mean ± S.D. (n = 3), with a $p \leq 0.05$ significance level. 46

3.4 Effect of ALA, QDs, and ALA-QDs on the growth inhibition of planktonic cells of *P.aeruginosa* was measured both with and without laser irradiation. Control: No substances were applied to planktonic cells. Each laser experiment was conducted under 640 nm laser irradiation for 10 minutes. The data are presented as mean ± S.D. (n = 3), with a $p \leq 0.05$ significance level. 47

3.5 Effect of ALA, QDs, and ALA-QDs on the growth inhibition of biofilms of *S. epidermidis* was measured both with and without laser irradiation. Control: No substances were applied to planktonic cells. Each laser experiment was conducted under 640 nm laser irradiation for 10 minutes. The data are presented as mean ± S.D. (n = 3), with a $p \leq 0.05$ significance level. 48

3.6 Effect of ALA, QDs, and ALA-QDs on the growth inhibition of biofilms of *P.aeruginosa* was measured both with and without laser irradiation. Control: No substances were applied to planktonic cells. Each laser experiment was conducted under 640 nm laser irradiation for 10 minutes. The data are presented as mean ± S.D. (n = 3), with a p $\leq$ 0.05 significance level. 49

3.7 Confocal microscopy images of P. aeruginosa biofilms at 40X magnification. Blue: Bacteria stained with DAPI (Ex/Em:325/375 nm), Red:Luminescence from QDs (Ex/Em:488/580-780 nm), Leica dmi8/SP Microscope. 50

3.8 Intracellular quantification of QDs and ALA-QDs in *P.aeruginosa* and *S.epidermidis* biofilms. 51

3.9 Intracellular formation of PpIX through administration of ALA and ALA-QDs after 24h incubation. (PpIX: λex: 405 nm and λem: 635 nm) *P.aeruginosa*(Left) and *S.epidermidis* (Right) planktonic cells. The data are expressed as mean ± S.D. (n = 3), (p $\leq$ 0.05). 52

3.10 ROS production in *P.aeruginosa* (left) and *S.epidermidis* (right) planktonic cells upon 24 h incubation with ALA (3 mM ALA), QD, and, ALA-QD at 500 ug/mL Ag dose after laser irradiation for 10 min. The data are expressed as mean ± S.D. (n = 3), (p $\leq$ 0.05). 53

ABBREVIATIONS

ALA	Aminolevulinic Acid
$AgNO_3$	Silver(I)Nitride
Ag_2S	Silver(I)Sulfide
aPDT	Antimicrobial Photodynamic Therapy
aPTT	Antimicrobial Photothermal Therapy
CB	Conduction Band
DAPI	4',6-diamidino-2-phenylindole
DLS	Dynamic Light Scattering
DMSO	Dimethyl Sulfoxide
Fe_2O_3	Maghemite
Fe_4O_4	Magnetite
ICP-MS	Inductive coupled-mass spectroscopy
kDa	Kilo Dalton
ITC	Isothermal Titration Calorimetry
MRI	Magnetic resonance imaging
MTT	Thiazolyl blue tetrazolium bromide
NAC	N-Acetyl-L-cysteine
NaOH	Sodium Hydroxide
Na_2S	Sodium sulfide
NH_4OH	Ammonium hydroxide
NIR	Near Infrared
PAA	Polyacrylic acid
PBS	Phosphate buffer saline
PL	Photo-Luminescence
PpIX	Protoporphyrin IX
PS	Photosensitizer
QD	Quantum Dots xxi
ROS	Reactive Oxygen Species
SPION	Superparamagnetic iron oxide nanoparticle
VB	Valence Band

Chapter 1

INTRODUCTION

1.1 Photodynamic Therapy (PDT)

Photodynamic therapy (PDT) has emerged as an alternative treatment method for variety of cancer types and infectious diseases [Bhattacherjee et al., 2019, Agostinis et al., 2011, dos Santos et al., 2019]. Antimicrobial resistance of pathogens has resulted in severe challenges of public health with high morbidity and mortality [Akova, 2016, Frieri et al., 2017]. Antimicrobial PDT has gained great attention due to its invasiveness, high locality, high specificity to microorganisms, and lack of the development of resistance to aPDT [Ornellas et al., 2018, Liu et al., 2015, Bartolomeu et al., 2016]. aPDT utilizes photosensitizer (PS), oxygen, and appropriate light source to produce reactive oxygen species (ROS) inside cells to destroy cellular structures [Maisch et al., 2011]. Upon light irradiation, excited PS either directly interacts with intracellular substrates such as proteins, lipids, or DNA/RNA to produce radical species (superoxide anion radical ($O_2^{-}\cdot$), a hydroxyl radical ($OH\cdot$), or hydrogen peroxide (H_2O_2) via electron or proton transfer (type I reaction), or excited PS interacts with molecular oxygen to produce singlet oxygen ($^1O_2$) via energy transfer (type II reaction) (Fig 1.) [Foote, 1991]. In general, membranous domains of microbial cells are affected by photoinactivation. Most of the actively used PS molecules preferentially locate at the level of cytoplasmic membrane except for the acridine which intercalate with DNA bases[Wainwright et al., 1997]. However, many investigators have been reported that photoinduced damage is in agreement with the lack of mutagenic effects even after repetative irradiations[Maisch et al., 2004, Malik et al., 1992].

For photodynamic killing of microbial pathogens, chemical structure of PS, cell-

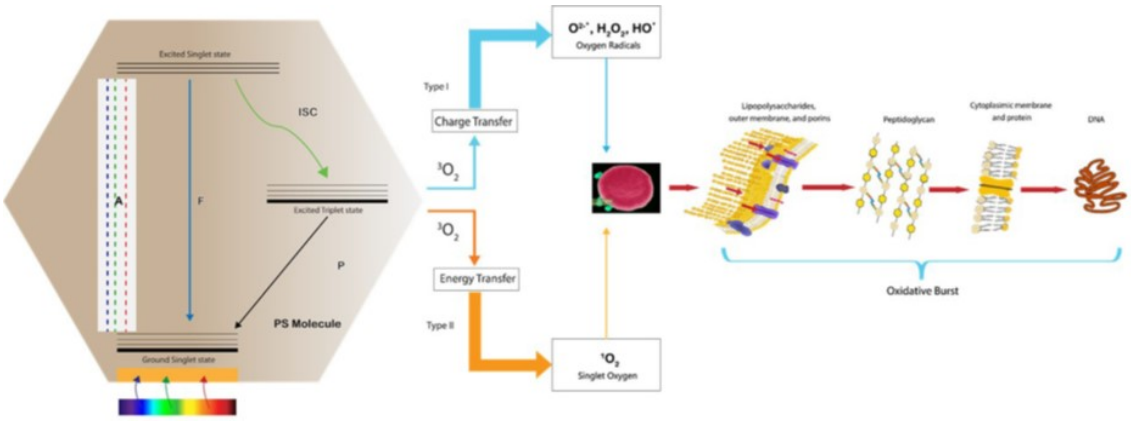

Figure 1.1: The Mechanism of PDT.

PS incubation time, fluence rate, and irradiation time determine the efficiency of therapy[Jori et al., 2011]. Different light sources, lasers, light-emitting diodes(LEDs), and lamps, are used for the activation of PS molecule[Kim and Darafsheh, 2020]. The use of light source depends on the type of PS, required light dose, and penetration depth of light to tissues. Lamps and LEDs are mostly preferred due to their low cost and ease of use. In order to minimize photosensitization of the healthy tissue, PS should absorb light in the longer wavelenghts, 600-900 nm. This optimal range wavelength is called "therapeutic window"[A., 2006]. Excitation of PS molecules at shorter wavelengths mostly prevent light penetration through tissue and may result in photosensitization of skin while excitation at long wavelengths may not provide sufficient energy for triplet state to transfer energy to the ground state oxygen to excite it[Kim and Darafsheh, 2020, Castano et al., 2005].

Different PS molecule derivatives have been synthesized since 1970s. In PDT research, hematoporphyrin derivatives (HpD), particularly commercial versions like Photofrin, were most frequently utilized. However, these PS had a number of significant drawbacks, including chemical heterogeneity, poor tumor selectivity, and weak light absorbance at therapeutically useful wavelengths[Nyman and Hynninen, 2004, Allison et al., 2004]. To overcome major drawbacks of first generation of PS molecules, the second generation of PS molecules have been synthesized[DeRosa, 2002, Sessler and Miller, 2000]. These PS molecules can be activated at therapeu-

tic window of 600-900 nm.Members of the majority of the main classes of second-generation PS are either clinically approved, participating in PDT clinical trials, or being patented.

1.1.1 ALA-mediated PDT

Endogenous photosensitization is a mechanism in which introducing naturally occurring molecules inside cells results in the generation of photosensitive molecules. These molecules can be later utilized to induce therapeutic levels of the photosensitizer. 5-aminolevulinic acid (ALA) is a naturally occurring intermediate in the heme biosynthetic pathway and precursor of the photosensitizing agent protoporphyrin IX (PpIX) (Fig 1.2)[Phillips, 2019, Harris and Pierpoint, 2012]. ALA has no intrinsic

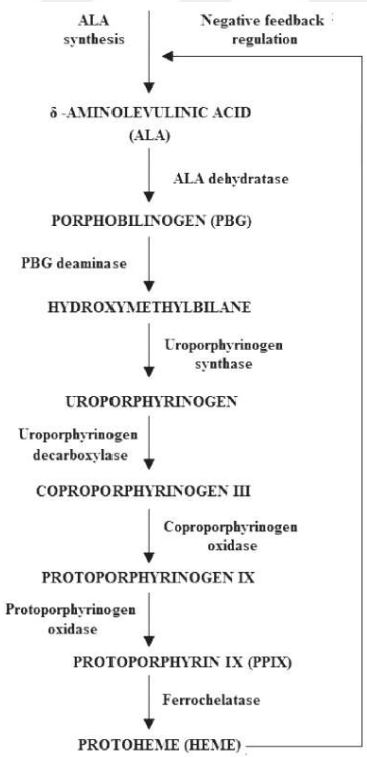

Figure 1.2: Heme Biosynthetic Pathway.

photosensitizing properties, it is internalized by cells and converted into the active agent PpIX (Fig. 1.3)[Tewari and Eggleston, 2018]. ALA has mainly been used as a prodrug in PDT applications for the treatment of different types of cancer, oral

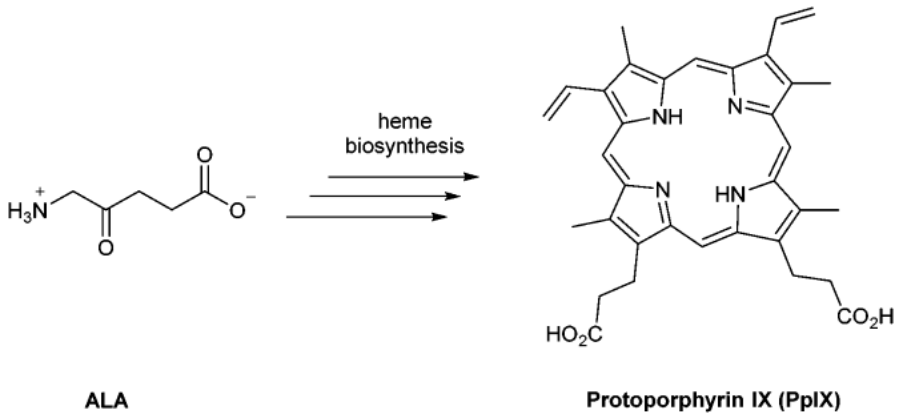

Figure 1.3: Chemical Structures of ALA and PpIX

diseases and microbial infections[Kennedy and Pottier, 1992, Sessler and Miller, 2000, dos Santos et al., 2019, Collaud, 2004]. It was shown that ALA-mediated therapies led to more accumulation of PpIX and other porphyrin intermediates in cancer cells, inflammatory cells and, bacteria compared to healthy cells[Hader and Jori, 2006, Collaud, 2004]. The heme biosynthesis pathway's intermediate porphyrins such as ALA, PPIX, and others are quickly removed from tissues. Therefore, ALA-based PDT applications has advantage over other therapeutic applications in terms of photosensitivity of the skin[Hader and Jori, 2006]. However, ALA is hydrophilic at physiological pH which renders its systemic delivery and topical application through hydrophobic barrier of cells. Different ALA derivatives with increased lipophilicity have been created in an effort to enhance the efficacy of ALA-mediated therapies[Novo et al., 1996, Kelty et al., 2002]. Another method to increase the permeability and amount of PS molecules is to use nanomaterials as a delivery vehicle. Poly(lactic-co-glycolic acid) (PLGA) nanoparticle technology was developed by Shi et al. to deliver ALA to human skin squamous cell cancer[Nitzan et al., 2004].

1.2 Photothermal Therapy (PTT)

The development of novel methods for temperature-induced cell death and alteration, as well as regulated and localized heating, has been heavily studied as a treatment for cancer[Fisher et al., 2010, Takahashi et al., 2006]. Depending on the

magnitude of the induced temperature increment and the duration of the treatment, thermal therapies can be classified as: diathermia, hyperthermia and thermal ablation (Figure 1.2)[Riadh W. Y. Habash and Alhafid, 2006].

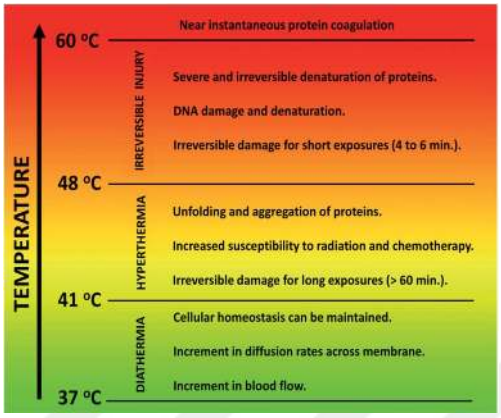

Figure 1.4: Different thermal treatments as classified by the corresponding operating temperature.

The maximum temperature of diathermia typically exceeds 41C for a brief amount of time, yet it does not significantly damage cells. Low temperature increase results in sensitivity of cells to additional therapies such as chemotherapy[Garrett et al., 2000, van Rijt and Sadler, 2009]. In hyperthermia, temperature usually reaches to 41-48C which is also accepted as clinical temperature range[Sapareto and Dewey, 1984]. It can be applied alone or in combination with other therapeutic modalities such as chemotherapy, immunotherapy or radiotherapy[Johannsen et al., 2005, Mendecki et al., 1980]. While, temperature increase up to 60°C causes protein denaturation, further temperature increase up to 80°C results in tissue explosion with thermal ablation therapies. Although, its application leads to efficient results, damage to adjacent healthy tissues can also take place[Corwin et al., 2001, Diederich, 2005]. The major focus of thermal therapies is to achieve well-localized heating in the disease area while keeping surrounding tissue temperature at a normal level[Rossmanna and Haemmerich, 2014]. Therefore, light irradiation of the disease area with high localization has received a great attention.

Photothermal therapy (PTT) is a light-based therapy in which, irradiation of NIR absorbing photothermal agents (PTAs) result in local temperature increase[Zou

et al., 2016]. The first and second biological windows, which are represented by the wavelength ranges between 700 and 980 nm and 1000 and 1400 nm, respectively, comprise the medical window (Figure 1.3) [Diederich, 2005]. Absorption and

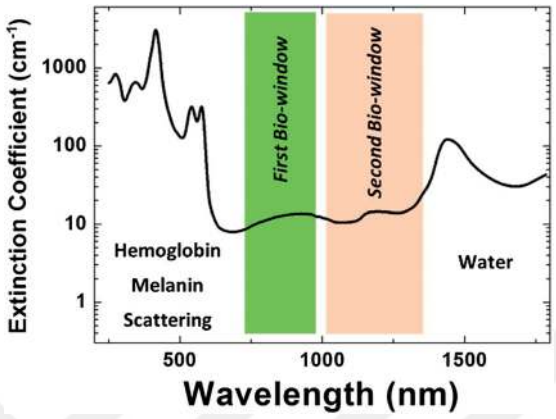

Figure 1.5: The spectral extensions of the medical window: First and Second Biological Windows

scattering of tissue are minimized at these wavelenghts. The major drawbacks of PTT are i) the limited depth of light penetration, ii) relatively low delivery efficiency of PTAs, iii) overheating of the tissue area and, iv) development of resistance to PTT by cells[Abadeer and Murphy, 2016]. The efficiency of PTT also depends on the ability of PTAs to convert light to heat especially in the nanotherapeutics. While numerous photothermal nanotherapeutics (PTN) have been widely synthesized, including noble metal nanostructures, transition metal oxide nanoparticles, nanocarbons, and organic nanomaterials, the use of nanotherapeutics-based clinical practice is still limited[Shanmugam et al., 2014, Orecchioni et al., 2015, Boca et al., 2011]. PTT has been extensively used in combination with multimodal-imaging, chemotherapy, radiotherapy and immunotherapy in animal models with lung, bone or lymph metastasis of many types of cancer[Yi et al., 2015, Zhou et al., 2015, Peng et al., 2014].

1.3 Superparamagnetic Iron Oxide Nanoparticles in PDT and PTT

Magnetic phenomena arises from electron-electron interactions and spin-couplings [Kaneyoshi, 1990]. Bulk magnetic materials do not have isotropic magnetization. As the material size is reduced from bulk to nano, the number of atoms per domain also decreases. These small portions of uniform spin alignments are called magnetic domains. A magnetic moment is created by the spontaneous magnetization of about 10(1–7)–10(2–1) atoms found in each domain. Large magnetic domains are contained inside the lattice structures of ferromagnetic materials. These domains become magnetized in a magnetic field as a result of the many aligned spins. Interaction between these domains results in magnetization of ferromagnetic materials even after magnetic field is removed [E. Blums, 1997]. Paramagnetic materials also have magnetization under magnetic field but they become demagnetized after magnetic field is removed. This property of paramagnetic materials is related to the weaker interactions between lower number of magnetic dipoles in domains. Magnetization dissipates at zero field when the number of atoms in magnetic domains decreases, or in other words, magnetic dipoles spontaneously randomly orient. When the quantity of atoms per domain is greatly reduced, ferromagnetic materials begin to behave like paramagnetic materials, and superparamagnetism arises. This can be seen in iron oxide nanoparticles smaller than 20 nm in size [Hofmann-Amtenbrink et al., 2010].

Superparamagnetic iron oxide nanoparticles (SPIONs) are small sized crystalline metal oxides which consist of a single magnetic domain [E. Blums, 1997]. Maghemite and magnetite are the two main crystal structures of SPIONs. A straightforward coprecipitation technique can be used to create SPIONs with any of the two alternative crystal structures by coprecipitating ferric (Fe^{3+}) and ferrous (Fe^{2+}) salts at high temperatures and in an alkaline environment [Reimers and Khalafalla, 1972, Zemann, 1965]. The overall chemical reaction of coprecipitation process can be written as in equation 1.1:

$$= \left[Fe^{3+} + Fe^{2+} + 8OH^{-} \quad \longrightarrow \quad Fe_3O_4 + 4H_2O \right] \tag{1.1}$$

The detailed coprecipitation reaction can be written as below equations:

$$= \begin{bmatrix} Fe^{3+} + H_2O & \longrightarrow & FeOH_x^{3-x} & (Deprotonation) \\ Fe^{2+} + H_2O & \longrightarrow & FeOH_y^{3-y} & (Deprotonation) \\ FeOH_x^{3-x} + FeOH_y^{3-y} & \longrightarrow & Fe_3O_4 & (Oxidation\&Dehydration) \end{bmatrix} \tag{1.2}$$

Magnetic moment of SPIONs arises from unpaired 3d electron in Fe^{3+} and Fe^{2+} cations. Between Fe^{3+} and Fe^{2+}, there are two types of coupling that occur: electron spin coupling on the octahedral sites and antiparallel couplings on the tetrahedral sites [Fleet, 1981]. Superexchange interactions, which are the cause of the magnetic behavior of SPIONs, are the outcome of exchange interactions between these two sites across oxygen anions. Superexchange interactions may be destroyed by oxygen vacancies, cationic vacancies, edge roughness, or loss of local symmetry [Kandasamy and Maity, 2015]. Magnetic properties of SPIONs are also determined by size, shape, crystallinity and surface coatings. Organic/inorganic coatings are applied in order to prevent agglomeration/precipitation of the nanoparticles in aqeuous solutions [Berry and Curtis, 2003, Yuen et al., 2012]. In addition to colloidal stability, coatings are applied to overcome the attractive forces including magnetic dipole-dipole and van der Waals interactions. The type of coating material, the ionic strength, and the pH of the media are the key factors that affect the repulsive forces that must be generated in the carrier liquid. Covalent bonds or electrostatic interactions between end groups of coating agents and nanoparticle surfaces are two possibilities. Most of these coating agents have end groups like -OH, -COOH, -NH, -PO(OH), and -(SO)-(2)-OH.[**?**]. The coating of material also effects cytotoxicity by reducing the risk of iron release from SPIONs in the biological environment. To further increase the biocompatibility of SPIONs, as well as to direct/target them to specific cells or tissues, the surface of SPIONs can be modified by attaching various functional groups, antibodies or ligands [Kaczyńska et al., 2016]. Moreover, nanoparticles with surface coatings can overcome the immune system defense and stay longer in circulation without being recognized. [Berry and Curtis, 2003].

SPIONs are mainly used in magnetic resonance imaging (MRI), magnetic hy-

perthermia, magnetofection, and drug delivery [Tietze et al., 2015, Barrow et al., 2015, Borlongan, 2007, Mykhaylyk et al., 2007]. Recently, SPIONs have been utilized as delivery system of PS molecules to the cells in PDT applications for various diseases [Unterweger et al., 2015]. The use of SPIONs as vehicles for the delivery of PS molecules is to overcome problems of the PDT is a growing field of research. de Santana et al., synthesized SPIONP-CUR by linking the keto-enol moiety of CUR with Fe atoms of SPIONs for the treatment of bacterial infections [de Santana et al., 2020]. In another study, the authors coated the surface of SPIONs with most commonly used porphyrin, PpIX, for simultaneous PDT application with imaging in a syngeneic murine tumor model [Yan et al., 2018]. SPIONs can also be used as multimodal contrast agent in combination with PTT. Sivakumar et al., encapsulated SPIONs and curcumin inside PLGA nanocapsules for the treatment of PANC-1 and MIA PaCa-2 cancer cell lines [Sivakumar et al., 2017]. Hyaluronan (HA)-modified SPIONs were developed for the diagnosis and treatment of CD44 HA receptor-overexpressing breast cancer in both in vitro and in vivo [Yang et al., 2016].

In the second chapter of the thesis, ALA combined aPDT and SPION aPTT in clinically safe doses of pro-drug ALA and low laser powers for planktonic and sessile cells of gram-positive *Staphylococcus epidermidis* (*S.epidermidis*) and gram-negative *Pseudomonas aeruginosa* (*P.aeruginosa*) bacteria was studied. Photothermal potential of SPIONs at 640 nm wavelength was shown. Complete eradication of planktonic cells of *P.aeruginosa* was observed with combination therapy. Significant growth inhibition rates were achieved for biofilms of *S.epidermidis* and *P.aeruginosa* (10-log and 13-log, respectively). Finally, imaging of biofilms was mediated through PpIX fluorescence.

1.4 Quantum Dots in PDT and PTT

Semiconducting nanoparticles (quantum dots) have attracted great attention in biomedical applications, photodetectors, light-emitting diode (LED) fabrication, solar cell technology or computing due to their unique size and shape dependent

electrical and optical properties [El-Sayed, 2001, Alivisatos, 1996]. A semiconductor nanocrystal is defined by its bandgap energy. Bandgap energy is the energy required to excite an electron from valence band (VB) to a higher energy level, conduction band (CB). This excitation results in an electron-hole pair known as an exciton. Electrons are not stable at CB, so they relax back from CB to VB, the exciton emits excess energy either in the form of photon (radiative) or nonradiative (vibrational relaxation, photochemical interaction). Exciton Bohr Radius (EBR) is the distance between the electron and hole pair and it is critical for confinement in semiconductors. When the size of the quantum dots (QDs) (2-10 nm) is smaller than EBR, strong confinement of QDs is observed. QDs in the nanoscale size have discrete energy levels that confine the motions of electrons and holes in all three directions. Therefore, the electronic structure of the confined QDs resides between a single molecule and the bulk material. As the size of the QDs decrease, the energy band gap increases and the emission wavelength decreases (Fig. 1.6) [Girma et al., 2017]. This is known as the quantum size effect. Thus, the band gap energy of the QDs becomes size dependent [Mattoussi et al., 2012, Bera et al., 2010].

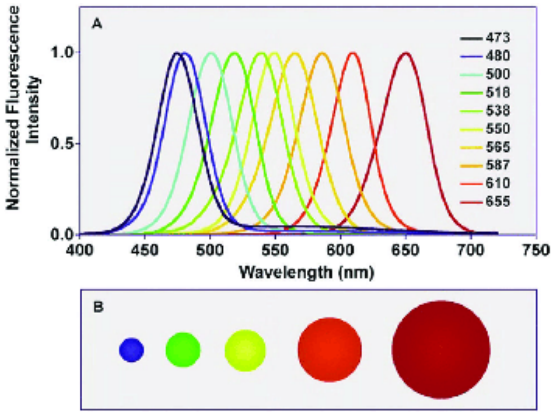

Figure 1.6: Size Dependent Fluorescence Properties of QDs.

Synthesis methods of semiconductor QDs are mainly traditional organic methods that result in hydrophobic surface properties with poor solubility and stability in aqeuous media [Pohanka, 2017]. Therefore, synthesis methods of QDs involved direct synthesis in water by using coating materials such as 2-mercaptopropionic acid, l-

cysteine, glutathione, and water-soluble polymers (PEG, polyethyleneimine (PEI), etc.). Synthesis of QDs in water provides a stable colloidal solution without any loss of luminescence and aggregation [Duman et al., 2015, Aydemir et al., 2020]. QDs are generally comprised of a metal, such as copper (Cu), cadmium (Cd), silver (Ag) or zinc (Zn) and a chalcogen atom, such as sulfur (S), selenium (Se) or tellurium (Te). Different coating materials are used to modify the surface of QDs by different techniques such as encapsulation, ligand exchange, and conjugation. While inorganic core is responsible for the size tunable color, coating material is responsible for stability and functionality of QDs. Coating material is also used for the controlled growth of the crystal surface during the synthesis of QDs. There have been a great effort to improve the cell/tissue specific NIR-imaging and diagnostic usages of QDs by changing the particle size, surface charge, and coating material [Bilan et al., 2016, Kumar, 2017].

QDs have been extensively used for the targeted tumor therapy and imaging, as the small size of QDs enhances the accumulation of QDs at the tumor site. In addition to small size, high surface to volume ratio of QDs provides the tailoring of coating material with therapeutic agents, targeting ligands, etc. [Cho et al., 2010]. Kim et al., synthesized nanospheres of CdTe/CdSe QDs that were loaded into poly(lactic-co-glycolic acid) (PLGA) for in vivo tumor imaging in the NIR-region. The particles had an emission peak around 760nm with 50% quantum yield [Kim et al., 2011]. Liu et al., developed NIR-emitting QDs capable of in vivo cation exchange for tumor imaging. The QDs were coated with PEG and the core was composed of Zn^{2+}, Hg^{2+}, Se^{2-}, and S^{2-} [Liu et al., 2017]. Nanocarriers that are composed of QDs with chemotherapeutic drug loadings have also been developed. Olerile et al., encapsulated paclitaxel along with CdTe/CdS/ZnS QDs in nanostructured lipid carriers with 77% tumor growth inhibition rate [Olerile et al., 2017]. PDT also has been extensively studied by using QDs [Samia et al., 2003, Park et al., 2012, Yong et al., 2015]. CdSe and CdTe QDs and carbon-based nanoparticles have been studied for PDT applications as either QDs alone, QDs with PS molecules, or QDs with PS molecules conjugations [Park et al., 2012, Juzenas et al., 2008, Choi et al., 2014]. However, most of the NIR emitting QDs contained heavy metals such

as Pb, Hg, and Cd which resulted in leaching of these heavy metals to cells leading to high cytotoxicity. Therefore, research was directed to the development of heavy-metal free QDs over the past decades. Ag_2S QDs with strong emission in the NIR-region with high biocompatibility have been of interest. Yang et al., developed Ag_2S QDs for in vivo elimination of tumor with fluorescence/photoacoustics imaging and photothermal tumor ablation [Yang et al., 2017]. These QDs have the ability to be used in PTT applications due to the surface plasmon resonance (SPR) effect. Gao et al., synthesized NIR-emitting Ag_2S QDs coated with GSH for photothermal therapy and monitoring the therapeutic effect for effective cancer treatment.[Gao et al., 2021] Ag_2S nanoparticles-decorated WS_2 system has been utilized for the treatment of bacterial infections caused by Staphylococcus aureus and Escherichia coli with the synergistic effect of photocatalytic and photothermal properties of QDs. The authors achieved 99.93% and 99.84% antibacterial efficacy against S.aureus and E.coli with 20 min NIR light irradiation, respectively [Lin et al., 2019]. Du et al., constructed a composite system composed of Ag_2S QDs with $mSiO_2$ hydrogel by free radical polymerization to achieve antibacterial activitiy. They observed 99.7% and 99.8% inhibition rates against E. coli and methicillin-resistant S.aureus (MRSA) with irradiation at NIR region, respectively [Du et al., 2022].

In the third chapter of the thesis, image-guided antimicrobial PTT&PDT applications of ALA-loaded NAC-Ag_2S QDs was studied against gram-positive and gram-negative bacteria at 640 nm laser irradiation. The photothermal potential of NAC-QDs was investigated at 640 nm wavelength. Significant growth inhibition rates were achieved against gram-negative bacteria, *Pseudomonas aeruginosa* (*P.aeruginosa*), with ALA-loaded QDs. Biofilms were imaged at NIR region. Finally, PpIX formation and ROS production were measured.

Chapter 2

ENHANCED ANTIMICROBIAL PDT OF 5-ALA IN COMBINATION WITH ANTIMICROBIAL PTT USING SPIONS

2.1 Abstract

Due to the limitations of efficient treatment of drug-resistant bacterial infections, new alternatives to antibiotics have been of interest. Here, we propose the combination of antimicrobial photodynamic therapy prodrug, 5-aminolevulinic acid (5-ALA), with carrier and antimicrobial photothermal superparamagnetic iron oxide nanoparticles, SPIONs, for enhanced dual therapy of bacterial infections. Antibacterial activity experiments demonstrated that the combination of ALA with SPIONs showed successful antimicrobial efficacy against both gram-positive and gram-negative bacteria. The use of low and clinically safe doses of 2 mM ALA in combination with SPIONs (with 600 µg/ml Fe) completely inhibited *P.aeruginosa* planktonic cells under dual laser (640 nm + 808 nm) irradiation for 10 minutes. ALA-SPION caused via SPIONs, 10 and 13-log inhibition within *S.epidermidis* and *P.aeruginosa* biofilms, respectively. To our knowledge, this is the first study that has combined aPDT effect of ALA with aPTT effect of SPIONs under dual laser irradiation. Successful antibacterial and antibiofilm activity achieved with combined aPDT and aPTT of ALA-SPION, may initiate an alternative treatment option for drug resistant biofilm related infections bacteria and their related infections.

2.2 Introduction

Multidrug resistance (MDR) of bacteria has become significantly important in the treatment of patients especially with biofilm related infections. Due to adher-

ence on various surfaces such as catheters or implants and embedded protection of bacteria within exopolysaccharide matrix of biofilms, penetration of antimicrobial drugs through the biofilm and thus efficient elimination of bacteria is highly limited [Costerton et al., 1987]. One of the common cause of implant-related infections as well as wound infections is staphylococci[Rogers et al., 2009, Sievert et al., 2013]. Increased and inappropriate use of antibiotics has resulted in elevated number of infections caused by methicillin resistant *Staphylococcus epidermidis* which hardens both the infection treatment and usage of medical devices such as implants and catheters[Campoccia et al., 2010, Tan et al., 2012]. Another MDR pathogen commonly causing biofilm-related infections is *Pseudomonas aeruginosa* which can lead to nosocomial infections as well as chronic lung infections in cystic fibrosis (CF) patients [Langton Hewer and Smyth, 2014, Gibson et al., 2003]. Treatment of *P.aeruginosa* infections still remains challenging because of its number of different resistance mechanisms [Yero et al., 2021, Breidenstein et al., 2011]. Increased antibiotic resistance rate of biofilms due to limited penetration of drugs as well as various acquired resistance mechanisms, current antibiotics are not efficient anymore and developing alternative treatments is critical [Mah and O'Toole, 2001, Donlan and Costerton, 2002].

Antimicrobial photodynamic therapy (aPDT) has become an alternative non-invasive strategy against MDR bacteria both in vitro and in vivo [Merchat et al., 1996, Zolfaghari et al., 2009, Dai et al.,]. Main mechanism of PDT is based on utilization of a photosensitizer (PS), appropriate light source and presence of molecular oxygen in the environment. Administration of PS, subsequent uptake and accumulation of PS by cells is followed by irradiation at a specific wavelength. Light energy causes excitation of PS molecule from ground state to the excited triplet state and this energy is later transferred to the substances in the environment via two oxidative mechanisms: type I and type II. In type I oxidative mechanism, electron transfer occurs between this excited triplet state PS and substances and generates radical species which further react with molecular oxygen to yield reactive oxygen species. In type II oxidative mechanism, energy transfer occurs between excited triplet state PS and an acceptor, mainly molecular oxygen, and leads to the formation of singlet

oxygen (1O2) which in turn attacks surrounding biomolecules such as DNA, RNA, amino acids and lipids [Ochsner, 1997]. Several studies reported antimicrobial efficiency of different photosensitizers against gram-negative and gram-positive bacteria [Vera et al., , Mantareva et al., 2011, Sbarra et al., 2008].

Photoinactivation of bacterial species by using 5-ALA has been of interest recently[Liu et al., 2016, Huang et al., 2019, Lin et al., 2021, Sajjad et al., 2021]. 5-aminolevulinic acid (ALA) is an intermediate agent in the heme biosynthetic pathway of both prokaryotic and eukaryotic cells. This prodrug compound itself does not have any photosensitizing properties, but it is converted into photoactive PpIX during heme cycle in cells[Phillips, 2019]. ALA is clinically approved for PDT applications and fluorescence-based diagnosis of different types of cancers due to the rapid metabolism of the fluorescent PpIX in the tumor cells. Nonetheless, the highly hydrophilic nature of ALA decreases the blood-circulation time, increases rapid clearance from body and decreases penetration through lipid bilayer of cell membrane [Novo et al., 1996, Kelty et al., 2002]. Hence, different derivatives of ALA with improved bioavailability as well as lipophilicity via esterification, their peptide esters, and dendritic and liposomal formulations have been utilized recently [Giuntini et al., 2009, Venosa et al., 2009, Sangtani et al., 2018].

Besides the applications of PDT, photothermal therapy (PTT) is also utilized for phototherapeutics [Castillo-Martínez et al., 2015, Ng and Zheng, 2015, Jung et al., 2018, Xu et al., 2019]. Upon light irradiation, photosensitive thermal agents generate an increase in the local temperature via nonradiative transitions. PTT is applicable for biofilm-related infections as the local temperature increase enhances penetration of therapeutic agents into the biofilm in addition to the disruption of the biofilm matrix through thermal ablation [Ibelli et al., 2018]. However, control of the local temperature increase and resistance of some bacterial strains to high temperature have been challenging problems [Nguyen et al., 2016]. To overcome such challenges, studies were directed to the utilization of both photodynamic and photothermal therapy[Wang et al., 2019, Peng et al., 2020].

Inorganic nanoparticles have been used in photothermal therapy [Wang et al., 2013, Chai et al., , Chen et al., 2017]. Superparamagnetic iron oxide nanoparticles

(SPIONs) have been recognized as PTT agents under NIR laser irradiation [Chu et al., 2013, Zhou et al., 2014]. Our group has shown the combined PDT-PTT potential of ICG loaded 3-aminopropyltrimethoysilane (APTMS) coated SPIONs on three clinically important biofilm producing gram-negative bacteria (Klebsiella pneumoniae, Escherichia coli, *Pseudomonas aeruginosa*) and one gram-positive, strong biofilm producing bacteria, *Staphylococcus epidermidis* by irradiating at a single wavelength (795 nm) which resulted in the total inhibition of planktonic cells of all bacteria strains [Bilici et al., 2020].

In this study, we investigated the antibacterial and antibiofilm activity of free ALA, PAA@SPIONs and ALA-PAA@SPIONs against gram-negative *P.aeruginosa* and gram-positive *S.epidermidis*, with and without laser irradiation. 640 nm, 808 nm and dual irradiation (640 nm + 808 nm) were applied at clinically safe laser powers (300 mW, 1000 mW and 300&1000 mW, respectively) for a short time duration (10 minutes). Herein, we report successful delivery of ALA into bacterial cells with enhanced aPDT in combination with aPTT effect of SPIONs. The use of low and clinically safe doses of 2 mM ALA with 600 µg/ml Fe completely inhibited *P.aeruginosa* planktonic cells under dual laser (640 nm + 808 nm) irradiation for 10 minutes. When ALA was delivered to biofilms via SPIONs, growth inhibition of biofilms of *S.epidermidis* and *P.aeruginosa* were 10-log and 13-log, respectively. To our knowledge, this is the first study that combines aPDT effect of 5-ALA with aPTT against planktonic cells and biofilms of gram-positive and gram-negative bacterial strains. This combination may become an alternative treatment against drug-resistant bacteria with broad-spectrum application.

2.3 Materials and Methods

2.3.1 Synthesis of Poly(acrylic Acid) Coated SPIONs

The coprecipitation method was utilized to synthesize poly(acrylic acid) coated SPIONs. Fe3+/Fe2+ was initially dissolved in deoxygenated water at a mole ratio of 2/1 using the iron salts FeCl36H2O and FeCl24H2O. PAA (1.2 g) was added while receiving constant nitrogen flow. 9.26 mL of 4.5 M NH4OH was introduced while

the suspension was being stirred vigorously at 85 °C. After being kept at this temperature for an hour, the solution was allowed to cool to room temperature. The solution was kept overnight on a magnet to remove any precipitated particles. Finally, NPs were stored at room temperature after being washed many times with DI water using Vivaspin 20 centrifugal filters (10 kDa MW cutoff).

2.3.2 ALA Loading on SPIONs

Dropwise additions of ALA (7 mg/ml) were introduced to the NPs solution (39.4 mg/ml), and the mixture was then stirred at 750 rpm for two hours at room temperature. Isothermal titration calorimetry was used to confirm the presence of electrostatic loading (Affinity ITC, USA). PAA@SPIONs (1 mL, 1 mg/mL in water) were titrated with ALA (total of 250 µgl from 5 mg/mL in water) at the rate of 5 µgL/s at 25°C. Complete electrostatic binding of ALA to PAA@SPIONs was verified by the strong binding exotherms throughout the titration. Therefore, no washing was done following the electrostatic loading of the ALA. The solution was kept at +4°C.

2.3.3 Characterization

UV-VIS-NIR spectrophotometer (Shimadzu) was used to measure absorbance. The hydrodynamic size and surface charge of nanoparticles were calculated using a Zetasizer from Malvern (NanoZS). To determine the iron content of nanoparticles, an inductively coupled plasma-mass spectrometer (Agilent 7700X ICP-MS) was employed. For the ICP-MS measurements, samples were etched with nitric acid (65% concentration) and sulfuric acid (96% concentration). A thermogravimetric analyzer was used to determine SPION's organic content (TGA, TGA 500). Under a nitrogen environment, samples were heated at a rate of 10°C min-1 from ambient temperature to 1000 °C.

2.3.4 Laser Irradiation of Aqueous Solutions

The temperature increase of aqueous solutions of PAA@SPIONs and aqueous colloidal ALA-PAA@SPION solutions was measured at 200, 600 and 1000 µg/ml Fe

concentration using 640nm laser irradiation with 200 mW laser power for 20 minutes.

2.3.5 Cell Culture

Healthy mouse fibroblast L929 cells were grown in DMEM media containing 10% fetal bovine serum and 1% streptomycin at 37 °C in a humidified incubator with 5% CO2.

2.3.6 Dark Toxicity

On L929 cells, the conventional MTT test was used to determine the dose-dependent toxicity of free ALA, PAA@SPION, and ALA-PAA@SPION at concentrations of 21-336 *simicrogram* ALA/mL or 37.5-600 *simicrogram* Fe/mL. In 96 well plates, cells were seeded at a density of 1x104 cells per well, and the plates were then incubated for 24 hours. After 24 hours of incubation with free ALA, SPIONs, and ALA-SPIONs in fresh culture medium, the medium was changed with 50 simicrograms/mL of MTT solution (5 mg/mL in PBS) and 150 simicrograms/mL of fresh medium. Purple formazan crystals produced by the live cells were dissolved using DMSO:ethanol (1:1 v/v) after 4 hours of incubation. A microplate reader (Synergy H1 Biotek Instruments) read the absorbance at 600 nm with a reference reading at 630 nm. The relative cell viability was calculated using the formula below:

Cell viability (%) = [Absorbance sample / Absorbance control] × 100 (n=3)

2.3.7 Antimicrobial activity and antibiofilm assays

Bacterial isolates

Pseudomonas aeruginosa ATCC® 700829™ and *Staphylococcus epidermidis* ATCC® 35984™ were used in the experiments.

Antibacterial activity on planktonic bacteria

A single colony of bacteria from overnight cultures was inoculated in Tryptic Soy Broth (TSB, BD™ Bacto™) and incubated overnight at 37 °C–135 rpm. A final concentration of 84 µg ml1 ALA/150 µg Fe per mL and 336 µg ml1 ALA/600 µg

Fe per mL of ALA, PAA@SPIONs, and ALA-PAA@SPIONs were added to the cell suspension. For control culture, TSB was added. Overnight, cultures were incubated at 37 °C. Colony counting following sequential 10-fold dilutions was used to evaluate bacterial survival. Significant inhibition was defined as a mean CFU/ml growth reduction of at least 2-log (99%). All studies were performed in triplicate.

Anti-biofilm activity

Merritt et al. technique was used to create biofilms in 96-well plates [**?**]. After carefully removing the media from the wells, fresh TSB-glucose, ALA, SPIONs, or ALA-SPIONs were added at a dose of 336 µg ml1 ALA and 600 µg Fe per mL dose. Colony counting was used to determine the bacteria's survival after an overnight incubation at 37 °C. Significant inhibition was defined as a mean CFU/ml value reduction of at least 2-log. All studies were performed with three replicates.

2.3.8 Laser Treatment of Bacteria

Planktonic bacteria and biofilms grown in well-plates were irradiated with laser light at wavelengths of 640 nm, 808 nm, and dual laser (640 nm 808 nm) with output laser powers of 300 mW, 1000 mW, and 300 mW 1000 mW for 10 minutes, respectively. Planktonic cells and biofilms were incubated at 37 °C overnight following laser treatment, and the survival rates were assessed using the same procedure as described above.

2.3.9 PpIX Detection

Qualitative analysis

The in vitro imaging of biofilms was performed using LEICA Live Cell Microscope at 20x magnification. Biofilms were fixed with 3.5% formaldehyde and mounted with DAPI (Mounting Medium with DAPI – Aqueous, Fluoroshield (ab104139)). PpIX was observed at a wavelength of 630 nm for emission and 590 nm for excitation.

Quantitative analysis

Planktonic bacteria were cultured and treated overnight with free ALA, only nanoparticles, and ALA-loaded nanoparticles. Each well's fluorescence was measured at 635 nm using a Synergy H1 microplate reader (Biotek) after an overnight incubation at 37 °C. The control group consisted of untreated cells.

2.3.10 Uptake of Nanoparticles

By measuring the Fe content in the NPs-treated biofilms, the quantitative analysis of NPs uptake was carried out. As previously noted, biofilms were grown for 24 hours at 37 °C. Next day, biofilms were treated with NPs at 600 g/mL [Fe] for overnight. The biofilms were then collected and washed with PBS to eliminate uninternalized NPs. Fe content was measured by (ICP-MS) (n = 3) after cells were digested with acid (HNO3/H2SO4: 9/1 v/v) for approximately 1 week at room temperature.

2.3.11 Statistical Analysis

For statistical analysis, a one-way ANOVA test was used by Graphpad Prism Software (Graphpad Prism8). Free ALA and ALA-SPIONs were compared with SPIONs in terms of bacterial growth reduction and growth reduction was considered as statistically significant if $p \leq 0.05$.

2.4 Results

2.4.1 Synthesis and Characterization of Nanoparticles

Anionic SPIONs were synthesized as described above. These nanoparticles have number-based hydrodynamic sizes of 12.39 nm and a zeta potential of -15.6 mV in PBS (Table 1).

PAA content of PAA-SPIONs was detected using TGA analysis under inert atmosphere (Fig. 2.1). These nanoparticles showed broad absorption in the UV-visible range of absorbance spectrum (Fig. 2.1).

Sample Name	Hydrodynamic Size (nm)	Zeta Potential (mV)
PAA@SPIONs	12.39	-15.6
ALA-PAA@SPIONs	12.44	-22.5

Table 2.1: Dynamic Light Scattering (DLS) Results of Nanoparticles.

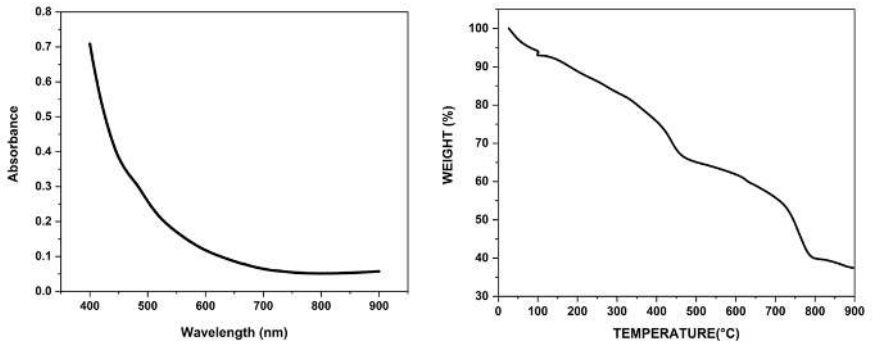

Figure 2.1: UV absorbance and TGA analysis of nanoparticles.

Zwitterionic ALA was loaded to these anionic SPIONs via electrostatic interaction. The pKa values of the two major amine and carboxylic acid groups in ALA are 4.05 and 8.9, respectively. Since ALA has a zwitterionic character between pH 7.2 and 7.4, electrostatic loading of ALA onto anionic SPIONs may be possible. This is made possible by the electrostatic contact between the COO(-) group of the SPIONs and the NH3(+) group of ALA. This electrostatic loading resulted in the slight decrease of zeta potential of nanoparticles from -15.6 to -22.5 mV with almost no dramatic increase in the number-based hydrodynamic sizes of nanoparticles from 12.39 to 12.44 nm. ITC has been used to study the interaction between ALA and the SPIONs. When SPIONs were titrated at pH 7.2 with ALA dissolved in dI water, an exotherm was produced, which is a sign of electrostatic binding (Fig. 2.2). With the addition of ALA, the exotherm consistently reduced until it nearly approached a constant value. This shows that at the investigated concentrations, ALA completely

binds to SPIONs.

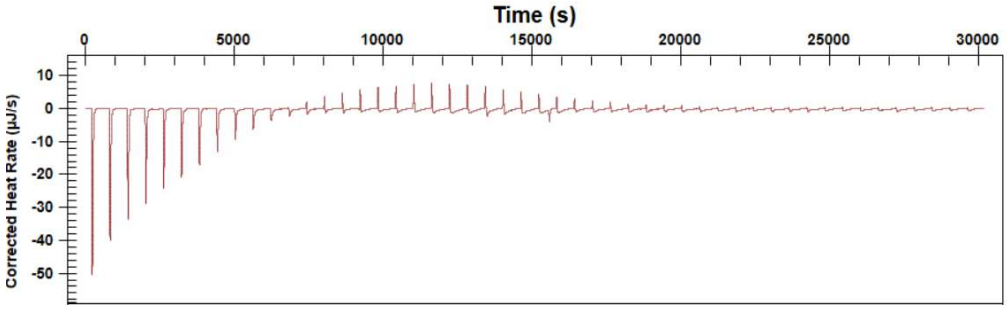

Figure 2.2: ITC Result.

2.4.2 Temperature Increase in Aqueous Solutions with 640 nm Irradiation

The photothermal effect of PAA@SPIONs was tested in aqueous solutions with respect to different Fe concentrations with 200 mW laser power at 640 nm irradiation. The temperature rise in the colloidal solutions increased with the Fe concentration. After 20 min laser irradiation at 200, 600 and 1000 µg/ml Fe concentrations, T was 3.93, 7.76 and 9.09C, respectively (Fig. 2.3).

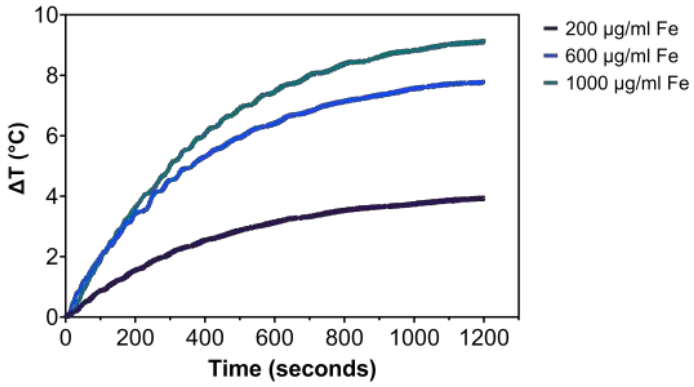

Figure 2.3: Time dependent change in the temperature of PAA@SPION solutions at different Fe concentrations irradiated at 200 mW. Excitation wavelength = 640 nm

Three cycles of laser on/off experiments were performed, and the temperature increase in three cycles was same which shows stability and reusability of SPIONs with repetitive laser irradiation (Fig. 2.4).

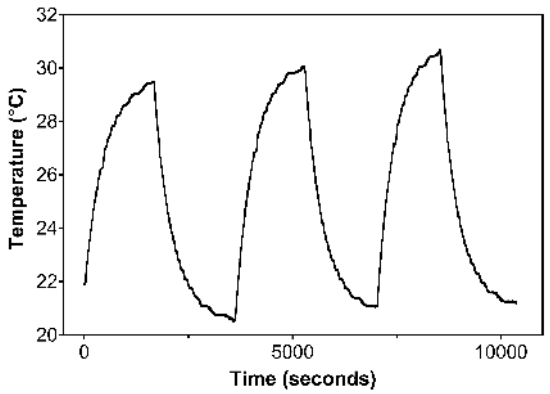

Figure 2.4: After laser on (20 min)/off (20 min) cycles (600 ug/mL, 200 mW). Excitation wavelength = 640 nm.

The photothermal conversion efficiency of the PAA@SPIONs at 600 ug/ml Fe concentration was determined as 89.73% by using the equation derived by Roper et al [Roper et al., 2007].

2.4.3 Antibacterial Activity

Dose dependent growth inhibition of ALA-SPIONs ([Fe]:150 and 600 µg/ml, [ALA]):84 and 336 µg/ml, respectively) with (640 nm, 808 nm and dual irradiation of 640&808 nm at 300 mW, 1000 mW and 300&1000 mW laser powers, respectively, for 10 minutes) and without laser irradiation were evaluated on planktonic cells of *S.epidermidis* and *P.aeruginosa*.

No significant inhibition was observed on *S.epidermidis* planktonic cells when cells were treated with free ALA, SPIONs and ALA-SPIONs without laser irradiation for each applied dose (Fig. 2.5). 640 nm laser irradiation did not cause any significant increase in the growth inhibition of *S.epidermidis* planktonic cells when cells were incubated with free ALA. Neither of the laser irradiations at the dose of 150 µg/ml Fe containing SPIONs did not cause any significant increase in the growth inhibition of *S.epidermidis* planktonic cells. ALA loading onto SPIONs at the same dose (150 µg/ml Fe) increased growth inhibition of *S.epidermidis* planktonic cells by 2-log at 640 nm laser irradiation. When *S.epidermidis* planktonic cells were incubated with 600 ug/ml Fe containing nanoparticles, 2-log growth inhibition

was observed for both 640 nm and 808 nm laser irradiations while 3-log growth inhibition was observed for the dual laser irradiation. ALA loading onto SPIONs at the same dose (600 µg/ml Fe) did not increase growth inhibition at 640 nm and 808 nm laser irradiation. However, ALA loading onto SPIONs at the dose of 600 µg/ml Fe increased the growth inhibition to 4-log in *S.epidermidis* planktonic cells with dual laser irradiation. Mean CFU/ml for control (without nanoparticle and laser) was found to be 6.73 10^{10} CFU/ml for *S.epidermidis*.

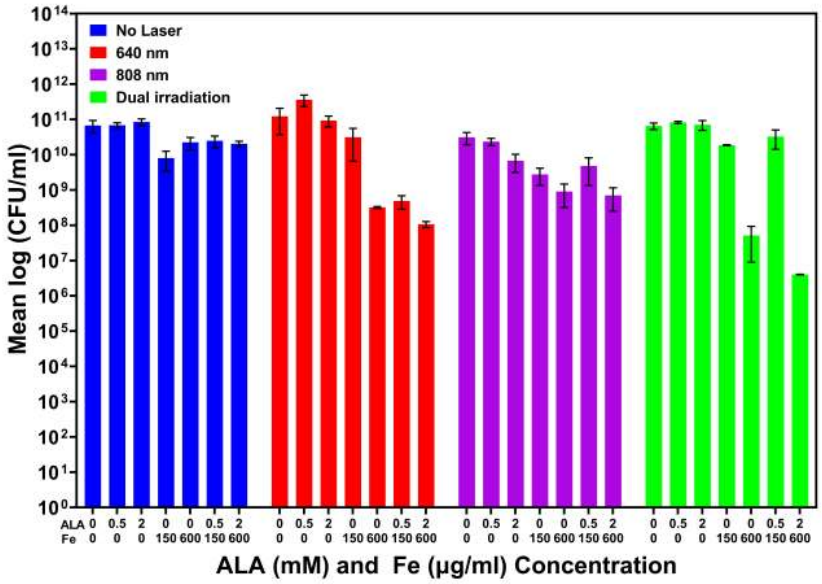

Figure 2.5: Effect of free ALA, only SPIONs, and ALA-SPIONs on the growth inhibition of planktonic cells of *S.epidermidis* were measured both with and without laser irradiation. Control: No substances were applied to planktonic cells. 640 nm, 808 nm, and dual laser irradiation at 300 mW, 1000 mW, and 300 mW 1000 mW for 10 minutes, respectively, were used in all laser experiments.

No significant inhibition was observed on *P.aeruginosa* planktonic cells when cells were treated with free ALA, SPIONs and ALA-SPIONs without laser irradiation for each applied dose (Fig. 2.7). Two different doses of free ALA caused 3-log growth inhibition in the *P.aeruginosa* planktonic cells with 640 nm laser irradiation while there was no significant increase in the growth inhibition of cells with 808 nm and dual laser irradition applications. 150 µg/ml Fe containing SPIONs caused 3-log reduction under application of 640 nm and dual laser irradiation where 808 nm

laser irradiation did not cause any significant increase in the growth inhibition of *P.aeruginosa* planktonic cells. ALA loading onto nanoparticles at the dose of 150 µg/ml Fe also caused 3-log growth inhibition when cells were irradiated with 640 nm laser application however 5-log growth inhibition was observed when cells were irradiated with dual laser application. 600 µg/ml Fe containing SPIONs caused 3-log, 4-log and 6-log growth inhibition in the *P.aeruginosa* planktonic cells with 640 nm, 808 nm and dual laser irradiation, respectively. When cells were incubated with ALA loaded nanoparticles at the same dose (600 µg/ml Fe), complete growth inhibition was observed for dual laser application in the *P.aeruginosa* planktonic cells. Mean CFU/ml for control (without nanoparticle and laser) was found to be 6.47 x 10^{10} CFU/ml for *P.aeruginosa* For biofilm applications only one dose (ALA:336, Fe:600 µg/ml) was chosen to apply both bacterial strains.

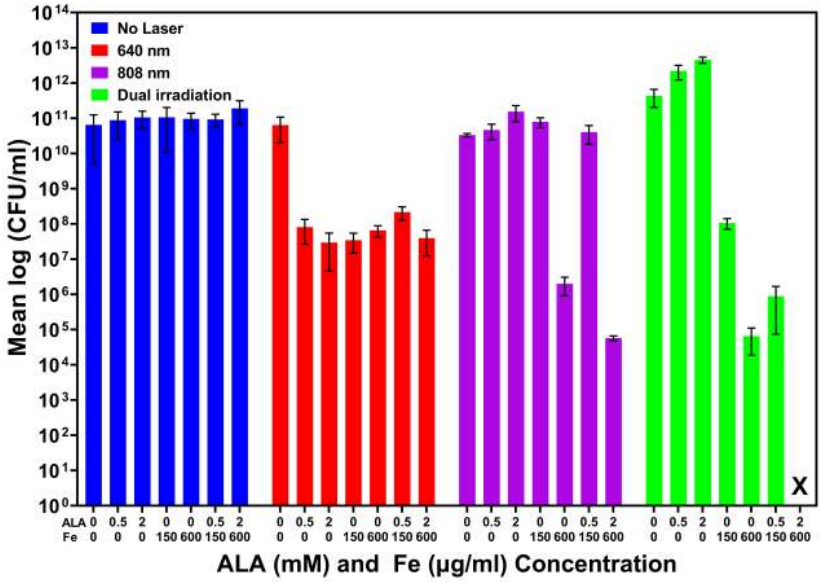

Figure 2.6: Effect of free ALA, only SPIONs, and ALA-SPIONs on the growth inhibition of planktonic cells of *P.aeruginosa* were measured both with and without laser irradiation. Control: No substances were applied to planktonic cells. 640 nm, 808 nm, and dual laser irradiation at 300 mW, 1000 mW, and 300 mW 1000 mW for 10 minutes, respectively, were used in all laser experiments.

2.4.4 Antibiofilm Bacterial Activity

Biofilm inhibition were evaluated by using free ALA, SPIONs and ALA-SPIONs (ALA:336, Fe:600 µg/ml) with (640 nm, 808 nm and dual irradiation, at 300 mW, 1000 mW and 300&1000 mW laser powers, respectively, for 10 min) and without laser irradiation on *S.epidermidis* and *P.aeruginosa*.

No significant inhibition was observed on *S.epidermidis* biofilms that were treated with free ALA, only SPIONs and ALA-SPIONs without laser irradiation for applied dose (Fig. 2.7). Free ALA caused no statistical inhibition on *S.epidermidis* biofilms even under applications of 640 nm, 808 nm and dual laser irradiations. Only SPIONs caused 3-log inhibition on *S.epidermidis* biofilms for all laser applications. While ALA loading onto SPIONs caused 5-log inhibition for 640 nm and 808 nm laser irradiations, 10-log inhibition was observed for dual laser irradiation on *S.epidermidis* biofilms. Mean CFU/ml for control (without nanoparticle and laser) was found to be 3.06 10^{15} CFU/ml for *S.epidermidis*

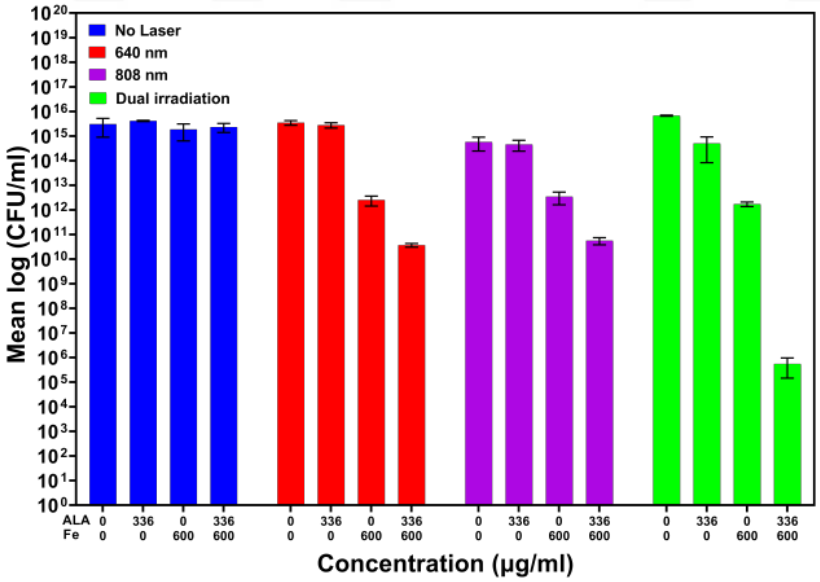

Figure 2.7: Effect of free ALA, only SPIONs, and ALA-SPIONs on the growth inhibition of *S.epidermidis* biofilms were measured both with and without laser irradiation. Control: No substances were applied to planktonic cells. 640 nm, 808 nm, and dual laser irradiation at 300 mW, 1000 mW, and 300 mW 1000 mW for 10 minutes, respectively, were used in all laser experiments.

No significant inhibition was observed on *P.aeruginosa* biofilms that were treated with free ALA, SPIONs and ALA-SPIONs without laser irradiation for applied dose (Fig. 2.8). Free ALA caused 1-log and 3-log inhibition on *P.aeruginosa* biofilms with 640 nm and dual laser irradiation, respectively. No significant inhibition was observed on *P.aeruginosa* biofilms that were treated with free ALA at 808 nm laser irradiation. SPIONs showed 3-log, 11-log and 10-log reduction on *P.aeruginosa* biofilms with laser irradiation at 640 nm, 808 nm and dual irradiation, respectively. ALA loading onto SPIONs increased inhibition of *P.aeruginosa* biofilms at all laser applications. 8-log inhibition on *P.aeruginosa* biofilms was observed with laser irradiation at 640 nm while 13-log inhibition was observed for both 808 nm and dual laser irradiation. Mean CFU/ml for control (without nanoparticle and laser) was found to be 3.06 x 10^{15} CFU/ml for *P.aeruginosa*.

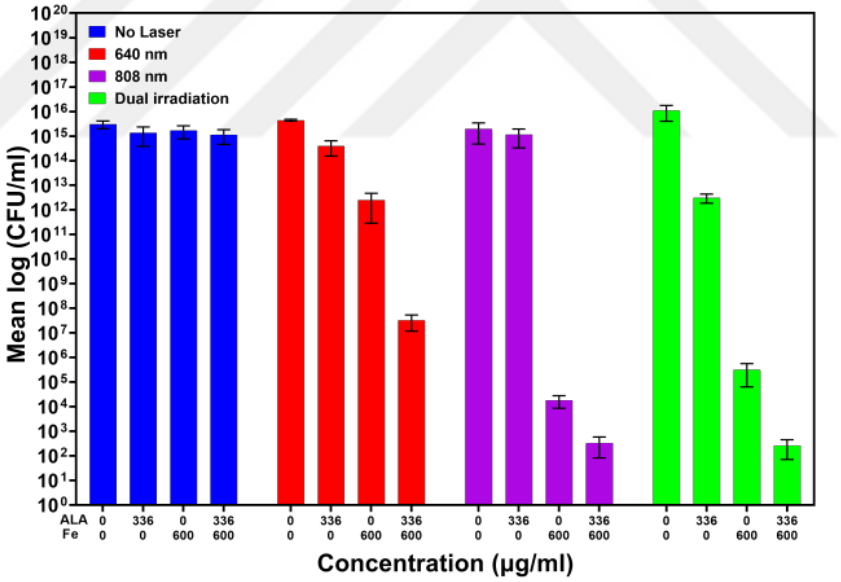

Figure 2.8: Effect of free ALA, only SPIONs, and ALA-SPIONs on the growth inhibition of *P.aeruginosa* biofilms were measured both with and without laser irradiation. Control: No substances were applied to planktonic cells. 640 nm, 808 nm, and dual laser irradiation at 300 mW, 1000 mW, and 300 mW 1000 mW for 10 minutes, respectively, were used in all laser experiments.

2.4.5 In vitro Uptake of Nanoparticles

To quantify the uptake of nanoparticles by biofilms of both bacteria, the concentration of Fe in the nanoparticle-treated biofilms was determined by ICP-MS. After overnight incubation with nanoparticles (600 µg/mL Fe), about 2.88% of SPIONs and 3% of ALA-SPIONs were internalized by biofilms of *P.aeruginosa* according to the ICP-MS analysis of the lysed biofilms with no significant difference between them. About 50% of SPIONs and 43% of ALA-SPIONs were internalized by biofilms of *S.epidermidis* according to the ICP-MS analysis of the lysed biofilms (Fig. 2.9).

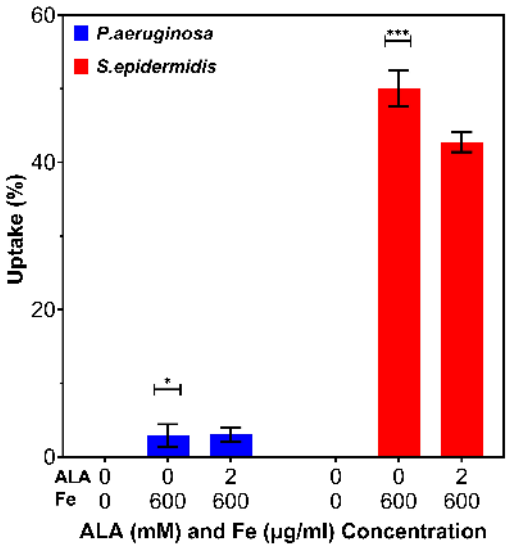

Figure 2.9: Intracellular quantification of SPIONs and ALA-SPIONs in *P.aeruginosa* and *S.epidermidis* biofilms.

2.4.6 PpIX Detection

Conversion of ALA into PpIX was quantitatively measured with fluorescence intensity of PpIX via its emission at 635 nm. Incubation of *P.aeruginosa* planktonic cells with 84 µg/ml free ALA resulted in the 60% increase of PpIX generation while 336 µg/ml free ALA resulted in 104% increase of PpIX generation inside the cells. When 84 and 336 µg/ml ALA was delivered into *P.aeruginosa* planktonic cells with nanoparticles, 117% and 185% increase in PpIX generation was observed, respec-

tively (Fig. 2.10). For *S.epidermidis*, incubation of planktonic cells with 84 and

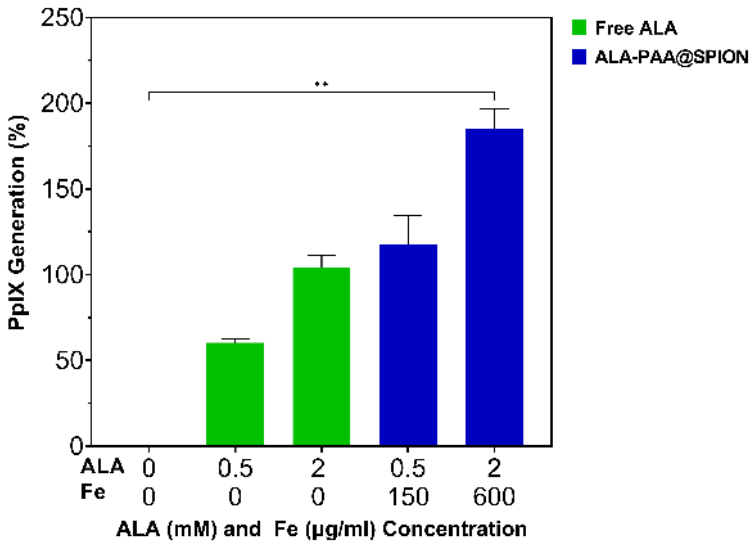

Figure 2.10: Intracellular formation of PpIX through administration of free ALA and ALA-PAA@SPION after overnight incubation. (PpIX: exc: 405 nm and em: 635 nm) *P.aeruginosa* planktonic cells.

336 µg/ml free ALA resulted in 26% and 105% increase of PpIX generation inside the cells, respectively. Delivery of 84 and 336 µg/ml ALA into the *S.epidermidis* planktonic cells resulted in 63% and 216% increase of PpIX generation, respectively (Fig. 2.11). Qualitative determination of PpIX inside *P.aeruginosa* biofilms was monitored with fluorescence microscopy using PpIX emission at 630 nm. After incubation of biofilms were incubated with 84 µg/ml free ALA, no PpIX emission was observed, however, delivery of ALA at the same concentration with SPIONs resulted in bright PpIX emission in biofilms (Fig. 2.12).

2.4.7 Photothermal Screening During Laser Treatment

A thermal camera was used to record the temperature increase during laser irradiation of Textit Textit P. aeruginosa biofilms treated with free ALA, only nanoparticles, and ALA loaded nanoparticles ([Fe]: 600 simicrogram/ml, [ALA]): 336 simicrogram/ml. Cells without laser treatment were used as control and the temperature increase of laser treated cells with respect to the control.

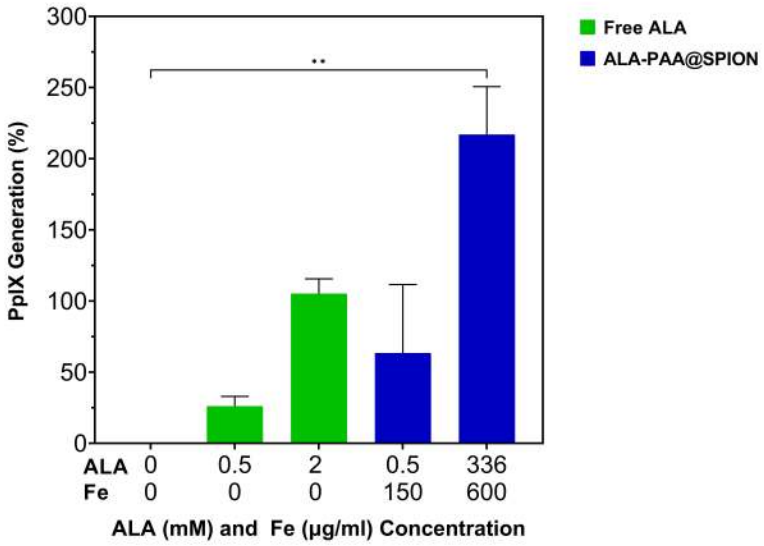

Figure 2.11: Intracellular formation of PpIX through administration of free ALA and ALA-SPIONs after overnight incubation. (PpIX: exc: 405 nm and em: 635 nm) S.aeruginosa planktonic cells.

640 nm laser application did not cause any temperature increase in control group and free ALA treated group however it resulted in 2.5 °C temperature increase in biofilms that were treated with SPIONs and ALA-SPIONs. 808 nm laser application resulted in 1.7 and 2.23°C temperature increase in control group and free ALA treated group, respectively. 8.16 and 8°C temperature increase were observed for biofilms treated with SPIONs and ALA-SPIONs at 808 nm laser irradiation, respectively. Dual irradiation resulted in 2.1 and 3.6°C temperature increase in control group and free ALA treated group while the highest temperature increase, 10.2°C was observed for biofilms that were treated with SPIONs. Biofilms that were treated with ALA-SPIONs showed 9.3 °C temperature increase with dual laser irradiation.

2.5 Discussion

The present study demonstrated the possibility of combined antimicrobial photodynamic and photothermal therapy on gram-positive and gram-negative bacteria after incubation with free ALA, SPIONs and ALA-SPIONs. 640 nm (300 mW), 808 nm (1000 mW) and dual laser irradiation (300&1000 mW) were applied for 10

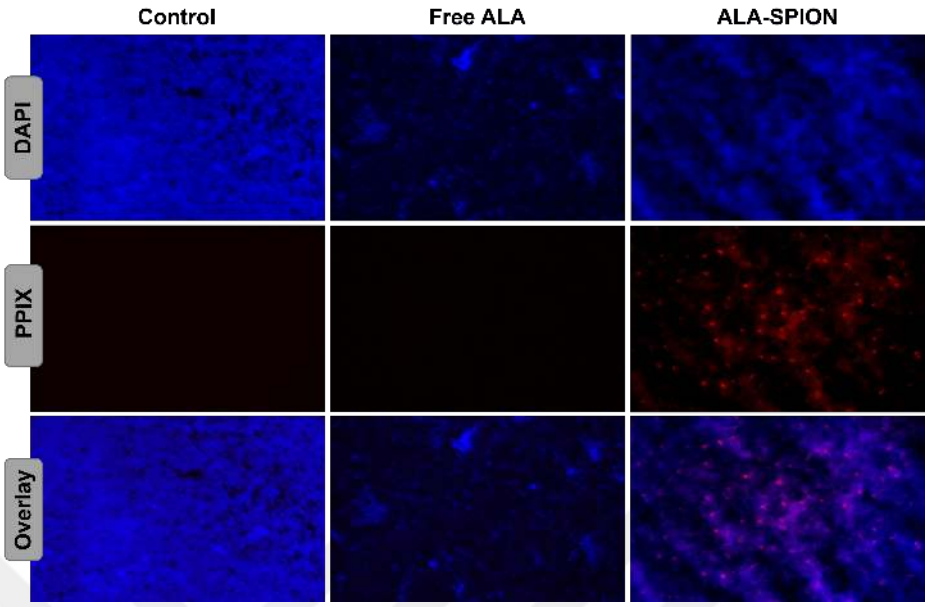

Figure 2.12: Fluorescence microscopy images of P. aeruginosa biofilm at 20X magnification. Blue: Bacteria stained with DAPI, Red: PPIX Fluorescence. LEICA Live Cell Microscope, DAPI Filter Ex:365, Em:465, Alexa 610 Filter Ex:590, Em:630.

minutes both against planktonic cells and biofilms. *S.epidermidis* and *P.aeruginosa* were selected due to their strong biofilm producing capacity and thus causing infections hard to treat. Their different cell wall structure properties resulted in different trends in particle internalization and thus killing activity showed differences with dual therapy.

There was no significant growth inhibition with any of the compound in the absence of laser irradiation which indicates no dark toxicity. Photothermal activity of SPIONs at only 640 and 808 nm wavelengths caused 3- and 4-log growth inhibition for *P.aeruginosa* planktonic cells at 600 ug/ml Fe dose, respectively. 2 mM ALA loading onto SPIONs and synergistic effect of dual laser irradiation resulted in complete eradication of *P.aeruginosa* planktonic cells. Synergistic effect was also observed for *S.epidermidis* planktonic cells. When *S.epidermidis* cells were incubated with 2 mM ALA loaded nanoparticles, 2-log growth inhibiton was observed for both only 640 and 808 nm laser irradiations while 4-log growth inhibition was observed for dual irradiation. In a similar study, In order to eliminate *E. coli* and *S. aureus*, Jeong et al. developed an iron oxide nanoparticle system made up of poly(3,4-

ethylenedioxythiophene) (PEDOT) and catechol-conjugated poly(vinylpyrrolidone) sulfobetaines-coated Fe3O4 NPs (Fe3O4@C-PVPs).[Jeong et al., 2015]. Nanoparticles containing 1 mg of Fe3O4@C-PVPS:PEDOT resulted in 100% killing in 5 min laser irradiation for both bacterial strains. In a different study, researchers coupled chlorin e6 (Ce6) with water-soluble chitosan-coated iron oxide nanoparticles to eradicate biofilms of drug-resistant bacteria *S. aureus* when exposed to a 660 nm laser at 100 mW/cm2. [Jin et al., 2022]. Combination of Ce6 with nanoparticles resulted in 9.4 log reduction in cell viability. Moreover, authors reported a heating potential of iron oxide nanoparticles with no dependence on concentration related temperature increase at 660 nm laser irradiation.

Herein, we have reported 89.73% heating efficiency of iron oxide nanoparticles with concentration dependent temperature increase under 640 nm laser application. In our study, dual laser irradiation of *P.aeruginosa* biofilms with only SPIONs resulted in 10.2 °C local temperature increase which is strong enough to provide aPTT. Staphylococci have been investigated for heat resistance and survival under thermal treatments, and the results have indicated that *S. epidermidis* can withstand a thermal treatment up to 80°C for 20 min.[Kennedy et al., 2005, Montanari et al., 2015]. We have observed lower growth inhibition rate in *S.epidermidis* compared to *P.aeruginosa* which is in line with the thermotolerance of *S.epidermidis* against heat treatments.

In the application of aPDT, photosensitizers absorb incident light and form cytotoxic reactive oxygen species which lead to oxidative damage to different components of microbial cells. ALA is a pro-drug itself and is converted into active photosensitizer PpIX when it is internalized by cells. There are studies showing that the outer membrane of gram-negative bacteria may contribute to the higher levels of resistance against ALA-based aPDT applications by inhibiting ALA uptake [**?**]. In our uptake studies, we did not observe a significant difference between uptake of SPIONs and ALA-SPIONs by *P.aeruginosa* biofilms. However, the percentages of internalized nanoparticles were 50 and 43% with only SPIONs and ALA-SPIONs in *S.epidermidis*, respectively. Moreover, gram-positive bacteria are reported to be more resistant to action mechanisms of NPs mainly because of the thick pepti-

doglycan layer which acts as a protective barrier [Cavassin et al., 2015]. Our NPs uptake finding indicated that NP internalization by *S.epidermidis* biofilm was higher compared to that of *P.aeruginosa*. It is noteworthy to mention that even though *P.aeruginosa* biofilm internalized less NPs than that of *S.epidermidis*, a significant inhibition (13-log) was observed for *P.aeruginosa* biofilms under dual laser irradiation with 2 mM ALA loaded nanoparticles. PpIX is not active at 808 nm wavelength, therefore we did not expect to see PDT effect of ALA under 808 nm laser irradiation. However, we still observed 13-log growth inhibition with 808 nm laser irradiation alone with 2 mM ALA loaded SPIONs for *P.aeruginosa* biofilms. The temperature increase in biofilms of *P.aeruginosa* with SPIONs and ALA-SPIONs were 10.2 and 9.3, respectively. Therefore, observation of similar growth inhibition rate with SPIONs and ALA-SPIONs might be related to this difference in temperature increase.

Hydrophilic nature of ALA at physiological pH reduces its penetration ability through hydrophobic barriers. Number of different ALA compounds were synthesized to improve higher levels of PpIX production inside cells [Giuntini et al., 2009, Fotinos et al., 2008, Vallinayagam et al., 2008]. Measurements of fluorescence intensity of PpIX showed that generation of PpIX was higher when ALA was delivered to the cells with nanoparticles than direct incubation of cells with free ALA. For both ALA dose (0.5 and 2 mM) loadings onto nanoparticles, almost 2 times more PpIX was generated inside the planktonic cells of *P.aeruginosa* and *S.epidermidis*.

Efficient conversion of prodrug ALA to active compound PpIX is required for ALA-based PDT therapies [Donnelly et al., 2007]. It was shown by laser scanning confocal microscopy that adsorption of nanoparticles on cell wall leads to cell wall depolarization and disintegration which alters negative charge of cell wall to become more permeable [Mukha et al., 2013]. Fluorescence intensity measurements of PpIX in planktonic cells indicated that delivery of ALA with nanocarriers resulted in higher amounts of PpIX generation in both bacteria species. Moreover, fluorescence microscopy images of biofilms of *P.aeruginosa* also demonstrated bright PpIX fluorescence in biofilms that were incubated with ALA-SPIONs. Free ALA did not give PpIX fluorescence in *P.aeruginosa* biofilm.

Biofilm formation is one of the critical protection feature of bacteria from various

antimicrobial treatment as well as the host immune responses. Increased minimum inhibitory concentration of drugs to kill the bacteria, as well as the ability to escape from host immune attack, leads to insufficient treatment and clearance of infections from the body[Stewart and William Costerton, 2001, Kristian et al., 2008]. Dual phototherapy which combines PDT and PTT can produce a higher therapeutic outcome via the synergistic effect. The combination of PTT and PDT has been extensively used to treat solid tumors [Sheng et al., 2014, Du et al., 2016, Li et al., 2016b]. Our antibiofilm activity results showed that, incubation of biofilms of *S.epidermidis* with 2 mM ALA loaded nanoparticles resulted in 5-log growth inhibition both for 640 and 808 nm laser irradiations. Under dual laser application, 10-log growth inhibition was observed for biofilms of *S.epidermidis*. This indicated the synergistic combination effect of PDT agent pro-drug,ALA, with PTT agent, SPIONs, against biofilms of *S.epidermidis*.

2.6 Conclusions

In this study, we showed increased efficiency of combined aPDT and aPTT in clinically safe doses of pro-drug ALA and low laser powers for planktonic and sessile cells of gram-positive and gram-negative bacteria. Combination therapy resulted in a higher growth inhibition rate with complete eradication of planktonic cells of *P.aeruginosa* than individual therapies. Significant growth inhibition rates were achieved for biofilms of *S.epidermidis* and *P.aeruginosa* (10-log and 13-log, respectively). Quantitative measurements of PpIX fluorescence intensity showed that pro-drug ALA was successfully delivered to planktonic cells of both bacteria and converted into the active component, PpIX. Furthermore, fluorescence images supported the enhanced delivery of ALA into *P.aeruginosa* biofilms with a bright fluorescence of PpIX recorded.

It is to our notice that this is the first study to combine ALA aPDT with SPIONs for enhanced aPDT with aPTT against both gram-positive and gram-negative bacterial species. Nanotherapeutics use different nanoparticle systems for antimicrobial approaches. It is important to emphasize that SPIONs are the only approved

nanoparticles, and they show low cytotoxicities. However, due to immune mechanisms, further in vivo studies are needed to verify enhanced combination therapy outcome of ALA with SPIONs for clinical use.

Chapter 3

NAC-AG2S QUANTUM DOTS FOR NIR-IMAGE GUIDED COMBINATION THERAPY OF ANTIMICROBIAL PDT AND PTT

3.1 Abstract

For image-guided antimicrobial PTT and PDT applications, quantum dots (QDs) with photothermal therapy (PTT) potential and loaded with the PDT drug 5-aminolevulinic acid (ALA) can be highly efficient therapeutic nanoparticles. Firstly, highly stable, small size (3 nm!!!!) and near-infrared region (NIR) emitting N-Acetyl-l-cysteine (NAC) coated QDs with peak emission at 760 nm were synthesized. The photothermal potential of NAC-QDs was investigated at 640 nm (200 mW laser power) for the first time and it was determined as 65.7%. 8-log and 6-log growth inhibition rates were achieved for *Pseudomonas aeruginosa* planktonic cells and biofilms, respectively. ALA loading onto QDs elevated both the amount of ROS production inside cells and uptake of nanoparticles by cells. These results indicate that single wavelength (640 nm) irradiation can combine antimicrobial PDT and PTT potential of QDs to overcome bacteria-related infections with image-guided approaches.

3.2 Introduction

Semiconductor nanoparticles (quantum dots [QDs]) have received great attention due to their size and shape-dependent physiochemical and biological properties that arise from quantum confinement and high surface-area-to-mass ratios[El-Sayed, 2001, Alivisatos, 1996]. Large absorption coefficient, size-tunable light emission, high quantum yield (QYs), photostability and resistance to photobleaching, and broad

excitation window with narrow emission peaks of quantum dots (QDs) make them an excellent candidate for bioimaging and biodiagnosis[Kairdolf et al., 2013]. Recently, there has been a great effort for the development of QDs with strong luminescence in the near-infrared region (NIR). Absorption and autofluorescence of tissues in the visible spectrum reduce the contrast of the image and require high amounts of signal-to-background intensity[Monici, 2005]. Water has absorbance above 900 nm which also limits optical imaging in living tissues[Matcher et al., 1994]. Therefore, the region between 650-950 nm (NIR I) is accepted as the "diagnostic window" because of the reduced autofluorescence of living tissues and deeper penetration depth[Chinnathambi and Shirahata, 2019]. In addition to bioimaging, high surface to volume ratio of QDs enables chemical conjugation and electrostatic loading of multiple therapeutic agents like chemotherapeutic drugs, targeting ligands, chemical agents for enhancement of the treatment efficacy and specificity.

Optical properties such as narrow band gap (Eg 1 eV), high absorption coefficient, emission in the NIR region and good chemical stability make Ag_2S as one of the most important metal sulfide semiconductor nanocrystal [Du et al., 2010, Duman et al., 2015, Hu et al., 2017]. Ag_2S nanocrystals were coated with a variety of substances to give them different functionalities [Yang et al., 2013, Hong et al., 2012, Chen et al., 2013, Aydemir et al., 2020, **?**]. Ag_2S quantum dots have been utilized for antibacterial applications against gram-positive and gram-negative bacteria[Bala Subramaniyan et al., 2019, Wei et al., 2022, Delgado-Beleño et al., 2018].

N-Acetyl-l-cysteine (NAC) is considered as one of the most smallest non-antibiotic drug that has anti-microbial properties[Roberts and Cole, 1981, Noszál et al., 2000]. The sulfhydryl moiety of NAC can act as a free radical scavenger via destroying disulfide bonds[Zafarullah et al., 2003, Yamada and Ogawa, 2009]. It was shown by many studies that NAC can reduce biofilm formation with a variety of bacteria[Schwandt et al., 2004, Pérez-Giraldo et al., 1997, Marchese et al., 2003]. NAC was also used in catheter lock solution for the treatment of catheter related bacterial infections[Ercan et al., 2021, Aslam et al., 2007].NAC reduced the cytotoxic effect of Ag nanoparticles at concentrations greater than their MIC value, according to research by Hamed et al. on the antibacterial effects of Ag nanoparticles combined

with NAC.[Hamed et al., 2017].

5-aminolevulinic acid (ALA) is another small molecule which has been utilized as photosensitizer (PS) for antimicrobial photodynamic therapy (aPDT) in both gram-positive and gram-negative bacteria[Hsieh et al., 2013, Huang et al., 2019, Sajjad et al., 2021]. ALA is not an active photosensitizer, but it is internalized and converted into PpIX in the heme biosynthesis pathway of cells. aPDT involves the action of PS, appropriate light source and oxygen in the environment, thus producing reactive oxygen species (ROS) to destroy cellular compartments[Vatansever et al., 2013]. However, aPDT can be limited in the treatment of gram-negative bacteria while using negatively charged PS due to the insufficient absorption of PS by bacteria [**?**]. In addition to the limitation of insufficient PS absorption, aPDT product, ROS, has a short life-time and a short diffusion distance, which affects the antibacterial efficacy of PSs[Baier et al., 2005]. Therefore, there has been a great effort for the enhancement of aPDT with combination therapies[Fischbach, 2011, Zhang et al., 2022, Feng et al., 2021].

Photothermal therapy (PTT) is an alternative method for the treatment of bacterial infections and cancer[Niu et al., 2022, Zou et al., 2016, Lin et al., 2015, Chen et al., 2020]. PTT agents can absorb light in NIR region and convert light energy into heat through non-radiative decay, thus leading to a local temperature increase in the environment. This local temperature increase can cause cells to be sensitive to combination therapies or even irreversible ablation of bacteria can be achieved by the denaturation of their proteins/enzymes[Li et al., 2021, Kim et al., 2015, Korupalli et al., 2017]. Recently, silica nanoparticles, quantum dots and gold nanoparticles have been utilized as PTT agents for therapeutic applications[Wang et al., 2020, Chu et al., 2012]. However, aPTT has some limitations such as; failure of aPTT to kill the heat-resistant bacteria and poor diffusion of phototherapy agents into the bacteria[Laport et al., 2003, Municoy et al., 2015]. Thus, antimicrobial therapies have been directed to the combination of aPDT and aPTT[Shi et al., 2022, Wei et al., 2020].

For the first time in the literature, our group designed highly luminescent, stable, and NIR-emitting aqueous Ag2S QDs to examine their potential as a ther-

anostic QD in particular cancer cells/types.[Buz et al., 2019]. Here, we report NIR-imaging guided combination therapy of gram-positive and gram-negative bacteria by using ALA loaded NAC-QDs. QDs were irradiated at 640 nm wavelength (300 mW laser power) where PpIX is active. The PTT potential of NAC-QDs were investigated in the visible region for the first time and 9C of temperature increase was obtained with irradiation of aqeuous QDs at 640 nm with 200 mW laser power. 2-log and 3-log growth inhibition rates were achieved with *Staphylococcus epidermidis*(*S.epidermidis*) planktonic cells and biofilms, respectively. In the case of *Pseudomonas aeruginosa*(*P.aeruginosa*), 8-log and 6-log growth inhibition rates were achieved for planktonic cells and biofilms, respectively. ALA loading onto QDs increased the uptake of QDs by bacteria that resulted in higher growth inhibition rates in *P.aeruginosa*. Radical scavenger effect of NAC coating led to the decrease in the production of ROS inside cells, however; ALA loading onto QDs elevated the amount of ROS production inside cells. Thus, combination therapy of aPDT and aPTT can be used to overcome bacteria-related infections with image-guided approaches that is superior than single therapies alone.

3.3 Materials and Methods

Silver nitrate (AgNO3, 99.9%) was purchased from Aldrich (MO, USA). Sodium sulfide (Na_2S) was purchased from Alfa-Aesar (Lancashire, England). NAC, sodium hydroxide (NaOH), acetic acid (CH_3COOH), sodium chloride (NaCl), Suprapur nitric acid (65%) and Suprapur sulphuric acid (96%) were obtained from Merck Millipore (MA, USA). Vivaspin 20 centrifugal filters (3000 Da MW cut-off) were obtained from Sartorius (Goettingen, Germany).

3.3.1 Synthesis of NAC-Ag2S QDs

In 37.5 ml of deionized (DI) water, 0.125 mmol of $AgNO_{(3)}$ and 0.25 mmol of NAC were dissolved, and the pH of the solution was changed to 10 by adding 1 M NaOH while working under argon flow. Na_2S (0.03125 mmol) was dissolved in 12.5 ml of DI water for 30 minutes in another flask with an Ar flow. Na_2S solution was

added to the reaction mixture at 70°C while being vigorously mechanically stirred. Following the injection of the Na_3S solution, the reaction mixture was cooled to room temperature (RT) and the QDs were washed with DI water using Vivaspin 20 centrifugal filters. Aqueous QDs are kept at 4°C in the dark.

3.3.2 Electrostatic Loading of ALA on NAC-Ag2S QDs

Zwitterionic ALA was dissolved in water (5 mg/ml ALA stock solution) and the pH of the stock solution was adjusted to 3 before loading onto QDs. The protonated amine groups of ALA and the deprotonated carboxyl groups of the 1 mg/ml QDs were titrated. Electrostatic binding was demonstrated by strong exothermic peaks by Isothermal Titration Calorimetry (ITC) measurement.

3.3.3 Characterization

An UV-VIS-NIR spectrophotometer from Shimadzu was used to measure absorbance. In order to determine the hydrodynamic size and surface charge of QDs, a NanoZS by Malvern Zetasizer was employed. The silver content of QDs was measured using an Agilent 7700X ICP-MS, an inductively coupled plasma-mass spectrometer. For the ICP-MS measurements, samples were etched with nitric acid (65% concentration) and sulfuric acid (96% concentration). Thermogravimetric analysis was used to determine the organic content of QDs (TGA, TGA 500). Under a nitrogen environment, samples were heated at a rate of 10 °C min-1 from ambient temperature to 1000 °C. A homemade device with a 600 L mm-1 grating on a 1/8 Newport Cornerstone 130 monochromator and a femtowatt-sensitive Si detector (Thorlabs PDF10A, 1.4 10-15 W Hz-1/2) was used to measure the intensity of photoluminescence (PL). The frequency-doubled output of a DPSS laser operating at 532 nm excitation wavelength was used to excite NAC-QDs. Using a 590 nm long-pass filter, the luminescence signal was filtered.

3.3.4 Laser irradiation of QD solutions

Concentration dependent temperature increase of aqeuous solutions of QDs was measured at 250, 500, 750 ug/ml Ag concentration using 640 nm laser irradiation with 200 mW laser power for 15 min.

3.3.5 Cytotoxicity assay

Using MTT (Thiazolyl blue tetrazolium bromide (3-(4, 5-dimethylthiazol-2-yl)-2, 5-diphenyltetrazolium bromide)) on Vero cells, the cytotoxicity of free NAC and NAC-Ag_2S was assessed. 1 x 104 cells were seeded into each well of 96-well plates, and the cells were then incubated for 24 hours in a humidified, 37 °C, 5 % CO2 environment. Then, in brand-new culture medium, cells were exposed to various doses of free NAC and NAC-Ag_2S. Cells were cultured for another 24 hours before being exposed to a 50 µL MTT (5 mg/mL in PBS) solution and a 150 µL medium for 4 hours. After that, DMSO:ethanol (1/1) solution was added to dissolve the purple formazan crystals the live cells had formed. Following formula was used to calculate the relative cell viability: Cell viability (%) = [Absorbance of sample / Absorbance of control] x 100 (n=3)

3.3.6 Antimicrobial activity and antibiofilm assays

Bacterial isolates

Pseudomonas aeruginosa ATCC® 700829™ and *Staphylococcus epidermidis* ATCC® 35984™ were used in the experiments.

Antibacterial activity on planktonic bacteria

A single colony of bacteria from overnight cultures was inoculated in Tryptic Soy Broth (TSB, BD™ Bacto™) and incubated overnight at 37 °C-135 rpm. F inal concentrations of 1.5, 2 and 3 mM ALA and 262, 352 and 525 ug/ml Ag, QDs, and ALA-QDs were added to the cell suspensions. Control cell cultures followed an overnight incubation at 37 °C with the addition of TSB. Colony counting following

sequential 10-fold dilutions was used to evaluate bacterial survival. Significant inhibition was defined as a mean CFU/ml growth reduction of at least 2-log (99%) in magnitude. All studies were performed in triplicate.

Antibiofilm activity

96-well plates were used to create biofilms. Briefly, 0.5 Macfarland cell suspension was seeded into wells with TSB-glucose medium for 24 hours after a single colony inoculation in TSB for an overnight period at 37 °C-135 rpm. After that, media were carefully removed from the wells and ALA, QDs, or ALA-QDs were introduced. The survival of the bacteria was assessed by colony counting after a 24-hour period of incubation at 37 °C. Significant inhibition was defined as a mean CFU/ml value reduction of at least 2-log. All studies were performed with three replicates.

3.3.7 Cell uptake of QDs

Qualitative analysis

To demonstrate the qualitative cell uptake, in vitro imaging of QDs was carried out on the biofilms using a confocal microscope (Leica dmi8/SP8). A single colony of bacteria from overnight cultures was inoculated in Tryptic Soy Broth (TSB, BD™ Bacto™) and incubated overnight at 37 °C-135 rpm. 200 ul of this solution was placed onto 12-well Ibidi glass chambers with Macfarland adjusted to 0.5 through TSB and 0.2% glucose, and the chambers were then incubated for 24 hours at 37°C with 5% CO2. After 24h of incubation, the biofilms were treated with QDs and ALA-QDs at 352 ug/mL [Ag] for another 24h incubation, and the cells were then washed three times with PBS to eliminate any uninternalized QDs. The biofilms were then dried at 60°C and fixed for 4–10 hours in a paraformaldehyde solution (3.5% in PBS). To get rid of excess paraformaldehyde, biofilms were washed three times with PBS before being allowed to air dry. Biofilms were air dried before being covered with a glass slide and incubated with a drop of DAPI mounting solution. Leica dmi8/SP8 confocal microscope with two distinct NIR filters (λexc: 510-550 nm and λem: 710 nm long pass) and DAPI filters (λexc: 325-375 nm and λem: 435-

485 nm) were used to study the fixed biofilms. The same experimental approach was also carried out on cells used as controls, which received no QD treatment.

Quantitative analysis

Ag content in the QD treated biofilms was determined in order to perform the quantitative analysis of QD uptake. On a 6-well plate with a 0.5 Macfarland, biofilms were produced for 24 hours at 37 °C and 5% CO2. The biofilms were treated with QD samples at a concentration of 525 ug/mL Ag for 24 hours. After being trypsinized, the biofilms were collected and washed with PBS to eliminate any uninternalized QDs. Ag content was assessed by ICP-MS (n = 3) after biofilms were digested with acid (HNO3/H2SO4: 9/1 v/v) for about one week at room temperature.

3.3.8 Measurement of PpIX formation

P.aeruginosa and *S.epidermidis* planktonic cells were seeded with ALA (1.5, 2 and, 3 mM) and QDs (262, 352 and, 525 ug/ml Ag) as described before. After 24 h of incubation, PpIX fluorescence from each well was measured at 635 nm (excitation at 420 nm; Synergy H1 microplate reader (Biotek)). Untreated cells were used as the control.

3.3.9 Determination of reactive oxygen species (ROS generation)

P.aeruginosa and *S.epidermidis* planktonic cells were incubated with ALA, QDs, and ALA-QDs for 24 hours before being irradiated with 640 nm laser for 10 minutes. Using the DCFDA/H2DCFDA-Cellular ROS Assay Kit (ab113851), cells were exposed to laser light before being incubated for 40 min. Using a Synergy H1 microplate reader and excitation/emission wavelengths of 485/535 nm as per the manufacturer's recommendations, the ROS levels in the cells were measured (Biotek).

3.4 Results

3.4.1 Synthesis and Characterization of NAC-QDs

A straightforward procedure was used to synthesize NAC-Ag_2S QDs in water utilizing $AgNO_3$, Na_2S, and NAC, where NAC is entirely deprotonated at pH 10 to produce stable NPs. NAC-Ag_2S QDs were produced in according to the previously established protocol (Buz et al., 2018). In a summary, 0.25 mmol of $AgNO_3$ and NAC were dissolved in 37.5 mL of water in an argon-filled flask. At 70 °C, NaOH (1M) was used to adjust the solution's pH to 10. Under argon gas in a separate flask, 12.5 mL of water was used to dissolve Na(2S), which was then added to the reaction mixture while being vigorously stirred. After stirring in the dark for 30 minutes, the reaction mixture was cooled to room temperature. The synthesized QDs were then stored at +4 °C after being washed with deionized water with 3 kDa ultracentrifuge tubes.

NAC-QDs have broad absorption in UV-VIS region and strong emission at 760 nm. The organic content was measured as 40 wt % by Thermogravimetric Analysis (TGA) (Fig. 3.1). The hydrodynamic size of NAC-QDs was measured as 2.286

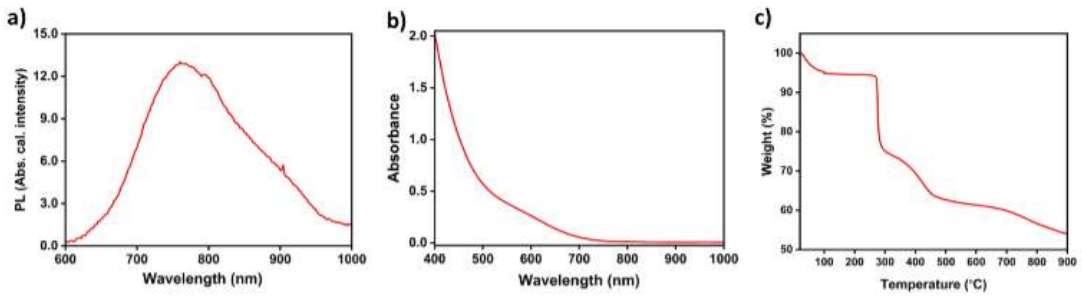

Figure 3.1: a) Absorbance calibrated photoluminescence, b) Absorbance and c) TGA spectra of QDs.

(number based size) by DLS and zeta potential was -27.2 mV. To confirm the interaction between ALA and QDs, Isothermal Titration Calorimetry (ITC) measurements were performed. Titration of 1 mg/ml QDs with 5 mg/ml ALA (pH=3) caused observation of exothermic peaks, indicating binding of ALA to QD. Therefore, after the electrostatic loading of ALA, no washing was performed. The loading amount

was calculated to be equaivalent to 40% mass ratio of QDs and this ratio was further used for bacteria experiments.

3.4.2 Measurement of photothermal potential

The photothermal potential of QDs was tested with different concentrations of Ag at 640 nm laser irradiation with 200 mW laser power for 15 min. The temperature increase was elevated with increasing concentrations of QDs. After 15 min of laser irradiation of 250, 500, and, 750 ug/ml Ag, ΔT was 5.6, 9.4 and 12°C, respectively (Fig. 3.2). The photothermal conversion efficiency of the QDs was determined as 65.7% by using the equation derived by Roper et al. [Roper et al., 2007]

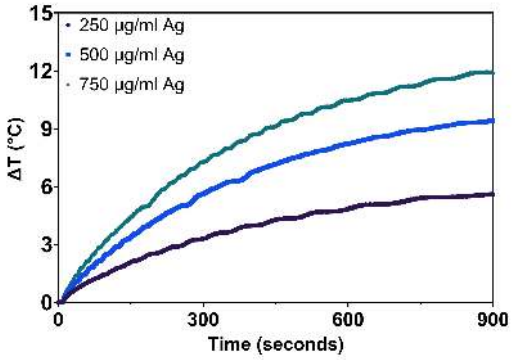

Figure 3.2: Time dependent change in the temperature of QD solutions at different Ag concentrations irradiated at 200 mW. (Ex = 640 nm). The data are expressed as mean ± S.D. (n = 3)

3.4.3 Antibacterial activity

Dose dependent growth inhibition of ALA, QDs and ALA-QDs with 640 nm laser irradiation at 300 mW laser power for 10 minutes and without laser irradiation were evaluated on planktonic cells of *S.epidermidis* and *P.aeruginosa*.

2-log growth inhibition was observed for *S.epidermidis* planktonic cells with laser application, independent from increasing concentrations of QDs and ALA-QDs (Fig. 3.3). All concentrations of ALA resulted in 1-log growth inhibition in cells with laser irradiation. When cells were incubated with ALA, QDs and ALA-QDs, 1-log

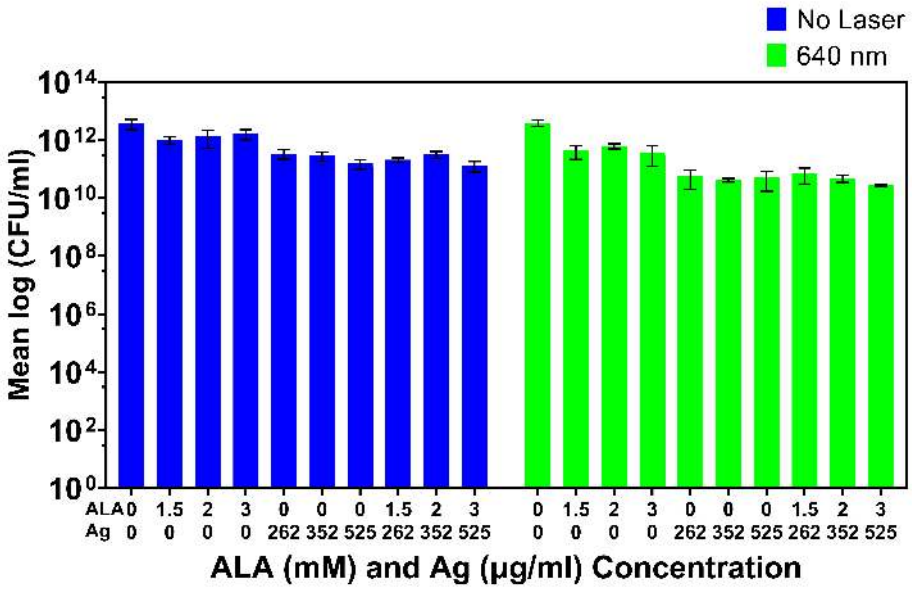

Figure 3.3: Effect of ALA, QDs, and ALA-QDs on the growth inhibition of planktonic cells of *S. epidermidis* was measured both with and without laser irradiation. Control: No substances were applied to planktonic cells. Each laser experiment was conducted under 640 nm laser irradiation for 10 minutes. The data are presented as mean ± S.D. (n = 3), with a $p \leq 0.05$ significance level.

growth inhibition was observed without laser application for all applied doses. Mean CFU/ml for control was found to be 3.68 x 1012 CFU/ml for *S.epidermidis* (without QDs and laser application).

Increasing growth inhibition rates were observed for *P.aeruginosa* planktonic cells with increasing concentrations of ALA-QDs after laser irradiation. 4-, 6-, and, 8-log growth inhibition were observed after laser irradiation of ALA-QDs (262, 352 and, 525 ug/ml Ag with 1.5, 2 and, 3 mM ALA loadings), respectively (Fig. 3.4). The incubation of cells with QDs (525 ug/ml Ag) resulted in 5-log growth inhibition after laser irradiation. 3-log growth inhibition was observed for two doses of QDs (262 and 352 ug/ml Ag) with laser irradiation. When cells were incubated with ALA, 2-log growth inhibition was observed with laser irradiation. The growth inhibition rate did not increase with increasing concentrations of ALA. No significant inhibition was observed when cells were incubated with ALA, QDs and ALA-QDs without laser irradiation for all applied doses. Mean CFU/ml for control was found to be 8.67 x

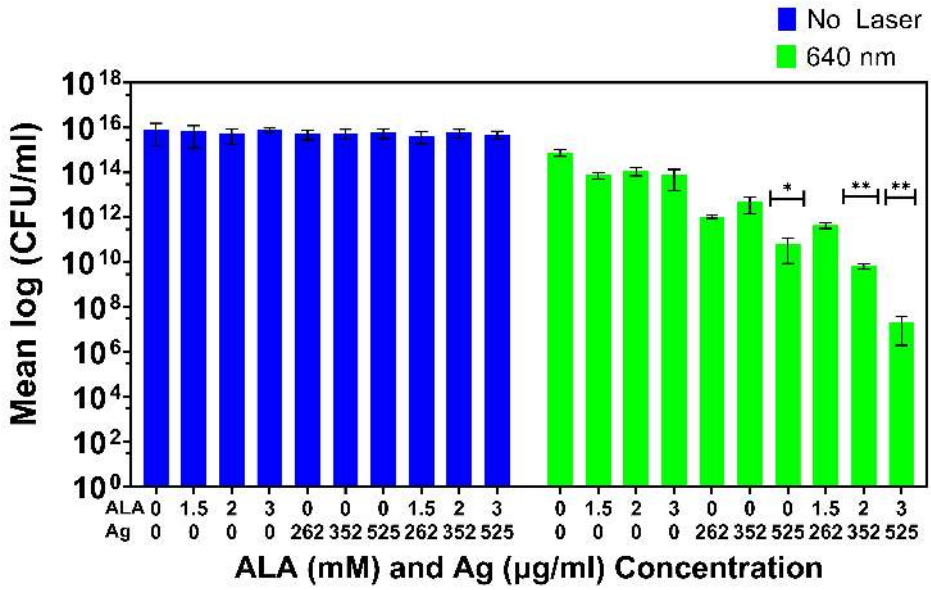

Figure 3.4: Effect of ALA, QDs, and ALA-QDs on the growth inhibition of planktonic cells of *P.aeruginosa* was measured both with and without laser irradiation. Control: No substances were applied to planktonic cells. Each laser experiment was conducted under 640 nm laser irradiation for 10 minutes. The data are presented as mean ± S.D. (n = 3), with a $p \leq 0.05$ significance level.

1015 CFU/ml for *P.aeruginosa* (without NPs and laser application).

3.4.4 Antibiofilm bacterial activity

Dose dependent biofilm inhibition of ALA, QDs and ALA-QDs with 640 nm laser irradiation at 300 mW laser power for 10 minutes and without laser irradiation were evaluated on *S.epidermidis* and *P.aeruginosa*.

For *S.epidermidis* biofilms, 3-log inhibition was observed with and without laser irradiation when biofilms were incubated with ALA, QDs and ALA-QDs for all applied doses (Fig 3.5). Mean CFU/ml for control was found to be 2.98 x 1014 CFU/ml for *S.epidermidis* biofilms (without QDs and laser application).

Increasing biofilm inhibition rates were observed for *P.aeruginosa* biofilms with increasing concentrations of ALA-QDs after laser irradiation. 5- and 6-log biofilm inhibitions were observed after laser irradiation when biofilms were incubated with two doses of ALA-QDs (352 and 525 ug/ml Ag with 2 and 3 mM ALA loadings),

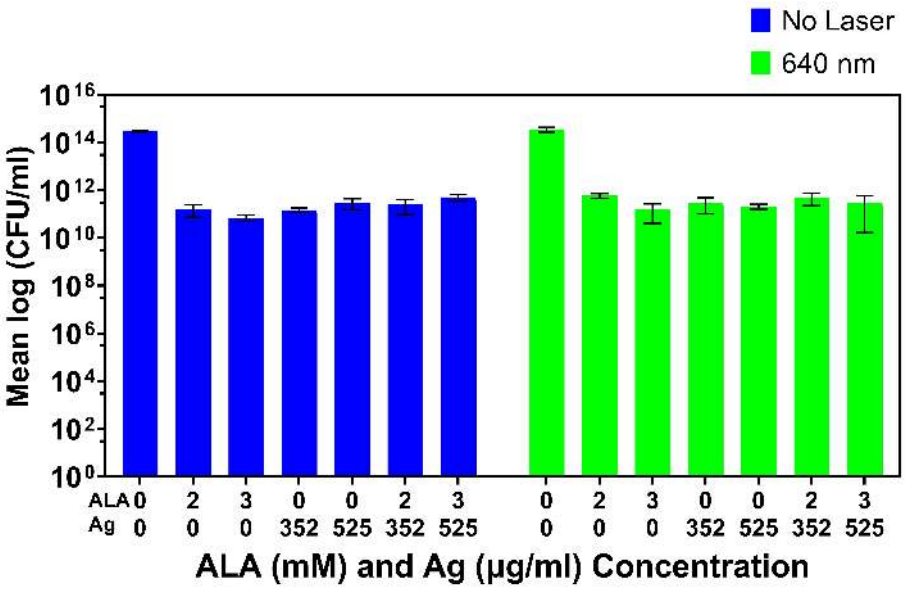

Figure 3.5: Effect of ALA, QDs, and ALA-QDs on the growth inhibition of biofilms of *S. epidermidis* was measured both with and without laser irradiation. Control: No substances were applied to planktonic cells. Each laser experiment was conducted under 640 nm laser irradiation for 10 minutes. The data are presented as mean ± S.D. (n = 3), with a $p \leq 0.05$ significance level.

respectively (Fig. 3.6). Incubation of biofilms with QDs (352 and 525 ug/ml Ag), resulted in 4- and 3-log inhibition after laser irradiation, respectively. When biofilms were incubated with 2 and 3 mM ALA, 2- and 1-log inhibition were observed after laser irradiation, respectively. No significant inhibition was observed when biofilms were incubated with ALA, QDs and ALA-QDs without laser irradiation for all applied doses. Mean CFU/ml for control was found to be 9.13 x 1013 CFU/ml for *P.aeruginosa* (without QDs and laser application).

3.4.5 Cell uptake of QDs

The internalization of QDs by biofilms were investigated qualitatively and quantitatively by confocal microscopy and ICP-MS techniques, respectively. The in vitro NIR imaging potential of QDs and ALA-QDs were examined at 352 ug/ml Ag concentration. The confocal microscopy images showed uptake of QDs and ALA-QDs with *P.aeruginosa* biofilms (Fig. 3.7). Quantitative analysis was performed with

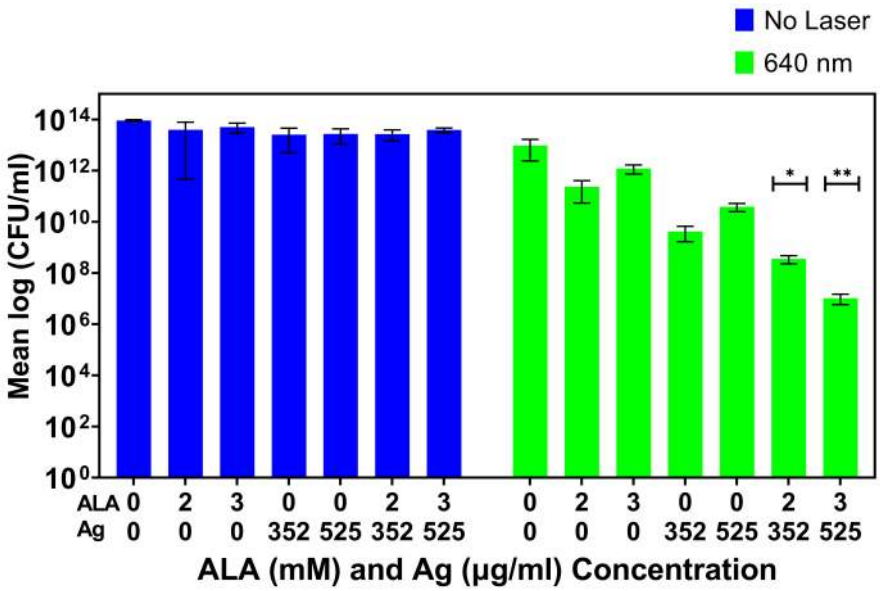

Figure 3.6: Effect of ALA, QDs, and ALA-QDs on the growth inhibition of biofilms of *P.aeruginosa* was measured both with and without laser irradiation. Control: No substances were applied to planktonic cells. Each laser experiment was conducted under 640 nm laser irradiation for 10 minutes. The data are presented as mean ± S.D. (n = 3), with a $p \leq 0.05$ significance level.

QDs and ALA-QDs (525 ug/ml Ag) for *S.epidermidis* and *P.aeruginosa* biofilms after 24h incubation of QDs. *P.aeruginosa* and *S.epidermidis* biofilms internalized about 1% and 1.4% of QDs while internalization of ALA-QDs significantly increased with ALA loading onto QDs in both bacteria (Fig. 3.8).

3.4.6 Measurement of PpIX formation

Intracellular PpIX generation was measured with three different concentrations of ALA (1.5, 2 and, 3 mM) and ALA-QDs (262, 352 and, 525 ug/ml Ag) for *S.epidermidis* and *P.aeruginosa* planktonic cells after 24h incubation. 1.5 and 3 mM ALA significantly increased PpIX formation inside *P.aeruginosa* cells (Fig. 3.9). About 2-folds higher PpIX fluorescence was measured for all applied ALA doses compared to ALA-QDs. 2 and 3 mM ALA significantly increased PpIX formation inside *S.epidermidis* cells. About 2-folds higher PpIX fluorescence was observed for all applied ALA doses compared to ALA-QDs. The intensity of PpIX fluorescence

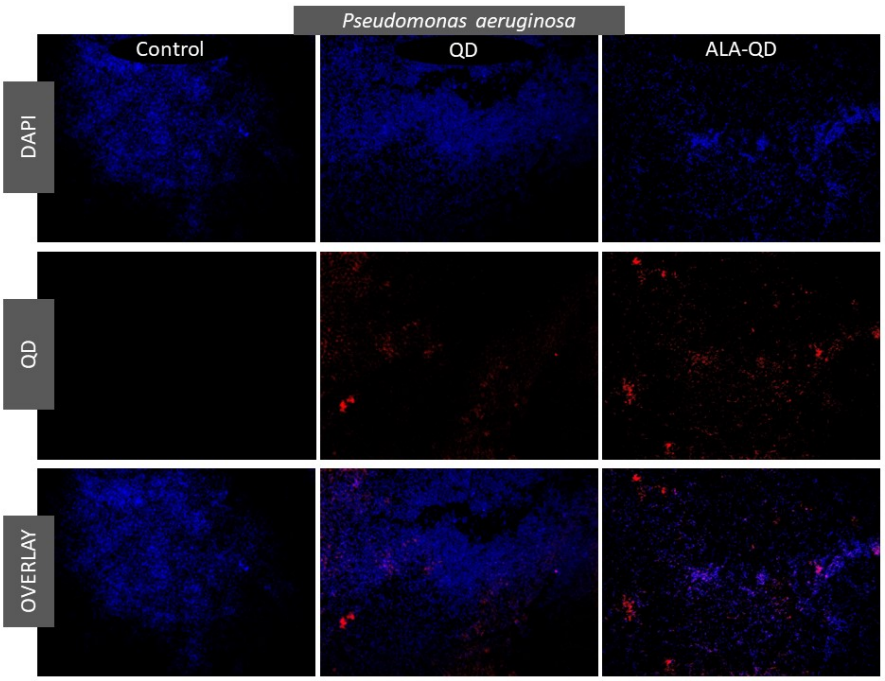

Figure 3.7: Confocal microscopy images of P. aeruginosa biofilms at 40X magnification. Blue: Bacteria stained with DAPI (Ex/Em:325/375 nm), Red:Luminescence from QDs (Ex/Em:488/580-780 nm), Leica dmi8/SP Microscope.

increased with increasing concentrations of ALA and ALA-QDs.

3.4.7 ROS generation

The amount of ROS generation was determined with a cell-permeable nonfluorescent dye 2',7'-dichlorofluorescein diacetate (DCFDA) with and without laser irradiation. The dye is oxidized to a green fluorescent dichlorofluorescein (DCF) by the presence of ROS. After incubation of *S.epidermidis* and *P.aeruginosa* with ALA, QDs and ALA-QDs (3 mM ALA, 525 ug/ml Ag), the production of ROS with and without laser irradiation is followed by the green fluorescence intensity at 535 nm. ROS production significantly increased after laser irradiation with ALA, QD and ALA-QD for *P.aeruginosa* (Fig. 3.11). No significant fluorescence intensity was observed without laser application. ALA-QD caused significant ROS production with and without laser irradiation in *S.epidermidis* (Fig. 3.11). Free ALA caused significant ROS production only after laser irradiation in *S.epidermidis*.

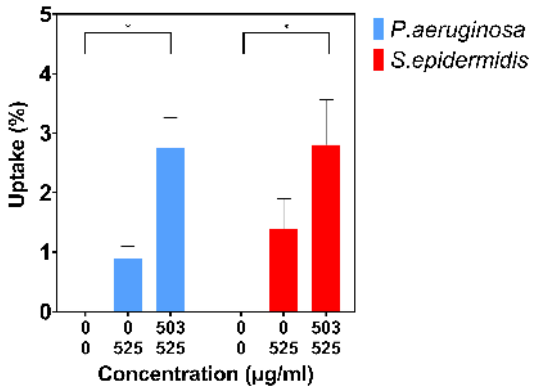

Figure 3.8: Intracellular quantification of QDs and ALA-QDs in *P.aeruginosa* and *S.epidermidis* biofilms.

3.5 Discussion

In this study, NIR-emitting NAC-Ag_2S QDs were synthesized in a simple aqueous method for combination therapy of aPDT and aPTT at a single wavelength. ALA was loaded onto QDs with different concentrations (1.5, 2 and 3 mM). *P.aeruginosa* and *S.epidermidis* planktonic cells and biofilms were incubated with free ALA, QDs and ALA-QDs for 24 h and irradiated at 640 nm (300 mW) for 10 min.

4-, 6-, and 8-log growth inhibition rates were observed with different concentrations of ALA-QDs (262, 352, and 525 ug/ml Ag with 1.5, 2, and 3 mM ALA loadings) after laser irradiation for *P.aeruginosa* planktonic cells, respectively. Growth inhibition rates were significantly increased with increasing concentrations of 2 and 3 mM ALA-QDs compared to control group. ALA loading onto QDs resulted in significantly higher uptake of NPs inside cells as shown by our uptake results. We have shown that QDs have concentration dependent PTT potential at 640 nm laser irradiation. It was also shown by in vitro studies that higher uptake of ALA-QDs resulted in higher killing activity. Surprisingly, PpIX fluorescence did not increase with higher uptake of ALA-QDs. QDs have broad absorption at visible region, therefore, observations of lower PpIX fluorescence with ALA-QD administration might be related to this phenomena [Nagasuna et al., 2011]. Measurements of ROS fluorescence showed lower ROS production for QDs and ALA-QDs compared to free

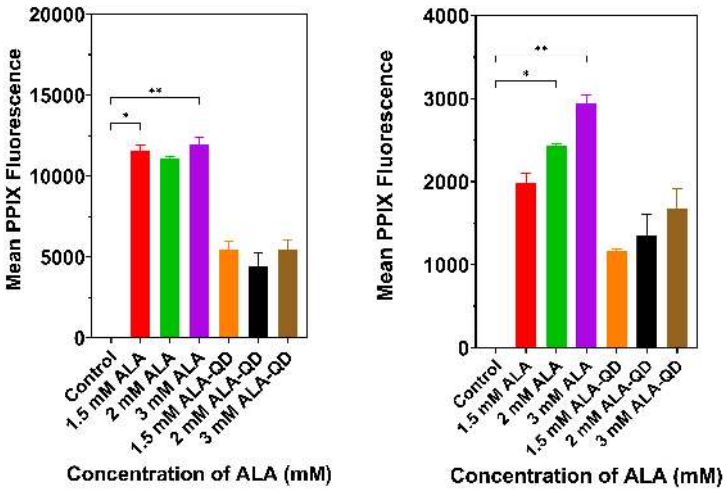

Figure 3.9: Intracellular formation of PpIX through administration of ALA and ALA-QDs after 24h incubation. (PpIX: λex: 405 nm and λem: 635 nm) *P.aeruginosa*(Left) and *S.epidermidis* (Right) planktonic cells. The data are expressed as mean $\pm$ S.D. (n = 3), ($p \leq 0.05$).

ALA. Coating material, NAC, has abilitiy to reduce ROS production inside cells when internalized. However, ROS production was significantly increased with ALA-QDs which shows successful delivery and conversion of ALA into PpIX inside cells. 3-, 3-, and 5-log growth inhibition rates were observed with different concentrations of QDs (262, 352, and 525 ug/ml Ag), respectively. It was shown that the killing activity of QDs is related to their PTT potential. Combination of ALA with QDs resulted in 3-log higher growth inhibition with 2 and 3 mM ALA concentrations which confirms synergistic effect of aPDT and aPTT. However, this effect was not observed with 1.5 mM ALA loading onto QDs (262 ug/ml Ag). Free ALA administration resulted in 2-log growth inhibition after laser irradiation. Inhibition rates and PpIX fluorescence did not increase with increasing concentrations of ALA which in accordance with the literature [Krammer and Überriegler, 1996]. No significant growth inhibition was observed with free ALA administration since PpIX is not an active compound without laser irradiation [Phillips, 2019]. QDs and ALA-QDs administration did not result in significant growth inhibition without laser irradiation which shows non-toxicity of QDs against *P.aeruginosa*.

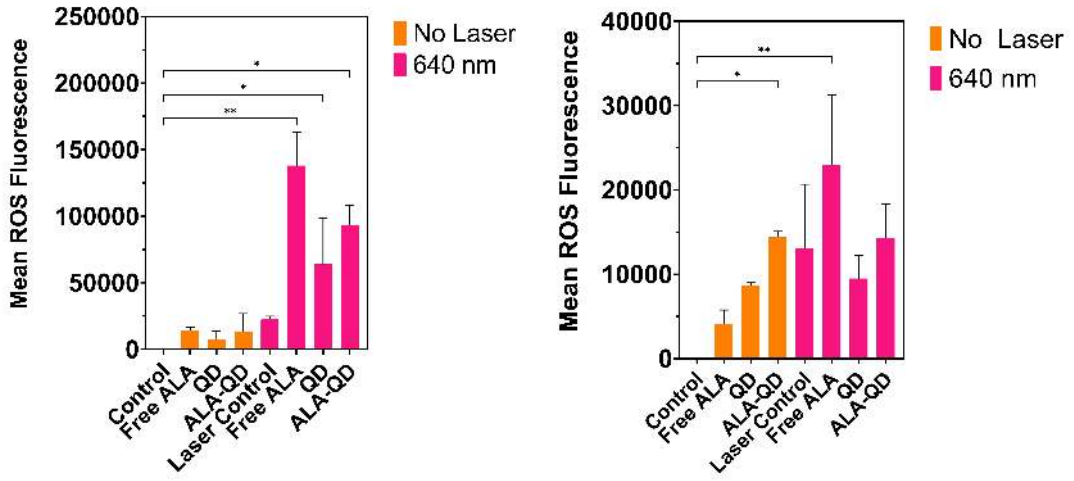

Figure 3.10: ROS production in *P.aeruginosa* (left) and *S.epidermidis* (right) planktonic cells upon 24 h incubation with ALA (3 mM ALA), QD, and, ALA-QD at 500 ug/mL Ag dose after laser irradiation for 10 min. The data are expressed as mean $\pm$ S.D. (n = 3), ($p \leq 0.05$).

For the photoinactivation of *S.epidermidis* Liet et al., used 40 mM ALA concentration[Li et al., 2013]. In our study, we used different concentrations of ALA up to 3 mM. No significant difference in growth inhibition rates was observed for the increasing concentrations of QDs and ALA-QDs (262, 352, and 525 ug/ml Ag with 1.5, 2, and 3 mM ALA loadings) with laser irradiation compared to control group in *S.epidermidis* planktonic cells. The heat resistance of *S.epidermidis* was extensively studied in the literature [Kennedy et al., 2005, Montanari et al., 2015]. Cell uptake studies showed that the uptake of ALA-QDs were significantly increased with ALA loading onto QDs. However, higher uptake of ALA-QDs did not result in higher antibacterial killing with increasing PTT effect which is in accordance with previous studies. Additionally, lower rates of PpIX formation was observed with the incubation of cells with ALA-QDs compared to the incubation of cells with free ALA at same doses. Nevertheless, mean PpIX fluorescence increased with increasing concentrations of ALA-QDs. All of the three concentrations of QDs and ALA-QDs resulted in 1-log growth inhibition without laser application. Dark toxicity of Ag2S QDs towards number of bacteria was also shown by other authors [Jabbar et al.,

2021, Prakash et al., 2020]. This phenomena can be explained by three possibilities. **1-** One of the possibilities of Ag2S dark toxicity is that the high surface energy of QDs led to the oxidative stress and formed radical species which further led to the disruption of cell components[Li et al., 2016a, Huo et al., 2018]. Measurements of ROS production in *S.epidermidis* also supported that QD and ALA-QD caused a slight increase in mean ROS fluorescence without laser application. **2-** Another possibility of darx toxicity of NAC-coated Ag2S QDs is either the adhesion of coating material onto to the *S.epidermidis* cell wall and the disruption of cell wall via elimination of disulfide bridges of cell wall components or competitive inhibition of cysteine utilization[Pérez-Giraldo et al., 1997]. **3-** The other possibility is that the oxygen containing groups of coating material, such as carboxyl and carbonyl groups led to the formation of hydrogen bonding with carbohydrate and proteins of cell wall, thus the integrity of cell wall was destroyed [Song et al., 2016]. All concentrations of free ALA caused 1-log growth inhibition with and without laser irradiation. Low pH culture medium was reported to lead to the death of S. epidermidis cells in another study [Cerca et al., 2011]. The growth inhibition of *S.epidermidis* with free ALA in the absence of laser apllication observed here is possibly due to the acidification of the culture with higher concentrations of ALA.

The complex structure of biofilm prevents treatment strategies against biofilm-related infections [Otto, 2008]. Behavior and adaptation of bacteria inside biofilm differ from planktonic bacteria. Change in the physiological state of bacteria in biofilm leads to higher antibiotic resistance, higher survival rates and adaptation to slow growing of bacteria [Flemming and Wingender, 2010]. Biofilm also prevents antibiotic penetration through complex extracellular polymeric matrix. Therefore, many studies were directed to eradication of biofilm structure [Donlan, 2008, Verderosa et al., 2019]. In our study, the most effective killing activity was achieved by the combination therapy for *P.aeruginosa* biofilms. 4- and 3-log growth inhibition rates were observed with *P.aeruginosa* biofilms incubated with QDs (352 and 525 ug/ml Ag), respectively. This effect was significantly increased with ALA loading onto QDs which is in line with the results of planktonic cells. 5- and 6-log growth inhibition rates were observed for ALA-QDs (352 and 525 ug/ml Ag with 2

and 3 mM ALA loadings) after laser irradiation, respectively. The physiochemical properties of QDs such as, size, shape, surface charge and coating material defines the interaction between biofilms and QDs [Joo and Aggarwal, 2018]. First contact of QDs with the macromolecules of biofilm results in the change of properties of QDs, hence change in the activity of QDs [Mu et al., 2014]. The observation of lower growth inhibition of *P.aeruginosa* biofilms compared to planktonic cells can be explained by this affect. However, significant increase in the growth inhibition was achieved with synergistic effect of aPDT and aPTT (6-log reduction). 2- and 1-log growth inhibition rates were seen with the free ALA incubation of biofilms with laser irradiation. No significant inhibition was observed without laser irradiation as in the case of planktonic cells. Higher killing activity was achieved for *S.epidermidis* biofilms compared to planktonic cells. 3-log inhibition was observed for all concentrations of groups with and without laser irradiation. Nanoparticles are taken up by tumors via passive targeting which relies on enhanced permeability and retention effect (EPR). This has also seen in biofilm-derived infections [Benoit and Koo, 2016]. It is expected to observe an increase in the growth inhibition rate of *S.epidermidis* biofilms compared to planktonic cells due to this EPR effect. Same killing activity trend was observed for biofilm as planktonic cells which supports previous results and claims in our study.

Ag_2S QDs with strong emission in the NIR-region with high biocompatibility have been of interest for bioimaging of tumors and inflammation sites [Kairdolf et al., 2013, Yang et al., 2017]. Internalization of QDs and ALA-QDs by *P.aeruginosa* biofilms were confirmed by confocal microscopy images in the NIR-region (Fig. 3.6). Strong luminescent signals coming from QDs were observed. This indicates the imaging property of these QDs as optical probes for biofilm imaging. Cell uptake studies showed significantly higher uptake for ALA-QDs compared to QDs and microscopy images were in agreement with these studies. QDs have advantages over common fluorescent dyes such as high quantum yield (QYs), resistance to photobleaching, broad excitation wavelength, and emission in NIR-region [Kairdolf et al., 2013]. Therefore, QDs have been utilized in vivo studies extensively. Liu et al., developed NIR-emitting PEG-coated QDs with the core composed of Zn^{2+}, Hg^{2+}, Se^{2-}, and

S^{2-} which is capable of in vivo cation exchange for tumor imaging [Liu et al., 2017]. For in vivo tumor imaging in the NIR-region, Kim et al. developed nanosphere systems in which poly(lactic-co-glycolic acid) (PLGA) was loaded with CdTe/CdSe QDs [Kim et al., 2011]. However, these QDs contain heavy metals that lead to cytotoxicity to healthy cells and tissues when utilized for in vivo studies. In addition to the advantage of NIR luminescence, the ultralow solubility of Ag-chalcogenides prevents Ag+ ion release and therefore renders them highly biocompatible compared to heavy metal-based QDs that suffer from heavy metal toxicity [Lu et al., 2018]. In our cytotoxicity study, QDs had no significant toxicity to Vero cells in the studied ranges which shows potential biocompability for further in vivo studies. NAC has been used in the treatment of bacterial infections because of its antibacterial and antibiofilm activities. Nonetheless, its antimicrobial activity against biofilm is found to be dependent on the bacterial strain and concentration. Additionally, it is mostly combined with different antibiotics or molecules for improved therapeutic outcome [del Prado et al., 2010, Silveira et al., 2013]. Coating material of QDs enhances distribution, bioavailability, and blood-circulation time when QDs are administrated into the body. NAC-Ag_2S-QDs are promising candidates for in vivo and clinical aPDT and aPTT studies against gram-positive bacteria infections with bioimaging property.

3.6 Conclusions

Theranostic nanoparticles, NAC-QDs, with NIR emission was developed to deliver ALA to *P.aeruginosa* and *S.epidermidis* planktonic cells and biofilms for effective antimicrobial PDT and PTT combination therapies with imaging properties. QDs emit strongly around 760 nm and have small sizes which is ideal for in vitro and in vivo imaging. PTT potential of QDs at 640 nm laser irradiation was investigated and reported as 65.7%. These QDs were mostly effective against gram-positive bacteria. Significant growth inhibition rates were observed as 8- and 6-log for *P.aeruginosa* planktonic cells and biofilms, respectively. Confocal microscopy images showed strong NIR emission highlighting the imaging potential of the QDs.

These NAC-Ag_2S-QDs are promising candidates for in vivo and clinical phototherapies against gram-positive bacteria related infections.

Chapter 4

CONCLUSIONS

Successfull, antibiotic-free phototherapy of gram-positive and gram-negative bacteria planktonic cells and biofilms under dual laser irradiation was demonstrated in this thesis utilizing aPDT with ALA and aPTT with either MRI trackable SPION or optically trackable Ag2S QDS. Idea was tested on P.aeruginosa and S.epidermidis planktonic cells and biofilms.

First, ALA loaded SPIONs combined with co-irradiation at 640 and 808 nm was studied, since laser irradiation at 640 nm is typical for ALA-PDT and 808 nm for SPION-PTT. It was also confirmed here that mild heating may be achieved by 640 nm irradiation of SPION, but not sufficient for combination therapy.

Yet, significant growth inhibition rates were achieved for both bacteria with complete eradication of P.aeruginosa plank-tonic cells and 10- and 13-log growth inhibition rates were observed for S.epidermidis and P.aeruginosa biofilms, respectively., when co-irradiaion was utilized. ALA loading onto SPIONs showed increased nanoparticle uptake by biofilms and hence, higher PpIX conversion was achieved. Disadvantages of free ALA treatment for PDT applications was eliminated by this combination with higher therapeutic outcome. Even though these SPIONs are not luminescent, fluorescence signals coming from PpIX was successfully monitored.

Next, same principle was tested with ALA loaded NIR-trackable NAC-Ag2S QDs to generate aPTT/aPDT combination at a single wavelength irradiation, at 640 nm. These NPs were utilized in antimicrobial studies for the first time. PTT potential of these QDs was calculated and reported to be 65.7% for the first time in the literature. These QDs were mostly effective against gram-positive bacteria. Significant growth inhibition rates were observed as 8- and 6-log for P.aeruginosa planktonic cells and biofilms, respectively. Imaging potential of biofilms by these QDs in the NIR region was shown by confocal microscopy images. Their biosafety

was shown by cytotoxi-city studies with Vero cells and reported to be non-toxic.

Overall, in this thesis, antibiotic-free highly effective amtimicrobial phototherapy utilizing safe nanoparticles and a FDA-approved photosensitizer under safe laser irradiation protocols is demonstrated.

BIBLIOGRAPHY

[A., 2006] A., D. P. (2006). Light activated compounds as antimicrobial agents - patently obvious? *Recent Patents on Anti-Infective Drug Discovery*, 1(2):181–199.

[Abadeer and Murphy, 2016] Abadeer, N. S. and Murphy, C. J. (2016). Recent progress in cancer thermal therapy using gold nanoparticles. *The Journal of Physical Chemistry C*, 120(9):4691–4716.

[Agostinis et al., 2011] Agostinis, P., Berg, K., Cengel, K. A., Foster, T. H., Girotti, A. W., Gollnick, S. O., Hahn, S. M., Hamblin, M. R., Juzeniene, A., Kessel, D., Korbelik, M., Moan, J., Mroz, P., Nowis, D., Piette, J., Wilson, B. C., and Golab, J. (2011). Photodynamic therapy of cancer: An update. *CA: A Cancer Journal for Clinicians*, 61(4):250–281.

[Akova, 2016] Akova, M. (2016). Epidemiology of antimicrobial resistance in bloodstream infections. *Virulence*, 7(3):252–266. PMID: 26984779.

[Alivisatos, 1996] Alivisatos, A. P. (1996). Perspectives on the physical chemistry of semiconductor nanocrystals. *The Journal of Physical Chemistry*, 100(31):13226–13239.

[Allison et al., 2004] Allison, R., Mota, H., and Sibata, C. (2004). Clinical pd/pdt in north america: An historical review. *Photodiagnosis and Photodynamic Therapy*, 1(4):263–277.

[Aslam et al., 2007] Aslam, S., Trautner, B. W., Ramanathan, V., and Darouiche, R. O. (2007). Combination of tigecycline and ¡i¿n¡/i¿-acetylcysteine reduces biofilm-embedded bacteria on vascular catheters. *Antimicrobial Agents and Chemotherapy*, 51(4):1556–1558.

[Aydemir et al., 2020] Aydemir, D., Hashemkhani, M., Acar, H. Y., and Ulusu, N. N. (2020). Evaluation of the biocompatibility of the gsh-coated ag2s quantum dots in vitro: a perfect example for the non-toxic optical probes. *Molecular Biology Reports*, 47(6):4117–4129.

[Baier et al., 2005] Baier, J., Maier, M., Engl, R., Landthaler, M., and Bäumler, W. (2005). Time-resolved investigations of singlet oxygen luminescence in water, in phosphatidylcholine, and in aqueous suspensions of phosphatidylcholine or ht29 cells. *The Journal of Physical Chemistry B*, 109(7):3041–3046. PMID: 16851318.

[Bala Subramaniyan et al., 2019] Bala Subramaniyan, S., Megarajan, S., Vijayakumar, S., Mariappan, M., and Anbazhagan, V. (2019). Evaluation of the toxicities of silver and silver sulfide nanoparticles against gram-positive and gram-negative bacteria. *IET Nanobiotechnology*, 13(3):326–331.

[Barrow et al., 2015] Barrow, M., Taylor, A., Nieves, D. J., Bogart, L. K., Mandal, P., Collins, C. M., Moore, L. R., Chalmers, J. J., Lévy, R., Williams, S. R., Murray, P., Rosseinsky, M. J., and Adams, D. J. (2015). Tailoring the surface charge of dextran-based polymer coated spions for modulated stem cell uptake and mri contrast. *Biomater. Sci.*, 3:608–616.

[Bartolomeu et al., 2016] Bartolomeu, M., Rocha, S., Cunha, , Neves, M. G. P. M. S., Faustino, M. A. F., and Almeida, A. (2016). Effect of photodynamic therapy on the virulence factors of staphylococcus aureus. *Frontiers in Microbiology*, 7.

[Benoit and Koo, 2016] Benoit, D. S. and Koo, H. (2016). Targeted, triggered drug delivery to tumor and biofilm microenvironments. *Nanomedicine*, 11(8):873–879. PMID: 26987892.

[Bera et al., 2010] Bera, D., Qian, L., Tseng, T.-K., and Holloway, P. H. (2010). Quantum dots and their multimodal applications: A review. *Materials*, 3(4):2260–2345.

[Berry and Curtis, 2003] Berry, C. C. and Curtis, A. S. G. (2003). Functionalisation of magnetic nanoparticles for applications in biomedicine. *Journal of Physics D: Applied Physics*, 36(13):R198.

[Bhattacherjee et al., 2019] Bhattacherjee, A., Hrynets, Y., and Betti, M. (2019). Improved bactericidal capacity of uv-b radiation against e. coli strains by photosensitizing bacteria with fructosazine – an advanced maillard reaction product. *Food Chemistry*, 271:354–361.

[Bilan et al., 2016] Bilan, R., Nabiev, I., and Sukhanova, A. (2016). Quantum dot-based nanotools for bioimaging, diagnostics, and drug delivery. *ChemBioChem*, 17(22):2103–2114.

[Bilici et al., 2020] Bilici, K., Atac, N., Muti, A., Baylam, I., Dogan, O., Sennaroglu, A., Can, F., and Yagci Acar, H. (2020). Broad spectrum antibacterial photodynamic and photothermal therapy achieved with indocyanine green loaded spions under near infrared irradiation. *Biomater. Sci.*, 8:4616–4625.

[Boca et al., 2011] Boca, S. C., Potara, M., Gabudean, A.-M., Juhem, A., Baldeck, P. L., and Astilean, S. (2011). Chitosan-coated triangular silver nanoparticles as a novel class of biocompatible, highly effective photothermal transducers for in vitro cancer cell therapy. *Cancer Letters*, 311(2):131–140.

[Borlongan, 2007] Borlongan, V. C. (2007). Nanotechnology as an adjunct tool for transplanting engineered cells and tissues. *Current Molecular Medicine*, 7(7):609–618.

[Breidenstein et al., 2011] Breidenstein, E. B., de la Fuente-Núñez, C., and Hancock, R. E. (2011). Pseudomonas aeruginosa: all roads lead to resistance. *Trends in Microbiology*, 19(8):419–426.

[Buz et al., 2019] Buz, P. T., Duman, F. D., Erkisa, M., Demirci, G., Ari, F., Ulukaya, E., and Acar, H. Y. (2019). Development of near-infrared region lumi-

nescent n-acetyl-l-cysteine-coated ag2s quantum dots with differential therapeutic effect. *Nanomedicine*, 14(8):969–987. PMID: 30917096.

[Campoccia et al., 2010] Campoccia, D., Montanaro, L., Speziale, P., and Arciola, C. R. (2010). Antibiotic-loaded biomaterials and the risks for the spread of antibiotic resistance following their prophylactic and therapeutic clinical use. *Biomaterials*, 31(25):6363–6377.

[Castano et al., 2005] Castano, A. P., Demidova, T. N., and Hamblin, M. R. (2005). Mechanisms in photodynamic therapy: part two-cellular signaling, cell metabolism and modes of cell death. *Photodiagnosis and photodynamic therapy*, 2(1):1—23.

[Castillo-Martínez et al., 2015] Castillo-Martínez, J., Martínez-Castañon, G.-A., Martínez-Gutiérrez, F., Zavala-Alonso, V., Patiño-Marín, N., Nino, N., Zaragoza-Magaña, V., and Cabral-Romero, C. (2015). Antibacterial and antibiofilm activities of the photothermal therapy using gold nanorods against seven different bacterial strains. *Journal of Nanomaterials*, 2015:1–7.

[Cavassin et al., 2015] Cavassin, E. D., de Figueiredo, L. F. P., Otoch, J. P., Seckler, M. M., de Oliveira, R. A., Franco, F. F., Marangoni, V. S., Zucolotto, V., Levin, A. S. S., and Costa, S. F. (2015). Comparison of methods to detect the in vitro activity of silver nanoparticles (agnp) against multidrug resistant bacteria. *Journal of Nanobiotechnology*, 13(1):64.

[Cerca et al., 2011] Cerca, F., França, , Guimarães, R., Hinzmann, M., Cerca, N., Lobo da Cunha, A., Azeredo, J., and Vilanova, M. (2011). Modulation of poly-n-acetylglucosamine accumulation within mature staphylococcus epidermidis biofilms grown in excess glucose. *Microbiology and Immunology*, 55(10):673–682.

[Chai et al.,] Chai, R., Xing, C., Gao, D., Yuan, H., Zhan, Y., and Wang, S. Remote-controlling potassium channels in living cells through photothermal inactivation of calmodulin. *Advanced Healthcare Materials*, 7(19):1800674.

[Chen et al., 2013] Chen, J., zhang, T., Feng, L., Zhang, M., Zhang, X., Su, H., and Cui, D. (2013). Synthesis of ribonuclease-a conjugated ag2s quantum dots clusters via biomimetic route. *Materials Letters*, 96:224–227.

[Chen et al., 2017] Chen, S., Tang, F., Tang, L., and Li, L. (2017). Synthesis of cu-nanoparticle hydrogel with self-healing and photothermal properties. *ACS Applied Materials & Interfaces*, 9(24):20895–20903. PMID: 28569057.

[Chen et al., 2020] Chen, Y., Gao, Y., Chen, Y., Liu, L., Mo, A., and Peng, Q. (2020). Nanomaterials-based photothermal therapy and its potentials in antibacterial treatment. *Journal of Controlled Release*, 328:251–262.

[Chinnathambi and Shirahata, 2019] Chinnathambi, S. and Shirahata, N. (2019). Recent advances on fluorescent biomarkers of near-infrared quantum dots for in vitro and in vivo imaging. *Science and Technology of Advanced Materials*, 20(1):337–355. PMID: 31068983.

[Cho et al., 2010] Cho, E. C., Glaus, C., Chen, J., Welch, M. J., and Xia, Y. (2010). Inorganic nanoparticle-based contrast agents for molecular imaging. *Trends in Molecular Medicine*, 16(12):561–573. Special Issue: Nanomedicine.

[Choi et al., 2014] Choi, Y., Kim, S., Choi, M.-H., Ryoo, S.-R., Park, J., Min, D.-H., and Kim, B.-S. (2014). Highly biocompatible carbon nanodots for simultaneous bioimaging and targeted photodynamic therapy in vitro and in vivo. *Advanced Functional Materials*, 24(37):5781–5789.

[Chu et al., 2012] Chu, M., Pan, X., Zhang, D., Wu, Q., Peng, J., and Hai, W. (2012). The therapeutic efficacy of cdte and cdse quantum dots for photothermal cancer therapy. *Biomaterials*, 33(29):7071–7083.

[Chu et al., 2013] Chu, M., Shao, Y., Peng, J., Dai, X., Li, H., Wu, Q., and Shi, D. (2013). Near-infrared laser light mediated cancer therapy by photothermal effect of fe3o4 magnetic nanoparticles. *Biomaterials*, 34(16):4078–4088.

[Collaud, 2004] Collaud, S. (2004). On the selectivity of 5-aminolevulinic acid-induced protoporphyrin ix formation. *Current Medicinal Chemistry - Anti-Cancer Agents*, 4(3):301–316.

[Corwin et al., 2001] Corwin, T. S., Lindberg, G., Traxer, O., Gettman, M. T., Smith, T. G., Pearle, M. S., and Cadeddu, J. A. (2001). Laparoscopic radiofrequency thermal ablation of renal tissue with and without hilar occlusion. *Journal of Urology*, 166(1):281–284.

[Costerton et al., 1987] Costerton, J. W., Cheng, K. J., Geesey, G. G., Ladd, T. I., Nickel, J. C., Dasgupta, M., and Marrie, T. J. (1987). Bacterial biofilms in nature and disease. *Annual Review of Microbiology*, 41(1):435–464. PMID: 3318676.

[Dai et al.,] Dai, T., Tegos, G. P., Zhiyentayev, T., Mylonakis, E., and Hamblin, M. R. Photodynamic therapy for methicillin-resistant staphylococcus aureus infection in a mouse skin abrasion model. *Lasers in Surgery and Medicine*, 42(1):38–44.

[de Santana et al., 2020] de Santana, W. M. O., Caetano, B. L., de Annunzio, S. R., Pulcinelli, S. H., Ménager, C., Fontana, C. R., and Santilli, C. V. (2020). Conjugation of superparamagnetic iron oxide nanoparticles and curcumin photosensitizer to assist in photodynamic therapy. *Colloids and Surfaces B: Biointerfaces*, 196:111297.

[del Prado et al., 2010] del Prado, G., Ruiz, V., Naves, P., Rodríguez-Cerrato, V., Soriano, F., and del Carmen Ponte, M. (2010). Biofilm formation by streptococcus pneumoniae strains and effects of human serum albumin, ibuprofen, n-acetyl-l-cysteine, amoxicillin, erythromycin, and levofloxacin. *Diagnostic Microbiology and Infectious Disease*, 67(4):311–318.

[Delgado-Beleño et al., 2018] Delgado-Beleño, Y., Martinez-Nuñez, C., Cortez-Valadez, M., Flores-López, N., and Flores-Acosta, M. (2018). Optical properties of silver, silver sulfide and silver selenide nanoparticles and antibacterial applications. *Materials Research Bulletin*, 99:385–392.

[DeRosa, 2002] DeRosa, M. C. (2002). Photosensitized singlet oxygen and its applications. *Coordination Chemistry Reviews*, 233:351–371.

[Diederich, 2005] Diederich, C. J. (2005). Thermal ablation and high-temperature thermal therapy: Overview of technology and clinical implementation. *International Journal of Hyperthermia*, 21(8):745–753. PMID: 16338857.

[Donlan, 2008] Donlan, R. M. (2008). *Biofilms on Central Venous Catheters: Is Eradication Possible?*, pages 133–161. Springer Berlin Heidelberg, Berlin, Heidelberg.

[Donlan and Costerton, 2002] Donlan, R. M. and Costerton, J. W. (2002). Biofilms: Survival mechanisms of clinically relevant microorganisms. *Clinical Microbiology Reviews*, 15(2):167–193.

[Donnelly et al., 2007] Donnelly, R. F., McCarron, P. A., and Woolfson, A. D. (2007). Derivatives of 5-aminolevulinic acid for photodynamic therapy. *Perspect Medicin Chem*, 1:49–63.

[dos Santos et al., 2019] dos Santos, A. F., de Almeida, D. R. Q., Terra, L. F., Baptista, M. S., and Labriola, L. (2019). Photodynamic therapy in cancer treatment - an update review. *Journal of Cancer Metastasis and Treatment*, 5:25.

[Du et al., 2016] Du, B., Gu, X., Zhao, W., Liu, Z., Li, D., Wang, E., and Wang, J. (2016). Hybrid of gold nanostar and indocyanine green for targeted imaging-guided diagnosis and phototherapy using low-density laser irradiation. *J. Mater. Chem. B*, 4:5842–5849.

[Du et al., 2022] Du, T., Xiao, Z., Cao, J., Wei, L., Li, C., Jiao, J., Song, Z., Liu, J., Du, X., and Wang, S. (2022). Nir-activated multi-hit therapeutic ag2s quantum dot-based hydrogel for healing of bacteria-infected wounds. *Acta Biomaterialia*, 145:88–105.

[Du et al., 2010] Du, Y., Xu, B., Fu, T., Cai, M., Li, F., Zhang, Y., and Wang, Q. (2010). Near-infrared photoluminescent ag2s quantum dots from a single source precursor. *Journal of the American Chemical Society*, 132(5):1470–1471. PMID: 20078056.

[Duman et al., 2015] Duman, F. D., Hocaoglu, I., Ozturk, D. G., Gozuacik, D., Kiraz, A., and Yagci Acar, H. (2015). Highly luminescent and cytocompatible cationic ag2s nir-emitting quantum dots for optical imaging and gene transfection. *Nanoscale*, 7:11352–11362.

[E. Blums, 1997] E. Blums, A. C. a. M. M. M. W. d. G. (1997). *Magnetic Fluids*, volume 354. Cambridge University Press.

[El-Sayed, 2001] El-Sayed, M. A. (2001). Some interesting properties of metals confined in time and nanometer space of different shapes. *Accounts of Chemical Research*, 34(4):257–264. PMID: 11308299.

[Ercan et al., 2021] Ercan, U. K., Yost, A. D., Wasko, K., Brooks, A. D., and Joshi, S. G. (2021). Evaluation of cellular and systemic toxicity of dielectric barrier discharge plasma-treated n-acetylcysteine as potential antimicrobial catheter lock solution. *Plasma*, 4(4):732–744.

[Feng et al., 2021] Feng, Y., Coradi Tonon, C., Ashraf, S., and Hasan, T. (2021). Photodynamic and antibiotic therapy in combination against bacterial infections: efficacy, determinants, mechanisms, and future perspectives. *Advanced Drug Delivery Reviews*, 177:113941.

[Fischbach, 2011] Fischbach, M. A. (2011). Combination therapies for combating antimicrobial resistance. *Current Opinion in Microbiology*, 14(5):519–523. Antimicrobials/Genomics.

[Fisher et al., 2010] Fisher, J. W., Sarkar, S., Buchanan, C. F., Szot, C. S., Whitney, J., Hatcher, H. C., Torti, S. V., Rylander, C. G., and Rylander, M. N. (2010).

Photothermal Response of Human and Murine Cancer Cells to Multiwalled Carbon Nanotubes after Laser Irradiation. *Cancer Research*, 70(23):9855–9864.

[Fleet, 1981] Fleet, M. E. (1981). The structure of magnetite. *Acta Crystallographica Section B*, 37(4):917–920.

[Flemming and Wingender, 2010] Flemming, H.-C. and Wingender, J. (2010). The biofilm matrix. *Nature Reviews Microbiology*, 8(9):623–633.

[Foote, 1991] Foote, C. S. (1991). Definition of type i and type ii photosensitized oxidation. *Photochemistry and Photobiology*, 54(5):659–659.

[Fotinos et al., 2008] Fotinos, N., Convert, M., Piffaretti, J.-C., Gurny, R., and Lange, N. (2008). Effects on gram-negative and gram-positive bacteria mediated by 5-aminolevulinic acid and 5-aminolevulinic acid derivatives. *Antimicrobial Agents and Chemotherapy*, 52(4):1366–1373.

[Frieri et al., 2017] Frieri, M., Kumar, K., and Boutin, A. (2017). Antibiotic resistance. *Journal of Infection and Public Health*, 10(4):369–378.

[Gao et al., 2021] Gao, M., Zhao, H., Wang, Z., Zhao, Y., Zou, X., and Sun, L. (2021). Controllable preparation of ag2s quantum dots with size-dependent fluorescence and cancer photothermal therapy. *Advanced Powder Technology*, 32(6):1972–1982.

[Garrett et al., 2000] Garrett, C., Draper, D., and Knight, K. (2000). Heat distribution in the lower leg from pulsed short-wave diathermy and ultrasound treatments. *Journal of athletic training*, 35:50–5.

[Gibson et al., 2003] Gibson, R. L., Burns, J. L., and Ramsey, B. W. (2003). Pathophysiology and management of pulmonary infections in cystic fibrosis. *American Journal of Respiratory and Critical Care Medicine*, 168(8):918–951. PMID: 14555458.

[Girma et al., 2017] Girma, W. M., Fahmi, M. Z., Permadi, A., Abate, M. A., and Chang, J.-Y. (2017). Synthetic strategies and biomedical applications of i–iii–vi ternary quantum dots. *J. Mater. Chem. B*, 5:6193–6216.

[Giuntini et al., 2009] Giuntini, F., Bourré, L., MacRobert, A. J., Wilson, M., and Eggleston, I. M. (2009). Improved peptide prodrugs of 5-ala for pdt: Rationalization of cellular accumulation and protoporphyrin ix production by direct determination of cellular prodrug uptake and prodrug metabolization. *Journal of Medicinal Chemistry*, 52(13):4026–4037. PMID: 19492812.

[Hader and Jori, 2006] Hader, D.-P. and Jori, G. (2006). *Photodynamic Therapy with ALA*. Comprehensive Series in Photochemical Photobiological Sciences. The Royal Society of Chemistry.

[Hamed et al., 2017] Hamed, S., Emara, M., Shawky, R. M., El-domany, R. A., and Youssef, T. (2017). Silver nanoparticles: Antimicrobial activity, cytotoxicity, and synergism with n-acetyl cysteine. *Journal of Basic Microbiology*, 57(8):659–668.

[Harris and Pierpoint, 2012] Harris, F. and Pierpoint, L. (2012). Photodynamic therapy based on 5-aminolevulinic acid and its use as an antimicrobial agent. *Medicinal Research Reviews*, 32(6):1292–1327.

[Hofmann-Amtenbrink et al., 2010] Hofmann-Amtenbrink, M., Hofmann, H., and Montet, X. (2010). Superparamagnetic nanoparticles – a tool for early diagnostics. *Swiss Medical Weekly*, 140(3738):w13081.

[Hong et al., 2012] Hong, G., Robinson, J. T., Zhang, Y., Diao, S., Antaris, A. L., Wang, Q., and Dai, H. (2012). Invivo fluorescence imaging with ag2s quantum dots in the second near-infrared region. *Angewandte Chemie International Edition*, 51(39):9818–9821.

[Hsieh et al., 2013] Hsieh, C.-M., Huang, Y.-H., Chen, C.-P., Hsieh, B.-C., and Tsai, T. (2013). 5-aminolevulinic acid induced photodynamic inactivation on staphylococcus aureus and pseudomonas aeruginosa. *J Food Drug Anal*, 22(3):350–355.

[Hu et al., 2017] Hu, X., Li, Y., Tian, J., Yang, H., and Cui, H. (2017). Highly efficient full solar spectrum (uv-vis-nir) photocatalytic performance of ag2s quantum dot/tio2 nanobelt heterostructures. *Journal of Industrial and Engineering Chemistry*, 45:189–196.

[Huang et al., 2019] Huang, J., Guo, M., Jin, S., Wu, M., Yang, C., Zhang, G., Wang, P., Ji, J., Zeng, Q., Wang, X., and Wang, H. (2019). Antibacterial photodynamic therapy mediated by 5-aminolevulinic acid on methicillin-resistant staphylococcus aureus. *Photodiagnosis and Photodynamic Therapy*, 28:330–337.

[Huo et al., 2018] Huo, P., Liu, C., Wu, D., Guan, J., Li, J., Wang, H., Tang, Q., Li, X., Yan, Y., and Yuan, S. (2018). Fabricated ag/ag2s/reduced graphene oxide composite photocatalysts for enhancing visible light photocatalytic and antibacterial activity. *Journal of Industrial and Engineering Chemistry*, 57:125–133.

[Ibelli et al., 2018] Ibelli, T., Templeton, S., and Levi-Polyachenko, N. (2018). Progress on utilizing hyperthermia for mitigating bacterial infections. *International Journal of Hyperthermia*, 34(2):144–156. PMID: 29498314.

[Jabbar et al., 2021] Jabbar, Z. H., Ammar, S. H., and Esmail Ebrahim, S. (2021). Enhanced visible-light photocatalytic bacterial inhibition using recyclable magnetic heterogeneous nanocomposites (fe3o4@sio2@ag2wo4@ag2s) in core/shell structure. *Environmental Nanotechnology, Monitoring Management*, 16:100601.

[Jeong et al., 2015] Jeong, C. J., Sharker, S. M., In, I., and Park, S. Y. (2015). Iron oxide@pedot-based recyclable photothermal nanoparticles with poly(vinylpyrrolidone) sulfobetaines for rapid and effective antibacterial activity. *ACS Applied Materials & Interfaces*, 7(18):9469–9478. PMID: 25905634.

[Jin et al., 2022] Jin, Y., Zhao, B., Guo, W., Li, Y., Min, J., and Miao, W. (2022). Penetration and photodynamic ablation of drug-resistant biofilm by cationic iron oxide nanoparticles. *Journal of Controlled Release*, 348:911–923.

[Johannsen et al., 2005] Johannsen, M., Gneveckow, U., Eckelt, L., Feussner, A., WaldÖFner, N., Scholz, R., Deger, S., Wust, P., Loening, S. A., and Jordan, A. (2005). Clinical hyperthermia of prostate cancer using magnetic nanoparticles: Presentation of a new interstitial technique. *International Journal of Hyperthermia*, 21(7):637–647. PMID: 16304715.

[Joo and Aggarwal, 2018] Joo, S. H. and Aggarwal, S. (2018). Factors impacting the interactions of engineered nanoparticles with bacterial cells and biofilms: Mechanistic insights and state of knowledge. *Journal of Environmental Management*, 225:62–74.

[Jori et al., 2011] Jori, G., Camerin, M., Soncin, M., Guidolin, L., and Coppellotti, O. (2011). Chapter 1 antimicrobial photodynamic therapy: Basic principles. 11:1–18.

[Jung et al., 2018] Jung, H. S., Verwilst, P., Sharma, A., Shin, J., Sessler, J. L., and Kim, J. S. (2018). Organic molecule-based photothermal agents: an expanding photothermal therapy universe. *Chem. Soc. Rev.*, 47:2280–2297.

[Juzenas et al., 2008] Juzenas, P., Chen, W., Sun, Y.-P., Coelho, M. A. N., Generalov, R., Generalova, N., and Christensen, I. L. (2008). Quantum dots and nanoparticles for photodynamic and radiation therapies of cancer. *Advanced Drug Delivery Reviews*, 60(15):1600–1614. 2008 Editors' Collection.

[Kaczyńska et al., 2016] Kaczyńska, A., Guzdek, K., Derszniak, K., Karewicz, A., Lewandowska-Łańcucka, J., Mateuszuk, , Skórka, T., Banasik, T., Jasiński, K., Kapusta, C., Chlopicki, S., and Nowakowska, M. (2016). Novel nanostructural contrast for magnetic resonance imaging of endothelial inflammation: targeting spions to vascular endothelium. *RSC Adv.*, 6:72586–72595.

[Kairdolf et al., 2013] Kairdolf, B. A., Smith, A. M., Stokes, T. H., Wang, M. D., Young, A. N., and Nie, S. (2013). Semiconductor quantum dots for bioimaging and

biodiagnostic applications. *Annual Review of Analytical Chemistry*, 6(1):143–162. PMID: 23527547.

[Kandasamy and Maity, 2015] Kandasamy, G. and Maity, D. (2015). Recent advances in superparamagnetic iron oxide nanoparticles (spions) for in vitro and in vivo cancer nanotheranostics. *International Journal of Pharmaceutics*, 496(2):191–218.

[Kaneyoshi, 1990] Kaneyoshi, T. (1990). Introduction to surface magnetism.

[Kelty et al., 2002] Kelty, C. J., Brown, N. J., Reed, M. W. R., and Ackroyd, R. (2002). The use of 5-aminolaevulinic acid as a photosensitiser in photodynamic therapy and photodiagnosis. *Photochem. Photobiol. Sci.*, 1:158–168.

[Kennedy et al., 2005] Kennedy, J., Blair, I., McDowell, D., and Bolton, D. (2005). An investigation of the thermal inactivation of staphylococcus aureus and the potential for increased thermotolerance as a result of chilled storage. *Journal of Applied Microbiology*, 99(5):1229–1235.

[Kennedy and Pottier, 1992] Kennedy, J. C. and Pottier, R. H. (1992). New trends in photobiology: Endogenous protoporphyrin ix, a clinically useful photosensitizer for photodynamic therapy. *Journal of Photochemistry and Photobiology B: Biology*, 14(4):275–292.

[Kim et al., 2011] Kim, J. S., Cho, K. J., Tran, T. H., Nurunnabi, M., Moon, T. H., Hong, S. M., and kyu Lee, Y. (2011). In vivo nir imaging with cdte/cdse quantum dots entrapped in plga nanospheres. *Journal of Colloid and Interface Science*, 353(2):363–371.

[Kim and Darafsheh, 2020] Kim, M. M. and Darafsheh, A. (2020). Light sources and dosimetry techniques for photodynamic therapy. *Photochemistry and Photobiology*, 96(2):280–294.

[Kim et al., 2015] Kim, S. H., Kang, E. B., Jeong, C. J., Sharker, S. M., In, I., and Park, S. Y. (2015). Light controllable surface coating for effective photothermal killing of bacteria. *ACS Applied Materials & Interfaces*, 7(28):15600–15606. PMID: 26101891.

[Korupalli et al., 2017] Korupalli, C., Huang, C.-C., Lin, W.-C., Pan, W.-Y., Lin, P.-Y., Wan, W.-L., Li, M.-J., Chang, Y., and Sung, H.-W. (2017). Acidity-triggered charge-convertible nanoparticles that can cause bacterium-specific aggregation in situ to enhance photothermal ablation of focal infection. *Biomaterials*, 116:1–9.

[Krammer and Überriegler, 1996] Krammer, B. and Überriegler, K. (1996). In-vitro investigation of ala-induced protopoyphyrin ix. *Journal of Photochemistry and Photobiology B: Biology*, 36(2):121–126. Perspectives in Photodynamic Therapy.

[Kristian et al., 2008] Kristian, S. A., Birkenstock, T. A., Sauder, U., Mack, D., Götz, F., and Landmann, R. (2008). Biofilm Formation Induces C3a Release and Protects Staphylococcus epidermidis from IgG and Complement Deposition and from Neutrophil-Dependent Killing. *The Journal of Infectious Diseases*, 197(7):1028–1035.

[Kumar, 2017] Kumar, S. (2017). **Nanomaterials for Tumor Targeting Theranostics. A Proactive Clinical Perspective.** Edited by Mingqian Tan and Aiguo Wu. World Scientific, 2016. Pp. 432. Price GBP 120.00 (Hardcover). ISBN 978-981-4635-41-7. *Acta Crystallographica Section D*, 73(7):626–627.

[Langton Hewer and Smyth, 2014] Langton Hewer, S. and Smyth, A. (2014). Antibiotic strategies for eradicating pseudomonas aeruginosa in people with cystic fibrosis. *Cochrane Database of Systematic Reviews*, (11).

[Laport et al., 2003] Laport, M. S., da Silva, M. R., Silva, C. C., do Carmo de Freire Bastos, M., and Giambiagi-deMarval, M. (2003). Heat-resistance and heat-

shock response in the nosocomial pathogen enterococcus faecium. *Current Microbiology*, 46(5):0313–0317.

[Li et al., 2016a] Li, J., Gao, L., Sun, K., Xiao, D., Li, W., Xiang, L., and Qi, J. (2016a). Benzoate fraction from gentiana rigescens franch alleviates scopolamine-induced impaired memory in mice model in vivo. *Journal of Ethnopharmacology*, 193:107–116.

[Li et al., 2016b] Li, W., Peng, J., Tan, L., Wu, J., Shi, K., Qu, Y., Wei, X., and Qian, Z. (2016b). Mild photothermal therapy/photodynamic therapy/chemotherapy of breast cancer by lyp-1 modified docetaxel/ir820 co-loaded micelles. *Biomaterials*, 106:119–133.

[Li et al., 2013] Li, X., Guo, H., Tian, Q., Zheng, G., Hu, Y., Fu, Y., and Tan, H. (2013). Effects of 5-aminolevulinic acid–mediated photodynamic therapy on antibiotic-resistant staphylococcal biofilm: an in vitro study. *Journal of Surgical Research*, 184(2):1013–1021.

[Li et al., 2021] Li, Z., Bai, H., Jia, S., Yuan, H., Gao, L.-H., and Liang, H. (2021). Design of functional polymer nanomaterials for antimicrobial therapy and combatting resistance. *Mater. Chem. Front.*, 5:1236–1252.

[Lin et al., 2021] Lin, M.-H., Lee, J. Y.-Y., Pan, S.-C., and Wong, T.-W. (2021). Enhancing wound healing in recalcitrant leg ulcers with aminolevulinic acid-mediated antimicrobial photodynamic therapy. *Photodiagnosis and Photodynamic Therapy*, 33:102149.

[Lin et al., 2019] Lin, Y., Han, D., Li, Y., Tan, L., Liu, X., Cui, Z., Yang, X., Li, Z., Liang, Y., Zhu, S., and Wu, S. (2019). Ag2s@ws2 heterostructure for rapid bacteria-killing using near-infrared light. *ACS Sustainable Chemistry & Engineering*, 7(17):14982–14990.

[Lin et al., 2015] Lin, Z., Liu, Y., Ma, X., Hu, S., Zhang, J., Wu, Q., Ye, W., Zhu, S., Yang, D., Qu, D., and Jiang, J. (2015). Photothermal ablation of bone metas-

tasis of breast cancer using pegylated multi-walled carbon nanotubes. *Scientific Reports*, 5(1):11709.

[Liu et al., 2016] Liu, C., Zhou, Y., Wang, L., Han, L., Lei, J., Ishaq, H., Nair, S., and Xu, J. (2016). Photodynamic inactivation of klebsiella pneumoniae biofilms and planktonic cells by 5-aminolevulinic acid and 5-aminolevulinic acid methyl ester. *Lasers in medical science*, 31.

[Liu et al., 2017] Liu, X., Braun, G., Qin, M., Ruoslahti, E., and Sugahara, K. (2017). In vivo cation exchange in quantum dots for tumor-specific imaging. *Nature Communications*, 8.

[Liu et al., 2015] Liu, Y., Qin, R., Zaat, S., Breukink, E., and Heger, M. (2015). Antibacterial photodynamic therapy: overview of a promising approach to fight antibiotic-resistant bacterial infections. *Journal of Clinical and Translational Research*, 1:140–167.

[Lu et al., 2018] Lu, C., Chen, G., Yu, B., and Cong, H. (2018). Recent advances of low biological toxicity ag2s qds for biomedical application. *Advanced Engineering Materials*, 20(6):1700940.

[Mah and O'Toole, 2001] Mah, T.-F. C. and O'Toole, G. A. (2001). Mechanisms of biofilm resistance to antimicrobial agents. *Trends in Microbiology*, 9(1):34–39.

[Maisch et al., 2011] Maisch, T., Hackbarth, S., Regensburger, J., Felgenträger, A., Bäumler, W., Landthaler, M., and Röder, B. (2011). Photodynamic inactivation of multi-resistant bacteria (pib) – a new approach to treat superficial infections in the 21st century. *JDDG: Journal der Deutschen Dermatologischen Gesellschaft*, 9(5):360–366.

[Maisch et al., 2004] Maisch, T., Szeimies, R.-M., Jori, G., and Abels, C. (2004). Antibacterial photodynamic therapy in dermatology. *Photochemical & Photobiological Sciences*, 3(10):907–917.

[Malik et al., 1992] Malik, Z., Ladan, H., and Nitzan, Y. (1992). Photodynamic inactivation of gram-negative bacteria: Problems and possible solutions. *Journal of Photochemistry and Photobiology B: Biology*, 14(3):262–266.

[Mantareva et al., 2011] Mantareva, V., Kussovski, V., Angelov, I., Wöhrle, D., Dimitrov, R., Popova, E., and Dimitrov, S. (2011). Non-aggregated ga(iii)-phthalocyanines in the photodynamic inactivation of planktonic and biofilm cultures of pathogenic microorganisms. *Photochem. Photobiol. Sci.*, 10:91–102.

[Marchese et al., 2003] Marchese, A., Bozzolasco, M., Gualco, L., Debbia, E. A., Schito, G. C., and Schito, A. M. (2003). Effect of fosfomycin alone and in combination with n-acetylcysteine on e. coli biofilms. *International Journal of Antimicrobial Agents*, 22:95–100. Part 1 of the International Symposium Hot Topics in Urinary Tract Infection.

[Matcher et al., 1994] Matcher, S. J., Cope, M., and Delpy, D. T. (1994).

[Mattoussi et al., 2012] Mattoussi, H., Palui, G., and Na, H. B. (2012). Luminescent quantum dots as platforms for probing in vitro and in vivo biological processes. *Advanced Drug Delivery Reviews*, 64(2):138–166. Biological Interactions of Nanoparticles.

[Mendecki et al., 1980] Mendecki, J., Friedenthal, E., Botstein, C., Paglione, R., and Sterzer, F. (1980). Microwave applicators for localized hyperthermia treatment of cancer of the prostate. *International Journal of Radiation Oncology*Biology*Physics*, 6(11):1583–1588.

[Merchat et al., 1996] Merchat, M., Bertolini, G., Giacomini, P., Villaneuva, A., and Jori, G. (1996). Meso-substituted cationic porphyrins as efficient photosensitizers of gram-positive and gram-negative bacteria. *Journal of Photochemistry and Photobiology B: Biology*, 32(3):153–157.

[Monici, 2005] Monici, M. (2005). Cell and tissue autofluorescence research and diagnostic applications. *Biotechnology Annual Review*, 11:227–256.

[Montanari et al., 2015] Montanari, C., Serrazanetti, D. I., Felis, G., Torriani, S., Tabanelli, G., Lanciotti, R., and Gardini, F. (2015). New insights in thermal resistance of staphylococcal strains belonging to the species staphylococcus epidermidis, staphylococcus lugdunensis and staphylococcus aureus. *Food Control*, 50:605–612.

[Mu et al., 2014] Mu, Q., Jiang, G., Chen, L., Zhou, H., Fourches, D., Tropsha, A., and Yan, B. (2014). Chemical basis of interactions between engineered nanoparticles and biological systems. *Chemical Reviews*, 114(15):7740–7781. PMID: 24927254.

[Mukha et al., 2013] Mukha, I. P., Eremenko, A. M., Smirnova, N. P., Mikhienkova, A. I., Korchak, G. I., Gorchev, V. F., and Chunikhin, A. Y. (2013). Antimicrobial activity of stable silver nanoparticles of a certain size. *Applied Biochemistry and Microbiology*, 49(2):199–206.

[Municoy et al., 2015] Municoy, S., F. Desimone, M., N. Catalano, P., and G. Bellino, M. (2015). Antimicrobial surfaces from incorporated nano-agents. *Current Bionanotechnology*, 1(2):125–134.

[Mykhaylyk et al., 2007] Mykhaylyk, O., Sanchez-Antequera, Y., Vlaskou, D., and Plank, C. (2007). Generation of magnetic nonviral gene transfer agents and magnetofection in vitro. *Nature protocols*, 2:2391–411.

[Nagasuna et al., 2011] Nagasuna, K., Akita, T., Fujishima, M., and Tada, H. (2011). Photodeposition of ag2s quantum dots and application to photoelectrochemical cells for hydrogen production under simulated sunlight. *Langmuir*, 27(11):7294–7300. PMID: 21553826.

[Ng and Zheng, 2015] Ng, K. K. and Zheng, G. (2015). Molecular interactions in organic nanoparticles for phototheranostic applications. *Chemical Reviews*, 115(19):11012–11042. PMID: 26244706.

[Nguyen et al., 2016] Nguyen, H., Park, S., Hlaing, K., and Kang, H. W. (2016). Temperature feedback-controlled photothermal treatment with diffusing applicator: Theoretical and experimental evaluations. *Biomedical Optics Express*, 7:1932.

[Nitzan et al., 2004] Nitzan, Y., Salmon-Divon, M., Shporen, E., and Malik, Z. (2004). Ala induced photodynamic effects on gram positive and negative bacteria. *Photochemical & Photobiological Sciences*, 3(5):430–435.

[Niu et al., 2022] Niu, N., Yang, N., Yu, C., Wang, D., and Tang, B. Z. (2022). Nir-ii absorbing charge transfer complexes for synergistic photothermal–chemodynamic antimicrobial therapy and wounds healing. *ACS Materials Letters*, 4(4):692–700.

[Noszál et al., 2000] Noszál, B., Visky, D., and Kraszni, M. (2000). Population, acid-base, and redox properties of n-acetylcysteine conformers. *Journal of Medicinal Chemistry*, 43(11):2176–2182. PMID: 10841796.

[Novo et al., 1996] Novo, M., Hüttmann, G., and Diddens, H. (1996). Chemical instability of 5-aminolevulinic acid used in the fluorescence diagnosis of bladder tumours. *Journal of Photochemistry and Photobiology B: Biology*, 34(2):143–148.

[Nyman and Hynninen, 2004] Nyman, E. S. and Hynninen, P. H. (2004). Research advances in the use of tetrapyrrolic photosensitizers for photodynamic therapy. *Journal of Photochemistry and Photobiology B: Biology*, 73(1):1–28.

[Ochsner, 1997] Ochsner, M. (1997). Photophysical and photobiological processes in the photodynamic therapy of tumours. *Journal of Photochemistry and Photobiology B: Biology*, 39(1):1–18.

[Olerile et al., 2017] Olerile, L. D., Liu, Y., Zhang, B., Wang, T., Mu, S., Zhang, J., Selotlegeng, L., and Zhang, N. (2017). Near-infrared mediated quantum dots and paclitaxel co-loaded nanostructured lipid carriers for cancer theragnostic. *Colloids and Surfaces B: Biointerfaces*, 150:121–130.

[Orecchioni et al., 2015] Orecchioni, M., Cabizza, R., Bianco, A., and Delogu, L. G. (2015). Graphene as cancer theranostic tool: Progress and future challenges. *Theranostics*, 5:710–723.

[Ornellas et al., 2018] Ornellas, P. O., Antunes, L. S., Motta, P. C., Mendonça, C., Póvoa, H., Fontes, K., Iorio, N., and Antunes, L. A. A. (2018). Antimicrobial photodynamic therapy as an adjunct for clinical partial removal of deciduous carious tissue: A minimally invasive approach. *Photochemistry and Photobiology*, 94(6):1240–1248.

[Otto, 2008] Otto, M. (2008). *Staphylococcal Biofilms*, pages 207–228. Springer Berlin Heidelberg, Berlin, Heidelberg.

[Park et al., 2012] Park, Y. I., Kim, H. M., Kim, J. H., Moon, K. C., Yoo, B., Lee, K. T., Lee, N., Choi, Y., Park, W., Ling, D., Na, K., Moon, W. K., Choi, S. H., Park, H. S., Yoon, S.-Y., Suh, Y. D., Lee, S. H., and Hyeon, T. (2012). Theranostic probe based on lanthanide-doped nanoparticles for simultaneous in vivo dual-modal imaging and photodynamic therapy. *Advanced Materials*, 24(42):5755–5761.

[Peng et al., 2014] Peng, J., Qi, T., Liao, J., Chu, B., Yang, Q., Qu, Y., Li, W., Li, H., Luo, F., and Qian, Z. (2014). Mesoporous magnetic gold "nanoclusters" as theranostic carrier for chemo-photothermal co-therapy of breast cancer. *Theranostics*, 4:678–692.

[Peng et al., 2020] Peng, R., Luo, Y., Cui, Q., Wang, J., and Li, L. (2020). Near-infrared conjugated oligomer for effective killing of bacterial through combination of photodynamic and photothermal treatment. *ACS Applied Bio Materials*, 3(2):1305–1311. PMID: 35019331.

[Phillips, 2019] Phillips, J. D. (2019). Heme biosynthesis and the porphyrias. *Molecular Genetics and Metabolism*, 128(3):164–177. Recent advances in Heme Biosynthesis and the Porphyrias.

[Pohanka, 2017] Pohanka, M. (2017). Quantum dots in the therapy: Current trends and perspectives. *Mini Reviews in Medicinal Chemistry*, 17(8):650–656.

[Prakash et al., 2020] Prakash, B., Katoch, V., Shah, A., Sharma, M., Devi, M. M., Panda, J. J., Sharma, J., and Ganguli, A. K. (2020). Continuous flow reactor for the controlled synthesis and inline photocatalysis of antibacterial ag2s nanoparticles. *Photochemistry and Photobiology*, 96(6):1273–1282.

[Pérez-Giraldo et al., 1997] Pérez-Giraldo, C., Rodríguez-Benito, A., Morán, F. J., Hurtado, C., Blanco, M. T., and Gómez-García, A. C. (1997). Influence of N-acetylcysteine on the formation of biofilm by Staphylococcus epidermidis. *Journal of Antimicrobial Chemotherapy*, 39(5):643–646.

[Reimers and Khalafalla, 1972] Reimers, G. and Khalafalla, S. (1972). *Preparing Magnetic Fluids by a Peptizing Method*. Bureau of Mines technical progress report. U.S. Department of the Interior.

[Riadh W. Y. Habash and Alhafid, 2006] Riadh W. Y. Habash, Rajeev Bansal, D. K. and Alhafid, H. T. (2006). Thermal therapy, part 2: Hyperthermia techniques. *Critical Reviewstrade; in Biomedical Engineering*, 34(6):491–542.

[Roberts and Cole, 1981] Roberts, D. and Cole, P. (1981). N-acetylcysteine potentiates the anti-pseudomonas activity of carbenicillin in vitro. *Journal of Infection*, 3(4):353–359.

[Rogers et al., 2009] Rogers, K., Fey, P., and Rupp, M. (2009). Coagulase-negative staphylococcal infections. infect dis clin north am. *Infectious disease clinics of North America*, 23:73–98.

[Roper et al., 2007] Roper, D. K., Ahn, W., and Hoepfner, M. (2007). Microscale heat transfer transduced by surface plasmon resonant gold nanoparticles. *The Journal of Physical Chemistry C*, 111(9):3636–3641. PMID: 19011696.

[Rossmanna and Haemmerich, 2014] Rossmanna, C. and Haemmerich, D. (2014). Review of temperature dependence of thermal properties, dielectric properties, and perfusion of biological tissues at hyperthermic and ablation temperatures. *Critical reviews in biomedical engineering*, 42(6):467—492.

[Sajjad et al., 2021] Sajjad, F., Sun, N.-N., Chen, T., Yan, Y.-J., Margetić, D., and Chen, Z.-L. (2021). Evaluation of antimicrobial photodynamic activities of 5-aminolevulinic acid derivatives. *Photodermatology, Photoimmunology & Photomedicine*, 37(4):296–305.

[Samia et al., 2003] Samia, A. C. S., Chen, X., and Burda, C. (2003). Semiconductor quantum dots for photodynamic therapy. *Journal of the American Chemical Society*, 125(51):15736–15737. PMID: 14677951.

[Sangtani et al., 2018] Sangtani, A., Petryayeva, E., Wu, M., Susumu, K., Oh, E., Huston, A. L., Lasarte-Aragones, G., Medintz, I. L., Algar, W. R., and Delehanty, J. B. (2018). Intracellularly actuated quantum dot–peptide–doxorubicin nanobioconjugates for controlled drug delivery via the endocytic pathway. *Bioconjugate Chemistry*, 29(1):136–148. PMID: 29191007.

[Sapareto and Dewey, 1984] Sapareto, S. A. and Dewey, W. C. (1984). Thermal dose determination in cancer therapy. *International Journal of Radiation Oncology*Biology*Physics*, 10(6):787–800.

[Sbarra et al., 2008] Sbarra, M. S., Poto, A. D., Arciola, C. R., Saino, E., Sharma, M., Bragheri, F., Cristiani, I., Speziale, P., and Visai, L. (2008). Photodynamic action of merocyanine 540 on staphylococcus epidermidis biofilms. *The International Journal of Artificial Organs*, 31(9):848–857. PMID: 18924098.

[Schwandt et al., 2004] Schwandt, L. Q., Weissenbruch, R. V., Stokroos, I., Mei, H. C. V. D., Busscher, H. J., and Albers, F. W. J. (2004). Prevention of biofilm formation by dairy products and n-acetylcysteine on voice prostheses in an artificial throat. *Acta Oto-Laryngologica*, 124(6):726–731. PMID: 15515498.

[Sessler and Miller, 2000] Sessler, J. and Miller, R. (2000). Texaphyrins: new drugs with diverse clinical applications in radiation and photodynamic therapy. *Biochemical pharmacology*, 59(7):733—739.

[Shanmugam et al., 2014] Shanmugam, V., Selvakumar, S., and Yeh, C.-S. (2014). Near-infrared light-responsive nanomaterials in cancer therapeutics. *Chem. Soc. Rev.*, 43:6254–6287.

[Sheng et al., 2014] Sheng, Z., Hu, D., Zheng, M., Zhao, P., Liu, H., Gao, D., Gong, P., Gao, G., Zhang, P., Ma, Y., and Cai, L. (2014). Smart human serum albumin-indocyanine green nanoparticles generated by programmed assembly for dual-modal imaging-guided cancer synergistic phototherapy. *ACS Nano*, 8(12):12310–12322. PMID: 25454579.

[Shi et al., 2022] Shi, J., Li, J., Wang, Y., and Zhang, C. Y. (2022). Tio2-based nanosystem for cancer therapy and antimicrobial treatment: A review. *Chemical Engineering Journal*, 431:133714.

[Sievert et al., 2013] Sievert, D. M., Ricks, P., Edwards, J. R., Schneider, A., Patel, J., Srinivasan, A., Kallen, A., Limbago, B., and Fridkin, S. (2013). Antimicrobial-resistant pathogens associated with healthcare-associated infections summary of data reported to the national healthcare safety network at the centers for disease control and prevention, 2009–2010. *Infection Control amp; Hospital Epidemiology*, 34(1):1–14.

[Silveira et al., 2013] Silveira, L. F. M., Baca, P., Arias-Moliz, M. T., Rodríguez-Archilla, A., and Ferrer-Luque, C. M. (2013). Antimicrobial activity of alexidine alone and associated with n-acetylcysteine against enterococcus faecalis biofilm. *International Journal of Oral Science*, 5(3):146–149.

[Sivakumar et al., 2017] Sivakumar, B., Aswathy, R. G., Romero-Aburto, R., Mitcham, T., Mitchel, K. A., Nagaoka, Y., Bouchard, R. R., Ajayan, P. M.,

Maekawa, T., and Sakthikumar, D. N. (2017). Highly versatile spion encapsulated plga nanoparticles as photothermal ablators of cancer cells and as multimodal imaging agents. *Biomater. Sci.*, 5:432–443.

[Song et al., 2016] Song, B., Zhang, C., Zeng, G., Gong, J., Chang, Y., and Jiang, Y. (2016). Antibacterial properties and mechanism of graphene oxide-silver nanocomposites as bactericidal agents for water disinfection. *Archives of Biochemistry and Biophysics*, 604:167–176.

[Stewart and William Costerton, 2001] Stewart, P. S. and William Costerton, J. (2001). Antibiotic resistance of bacteria in biofilms. *The Lancet*, 358(9276):135–138.

[Takahashi et al., 2006] Takahashi, H., Niidome, T., Nariai, A., Niidome, Y., and Yamada, S. (2006). Photothermal reshaping of gold nanorods prevents further cell death. *Nanotechnology*, 17(17):4431.

[Tan et al., 2012] Tan, H. L., Lin, W. T., and Tang, T. T. (2012). The use of antimicrobial-impregnated pmma to manage periprosthetic infections: Controversial issues and the latest developments. *The International Journal of Artificial Organs*, 35(10):832–839. PMID: 23138709.

[Tewari and Eggleston, 2018] Tewari, K. M. and Eggleston, I. M. (2018). Chemical approaches for the enhancement of 5-aminolevulinic acid-based photodynamic therapy and photodiagnosis. *Photochemical & Photobiological Sciences*, 17(11):1553–1572.

[Tietze et al., 2015] Tietze, R., Zaloga, J., Unterweger, H., Lyer, S., Friedrich, R. P., Janko, C., Pöttler, M., Dürr, S., and Alexiou, C. (2015). Magnetic nanoparticle-based drug delivery for cancer therapy. *Biochemical and Biophysical Research Communications*, 468(3):463–470. Nanomedicine.

[Unterweger et al., 2015] Unterweger, H., Subatzus, D., Tietze, R., Janko, C., Poettler, M., Stiegelschmitt, A., Schuster, M., Maake, C., Boccaccini, A. R., and Alex-

iou, C. (2015). Hypericin-bearing magnetic iron oxide nanoparticles for selective drug delivery in photodynamic therapy. *International journal of nanomedicine*, 10:6985—6996.

[Vallinayagam et al., 2008] Vallinayagam, R., Schmitt, F., Barge, J., Wagnieres, G., Wenger, V., Neier, R., and Juillerat-Jeanneret, L. (2008). Glycoside esters of 5-aminolevulinic acid for photodynamic therapy of cancer. *Bioconjugate Chemistry*, 19(4):821–839. PMID: 18341270.

[van Rijt and Sadler, 2009] van Rijt, S. H. and Sadler, P. J. (2009). Current applications and future potential for bioinorganic chemistry in the development of anticancer drugs. *Drug Discovery Today*, 14(23):1089–1097.

[Vatansever et al., 2013] Vatansever, F., de Melo, W. C., Avci, P., Vecchio, D., Sadasivam, M., Gupta, A., Chandran, R., Karimi, M., Parizotto, N. A., Yin, R., Tegos, G. P., and Hamblin, M. R. (2013). Antimicrobial strategies centered around reactive oxygen species – bactericidal antibiotics, photodynamic therapy, and beyond. *FEMS Microbiology Reviews*, 37(6):955–989.

[Venosa et al., 2009] Venosa, G. D., Hermida, L., Fukuda, H., Defain, M. V., Rodriguez, L., Mamone, L., MacRobert, A., Casas, A., and Batlle, A. (2009). Comparation of liposomal formulations of ala undecanoyl ester for its use in photodynamic therapy. *Journal of Photochemistry and Photobiology B: Biology*, 96(2):152–158.

[Vera et al.,] Vera, D. M. A., Haynes, M. H., Ball, A. R., Dai, T., Astrakas, C., Kelso, M. J., Hamblin, M. R., and Tegos, G. P. Strategies to potentiate antimicrobial photoinactivation by overcoming resistant phenotypes†. *Photochemistry and Photobiology*, 88(3):499–511.

[Verderosa et al., 2019] Verderosa, A., Totsika, M., and Fairfull-Smith, K. (2019). Bacterial biofilm eradication agents: A current review. *Frontiers in Chemistry*, 7.

[Wainwright et al., 1997] Wainwright, M., Phoenix, D. A., Marland, J., Wareing, D. R., and Bolton, F. J. (1997). In-vitro photobactericidal activity of aminoacridines. *Journal of Antimicrobial Chemotherapy*, 40(4):587–589.

[Wang et al., 2020] Wang, J., Wu, X., Shen, P., Wang, J., Shen, Y., Shen, Y., Webster, T. J., and Deng, J. (2020). Applications of inorganic nanomaterials in photothermal therapy based on combinational cancer treatment. *Int J Nanomedicine*, 15:1903–1914.

[Wang et al., 2019] Wang, W., Cheng, X., Liao, J., Lin, Z., Chen, L., Liu, D., Zhang, T., Li, L., Lu, Y., and Xia, H. (2019). Synergistic photothermal and photodynamic therapy for effective implant-related bacterial infection elimination and biofilm disruption using cu9s8 nanoparticles. *ACS Biomaterials Science & Engineering*, 5(11):6243–6253. PMID: 33405531.

[Wang et al., 2013] Wang, Y., Black, K. C. L., Luehmann, H., Li, W., Zhang, Y., Cai, X., Wan, D., Liu, S.-Y., Li, M., Kim, P., Li, Z.-Y., Wang, L. V., Liu, Y., and Xia, Y. (2013). Comparison study of gold nanohexapods, nanorods, and nanocages for photothermal cancer treatment. *ACS Nano*, 7(3):2068–2077. PMID: 23383982.

[Wei et al., 2020] Wei, G., Yang, G., Wang, Y., Jiang, H., Fu, Y., Yue, G., and Ju, R. (2020). Phototherapy-based combination strategies for bacterial infection treatment. *Theranostics*, 10(26):12241–12262.

[Wei et al., 2022] Wei, L., Chen, Y., Yu, X., Yan, Y., Liu, H., Cui, X., Liu, X., Yang, X., Meng, J., Yang, S., Wang, L., Yang, X., Chen, R., and Cheng, Y. (2022). Bismuth tungstate–silver sulfide z-scheme heterostructure nanoglue promotes wound healing through wound sealing and bacterial inactivation. *ACS Applied Materials & Interfaces*, 14(48):53491–53500. PMID: 36416503.

[Xu et al., 2019] Xu, J.-W., Yao, K., and Xu, Z.-K. (2019). Nanomaterials with a photothermal effect for antibacterial activities: an overview. *Nanoscale*, 11:8680–8691.

[Yamada and Ogawa, 2009] Yamada, M. and Ogawa, T. (2009). Chemodynamics underlying n-acetyl cysteine-mediated bone cement monomer detoxification. *Acta Biomaterialia*, 5(8):2963–2973.

[Yan et al., 2018] Yan, L., Amirshaghaghi, A., Huang, D., Miller, J., Stein, J. M., Busch, T. M., Cheng, Z., and Tsourkas, A. (2018). Protoporphyrin ix (ppix)-coated superparamagnetic iron oxide nanoparticle (spion) nanoclusters for magnetic resonance imaging and photodynamic therapy. *Advanced Functional Materials*, 28(16):1707030.

[Yang et al., 2013] Yang, H.-Y., Zhao, Y.-W., Zhang, Z.-Y., Xiong, H.-M., and Yu, S.-N. (2013). One-pot synthesis of water-dispersible ag2s quantum dots with bright fluorescent emission in the second near-infrared window. *Nanotechnology*, 24(5):055706.

[Yang et al., 2016] Yang, R.-M., Fu, C., Fang, J., Xu, X., Wei, X., Tang, W., Jiang, X., and Zhang, L. (2016). Hyaluronan-modified superparamagnetic iron oxide nanoparticles for bimodal breast cancer imaging and photothermal therapy. *International Journal of Nanomedicine*, Volume 12:197–206.

[Yang et al., 2017] Yang, T., Tang, Y., Liu, L., Lv, X., Wang, Q., Ke, H., Deng, Y., Yang, H., Yang, X., Liu, G., Zhao, Y., and Chen, H. (2017). Size-dependent ag2s nanodots for second near-infrared fluorescence/photoacoustics imaging and simultaneous photothermal therapy. *ACS Nano*, 11(2):1848–1857. PMID: 28117993.

[Yero et al., 2021] Yero, D., Díaz-Lobo, M., Costenaro, L., Conchillo-Solé, O., Mayo, A., Ferrer-Navarro, M., Vilaseca, M., Gibert, I., and Daura, X. (2021). The pseudomonas aeruginosa substrate-binding protein ttg2d functions as a general glycerophospholipid transporter across the periplasm. *Communications biology*, 4(1):448.

[Yi et al., 2015] Yi, X., Yang, K., Liang, C., Zhong, X., Ning, P., Song, G., Wang, D., Ge, C., Chen, C., Chai, Z., and Liu, Z. (2015). Imaging-guided combined pho-

tothermal and radiotherapy to treat subcutaneous and metastatic tumors using iodine-131-doped copper sulfide nanoparticles. *Advanced Functional Materials*, 25(29):4689–4699.

[Yong et al., 2015] Yong, Y., Cheng, X., Bao, T., Zu, M., Yan, L., Yin, W., Ge, C., Wang, D., Gu, Z., and Zhao, Y. (2015). Tungsten sulfide quantum dots as multifunctional nanotheranostics for in vivo dual-modal image-guided photothermal/radiotherapy synergistic therapy. *ACS Nano*, 9(12):12451–12463. PMID: 26495962.

[Yuen et al., 2012] Yuen, A. K. L., Hutton, G. A., Masters, A. F., and Maschmeyer, T. (2012). The interplay of catechol ligands with nanoparticulate iron oxides. *Dalton Trans.*, 41:2545–2559.

[Zafarullah et al., 2003] Zafarullah, M., Li, W. Q., Sylvester, J., and Ahmad, M. (2003). Molecular mechanisms of n-acetylcysteine actions. *Cellular and Molecular Life Sciences CMLS*, 60(1):6–20.

[Zemann, 1965] Zemann, J. (1965). Crystal structures, 2nd edition, vol. 2 by r. w. g. wyckoff. *Acta Crystallographica*, 19(3):490–490.

[Zhang et al., 2022] Zhang, Y., Li, P., Su, R., Wen, F., Jia, Z., Lv, Y., Cai, J., and Su, W. (2022). Curcumin-loaded multifunctional chitosan gold nanoparticles: An enhanced pdt/pttdual-modal phototherapeutic andph-responsive antimicrobial agent. *Photodiagnosis and Photodynamic Therapy*, 39:103011.

[Zhou et al., 2015] Zhou, F., Li, X., Naylor, M. F., Hode, T., Nordquist, R. E., Alleruzzo, L., Raker, J., Lam, S. S., Du, N., Shi, L., Wang, X., and Chen, W. R. (2015). Incvax – a novel strategy for treatment of late-stage, metastatic cancers through photoimmunotherapy induced tumor-specific immunity. *Cancer Letters*, 359(2):169–177.

[Zhou et al., 2014] Zhou, Z., Sun, Y., Shen, J., Wei, J., Yu, C., Kong, B., Liu, W., Yang, H., Yang, S., and Wang, W. (2014). Iron/iron oxide core/shell nanoparticles

for magnetic targeting mri and near-infrared photothermal therapy. *Biomaterials*, 35(26):7470–7478.

[Zolfaghari et al., 2009] Zolfaghari, P. S., Packer, S., Singer, M., Nair, S. P., Bennett, J., Street, C., and Wilson, M. (2009). In vivo killing of staphylococcus aureus using a light-activated antimicrobial agent. *BMC MICROBIOLOGY*, 9.

[Zou et al., 2016] Zou, L., Wang, H., He, B., Zeng, L., Tan, T., Cao, H., He, X., Zhang, Z., Guo, S., and Li, Y. (2016). Current approaches of photothermal therapy in treating cancer metastasis with nanotherapeutics. *Theranostics*, 6:762–772.